PhD thesis

Pilot experiment to measure a complete triple of thermoviscoelastic response functions of equilibrium viscous liquids and an effect of thermoelastic coupling - cooling by heating

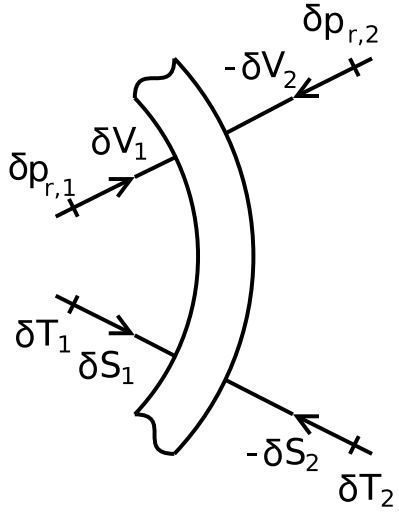

Author:
Jon Josef Papini

Supervisor:
Tage Christensen

Danish National Research Foundation Centre "Glass and Time",
IMFUFA, Department of Science, Systems, and Models
Roskilde University, Denmark

Abstract in English

The present PhD thesis dissertation is a report on two main projects: (1) A study of thermoviscoelastic phenomena, and (2) a pilot experiment to test if relaxation of highly viscous liquids can be described by a single internal parameter.

The first part is a study of a peculiar thermoelastic effect - cooling by heating: If a solid sphere is heated at the surface, temperature will drop in the middle of the sphere. The study gives a theoretical explanation in terms of an analysis of the full thermoviscoelastic problem in spherical geometry. The effect is shown to be the consequence of a non-trivial thermomechanical coupling which exist if there is a difference between the longitudinal and the isobaric specific heat. Through extensive mathematical modeling I derive a formula that predicts the size of the cooling by heating effect when a finite amount of heat is added at the surface of a thermoelastic solid. Numerical simulations prove that the effect also exists in the thermoviscoelastic case, and it is shown that the effect is present in the liquid, even in the case where the effect is non-present in the solid. The modeling also shows that the effect is not limited to the center of the sphere and thus a detection of the phenomenon is not dependent on a very precise central placement of a thermometer. Besides the theoretical work I have done molecular dynamics simulations of a nano-sized droplet proving that cooling by heating is present also on the molecular level. Finally, I have performed measurements in the lab on a sphere of glucose. The experiments show that the effect is present also in real systems.

The second part is a pilot experiment. I explore the possibility of measuring a complete set of thermoviscoelastic response functions on the same sample under identical conditions, by combining two devices used and developed in the Glass & Time group at Roskilde University. The motive for this is the scientific question whether one or more internal parameters are needed to describe the relaxation dynamics of highly viscous liquids. This question is a part of the long term research plan of the group. The first device is the Piezoelectric Bulk modulus Gauge (PBG), which is a spherical piezoelectric shell coated with electrodes on both sides. Applying an oscillation electric field to the liquid filled PBG one measures the mechanical auto response function $K_S(\omega)$ - the adiabatic bulk modulus. The second device is a thermistor. Employing the 3ω-method one measures the thermal auto response function $c_l(\omega)$ - the longitudinal specific heat. Placing the thermistor in the center of the PBG, one can perform the third experiment: The measurement of the cross response function $\beta_S(\omega) \equiv \left(\frac{\partial V}{\partial S}\right)_p(\omega)$ - the adiabatic pressure coefficient. Here a heat current is generated in the center with the thermistor while the resulting deformation of the PBG as the liquid expands is measured as a piezoelectric voltage. This is a novel measurement never done before, and in order to deduce β_S one first need to measure the two auto response functions. This part of the thesis briefly presents the measurements of K_S and c_l. Also I show how to model the third combined experiment, and perform a first pilot measurement

of the cross response function. The measurement gives a good signal to noise ratio, but the deduced spectrum found for β_s have peculiar characteristics. The absolute value of the measured property is in the correct range, but the temperature dependence of the dispersion is not understood. It is suggested that the model used is to simple and that the thermal structure of the thermistor bead needs to be included in the model. A test of "single parameterness" of relaxation in an equilibrium liquids is not possible due to the quality of the data.

Abstract in Danish

Denne philosophiæ doctor afhandling består af to dele: (1) Den første del omhandler termoelastiske fænomener, og (2) omhandler et pilot forsøg til måling af en komplet tripel af termoviskoelastiske respons funktioner.

Den første del undersøger en pudsig effekt- cooling by heating: Hvis man varmer på overfladen af en kugle falder temperaturen i dens midte. Dette studie giver den teoretiske forklaring på effekten i termer af det fulde termoviskoelastiske problem i sfærisk geometri. Effekten viser sig at skyldes en ikke-triviel termoelastisk kobling som kun er til stede når den longitudinale og isobare varmefylde adskiller sig. Omfattende matematisk modellering leder frem til en formel der forudsiger størrelsen af effekten når en endelig varmemængde appliceres på overfladen af en fast kugle. Numeriske beregninger viser at effekten også er til stede i det viskoelastiske tilfælde. Det viser sig at effekten er til stede i væsken, selv om den ikke er det i den faste tilstand. Modelleringerne viser også at effekten er til stede ikke bare i midten af kuglen, men i alle afstande fra centrum. Udover det teoretisk arbejde har jeg udført MD-simuleringer der viser at effekten også er til stede i en dråbe af nano-størrelse. Ydermere giver jeg et eksperimentelt bevis for fænomenet ved målinger på en kugle støbt af glukose.

Den anden del er et eksperimentelt pilotprojekt. Formålet er at måle et komplet set af termoviskoelastiske respons funktioner - med sådan en metode vil man kunne undersøge en central videnskabelig problemstilling, nemlig hvorvidt relaksations fænomener i viskøse væsker skal beskrives med en eller flere ordens parametre. For at undersøge dette kombinerer jeg to tekniker der bruges flittigt i Glas og Tid ved Roskilde Universitet. Den første metode bruges til at måle det frekvensafhængige bulk modul $K_S(\omega)$. Til det bruges den piezoelektriske bulk transducer (PBG) som er en sfærisk keramisk skal pålagt elektroder. Ved at pålægge en oscillerende spænding på den væske-fyldte PBG kan bulk modulet bestemmes. Den anden metode udnytter 3ω-signalet i en temperatur afhængig modstand til at måle den frekvensafhængige longitudinale varmefylde $c_l(\omega)$. Hvis man placerer termistoren i midten af PBG kan man udføre det tredje eksperiment: Måling af den adiabatiske tryk stignings koefficient $\beta_S(\omega) \equiv \left(\frac{\partial V}{\partial S}\right)_p(\omega)$. I dette forsøg genererer man en varmestrøm med termistoren. Den resulterende deformation af PBG'en når væsken ekspanderer måles som en piezoelektrisk spænding. Dette er en ny metode og for at udføre den skal man først kende de to andre respons funktioner. I denne afhandling gøres der rede for modelleringen af forsøget og et første pilot forsøg udføres. Målingerne giver et fint signal men det udledte spektrum for β_S udviser mærkelige træk. Størrelsesorden af trykstignings koefficienten er dog rigtig, men dispersionens temperatur afhængighed er ikke helt forstået. Det skønnes at den anvendte model er for simpel og at modellen bør udvides til at omfatte termistorens termiske struktur. De opnåede data er ikke gode nok til at teste spørgsmålet om antallet af nødvendige ordens-parametre i beskrivelsen af viskøse væskers dynamik.

Preface

Acknowledgemets

The last three years as a PhD student in the Danish National Research Foundation Centre 'Glass & Time' at Roskilde University has been a wonderful experience. Thanks to the warn, free and easy atmosphere, it has been a joy to meet in the office every single day of the week. My colleagues, both in the group and at Imfufa in general have become an important part of my life that I will never forget.

I would like to thank my supervisor Tage Christensen for always being positive and his supporting attitude. I am grateful for all the hours he spent with me in the lab or at a table working on mathematical problems. I enjoyed our walks and drinking wine in his company.

Also I would like to thank Jeppe Dyre for the first year of supervising and him believing in me. I believe Jeppe is an inspiration to all of us, with his broad knowledge and wholehearted commitment to the field.

The technical staff at IMFUFA, Preben Olsen, Torben Rasmussen, Ebbe H. Larsen, Ib Høst, and Heine Larsen, have all contributed in some way to my project. Especially I would like to thank Preben for the many hours he spent helping me to mold lollipops.

Finally, I am grateful for the support of my family, especially from the three persons that mean the most to me: My two children Selma and Loui and my wife Line. Without the support from Line, I would have lost my self on the way.

Jon Josef Papini

June, 2011

Contents

1 Introduction

When cooling a liquid through the glass transition range, the properties of the supercooled melt change to those of the corresponding glass. One such property is the specific heat. A way to obtain the temperature dependence of the specific heat is to do Differential Scanning Calorimetry (DSC). DSC is based on quite a basic idea. It is done by placing a sample that you wish to study in a pan that rests on top of a heater. But there is also an other pan sitting on another heater, the reference pan, which is empty but otherwise identical to the pan containing the sample. Then the two heaters are turned on, and continue to heat at a specific rate, that stay exactly the same throughout the experiment. This is regulated with the aid of a computer, which also makes sure, that the two separate pans, with their two separate heaters, heat at exactly the same rate. Now, since one pan contains the sample, and the other is empty, more heat has to be transferred to the pan with the sample in order to keep the temperature of the sample pan increasing at the same rate as the reference pan. The quantity that is measured in a DSC experiment is thus the difference in the heat that the two heaters have to put out. Plotting the difference in heat output of the two heaters against temperature, one obtains a graph that tells how much heat is put in to the sample at any given temperature. Since the heating rate is constant, the heat capacity is obtained by the ratio of heat flow and temperature rate $c_p(T) = \frac{dQ}{dt}/\frac{dT}{dt}$. So, if a sample has been brought down in temperature below T_g without crystallizing, one can perform a DSC scan going up in temperature. Such a scan is depicted in Figure 1.1. The data shown here was obtained in the late twenties by Simon and Lange [1]. Their data shows how the property changes differently depending on the starting configuration. Bringing the crystal up in temperature a discontinuous change will occur at the melting point, whereas coming from a glassy state the change occurs below the melting temperature, smoothly from one plateau to another. Below T_g the heat capacity of the glass follows (almost) that of the crystal, reflecting a loss of the configurational contribution to the free energy going from the liquid to the glassy state.

The behavior described is a general characteristic of substances that can form a glass. In all cases there is a temperature range where relaxation phenomena can be observed and quantities such as the specific heat changes quite much over a small temperature range. Attempts to find a microscopic explanation has been made [2, 3]. One such attempt was given by Simon [1] in 1931. The idea was to associate a degree of order to each state of a substance, represented by some parameter that depends on temperature (and pressure). As energy is added to, or removed from the system, the parameter changes, thus representing the changing potential energy that follows with a changing configuration. Simons idea was, that as a liquid substance is cooled through its glass transition region, the mobility of the constituent molecules is lowered. This would mean that any structural change that is appropriate with respect to the changing conditions is being increasingly hindered and finally brought to a halt. At this point the parameter

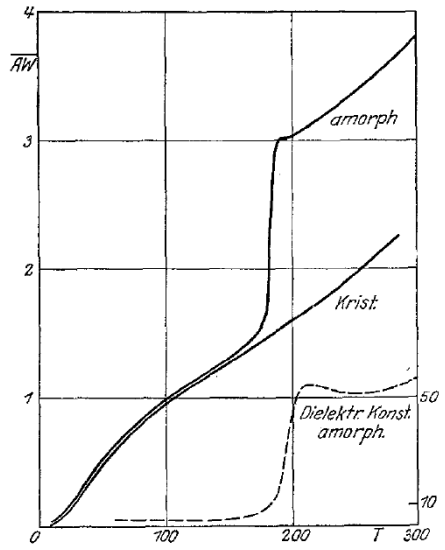

Fig. 2. Atomwärmen des Glycerins. Von 300 bis 70⁰ abs. nach Simon (l. c.) und Gibson und Giauque, unterhalb 70⁰ nach dieser Arbeit.

Figure 1.1 Typical $C_p = C_p(T)$ curves for crystalline, liquid and glassy Glycerol [1].

descriptive of the order is fixed and the part of the specific heat corresponding to changes in potential energy vanishes. This is manifested as a jump in isobaric specific heat per unit volume Δc_p. That fingerprint would also be seen in other quantities, with jumps in isobaric expansion coefficient, $\Delta\alpha_p$, and isothermal compressibility, $\Delta\kappa_T$ around T_g.

Taking the view of Simon [1] of glass formation as being a freezing-in process, several authors, beginning with [4–6] in the Fifties, and later [7–9], used the concept of structural internal parameters [10] in order to treat the glass transition as a genuine phase transition. The internal parameters were included as extra terms in the free energy of the system, which in the liquid are functions of temperature and pressure, whereas in the glass they are frozen in. From this approach it was possible to correlate the jumps of the different quantities in the so called Prigogine-Defay (PD) ratio, Π, defined as follows.

$$\Pi = \frac{1}{T}\frac{\Delta c_p \Delta\kappa_T}{(\Delta\alpha_p)^2}\bigg|_{T=T_g} \tag{1.1}$$

Despite the debate in the Seventies [9, 11–15], consensus was reached, that the original prediction made by [5, 6] was correct: In a homogeneous system , $\Pi = 1$ if there is just a single internal parameter, whereas if more than one internal parameter determines the structural relaxation, then $\Pi > 1$.

In most cases values of $\Pi > 1$ are found experimentally [5, 6, 9, 16–18] making it conventional wisdom that generally there is a need for more than one internal parameter. However, Gupta [19] showed that in a system with inhomogeneities, assuming a single

internal parameter gives a PD-ratio greater than unity, i.e., the inhomogeneities behave like additional internal parameters. Since almost all systems are inhomogeneous to some extent, there is no reason to expect that a PD-ratio equal to unity should be obtained experimentally. Another point to be made, also due to Gupta [19], is that glass formation is not a sharp transition in an instantaneously quenched system, but rather occurs at finite rates of cooling, with a gradual falling out of (metastable) equilibrium. Schmelzer [20] pointed out this weakness of the classical approach (Simon's picture) where the glass transition is regarded as a freezing in process, and showed that, assuming a single internal parameter in a framework of thermodynamics of irreversible processes, a PD-ratio greater than unity is obtained.

In addition to the above critique, the authors of [21] pointed out that the classical PD-ratio, as defined in Eq. 1.1, is conceptually ill defined. First of all, the changes in the different responses in the PD-ratio are experimentally obtained by extrapolating the properties from glass and liquid values respectively, to a temperature, T_g, which is not rigorously defined. Second, the glass phase is not well defined either - it is aging, in principal making the glass properties time dependent. These two points, led the authors to the conclusion that instead of the classical PD-ratio, in order to make the problem well defined, one should consider a version of Π suggested by [22, 23], which refers to the linear responses in the equilibrium viscous liquid phase. The constitutive parameters are in general complex frequency dependent functions, and using the low- ($\omega \to 0$) and high- ($\omega \to \infty$) frequency limits of the response, the *linear* PD-ratio, Π_{Tp}^{lin} can be calculated:

$$\Pi_{Tp}^{lin} = \frac{\left[c_p\left(\omega \to 0\right) - c_p\left(\omega \to \infty\right)\right]\left[\kappa_T\left(\omega \to 0\right) - \kappa_T\left(\omega \to \infty\right)\right]}{T\left[\alpha_p\left(\omega \to 0\right) - \alpha_p\left(\omega \to \infty\right)\right]^2}. \tag{1.2}$$

The indecis in the PD-ratio given by Eq. 1.2 refers to a situation where you control temperature T and pressure P. The linear PD-ratio is unity if there is just a single internal parameter controlling the relaxation, while greater otherwise. Even though the linear PD-ratio constitutes a rigorously well defined quantity, the experimental determination of the involved constitutive parameters is difficult. First of all it requires measurements over a wide frequency range, and to my knowledge, a complete set of the three required frequency-dependent thermoviscoelastic linear-response functions, has not yet been measured. Furthermore, as pointed out in [25, 26], even the isobaric specific heat, $c_p(\omega)$ has not yet been measured reliably. Instead conventional methods measure another quantity, the *longitudinal* specific heat $c_l(\omega)$. In fact, Part I of this thesis, presents a new phenomenon which is a direct consequence of the difference between the longitudinal and isobaric specific heats.

In order to find a way to test "single parameterness", [24] suggested a "one-frequency" test, where the values of the imaginary parts from a complete set of frequency-dependent thermoviscoelastic linear-response functions, can be combined into a *dynamic* PD-ratio, $\Lambda_{XY}\left(\omega\right)$, where the indecis denotes the two variables one is controlling in experiment. If for example, the control variables are entropy (heat) and pressure, at a given temperature T, the dynamic PD-ratio reads [24]

$$\Lambda_{sp}(\omega) = -\frac{\left({}^{T}/_{c_p}(\omega)\right)'' \kappa_s''(\omega)}{\left[\left({}^{1}/_{\beta_s}(\omega)\right)''\right]^2}, \tag{1.3}$$

where $c_p''(\omega)$, $\kappa_s''(\omega)$ and $\beta_s''(\omega)$ are the imaginary parts of isobaric specific heat, adiabatic compressibility and adiabatic pressure coefficient respectively. Ellegard et. al. [24] show that if a single internal parameter contols the structural relaxation, then the dynamic PD-ratio is unity:

Consider the case of a thermovicoelastic experiment where you perturb a system with periodically varying input of heat (per unit volume) δs and pressure δp. Assuming the structural relaxation is given by a single internal parameter $\delta\varepsilon$, the response matrix relating the complex amplitudes of temperature δT and volume response per unit volume δv to the input variables is given by

$$\begin{aligned} \delta T &= \gamma_1 \delta\varepsilon + J_{11}^{\infty}\delta s - J_{12}^{\infty}\delta p & (1.4)\\ -\delta v &= \gamma_2 \delta\varepsilon + J_{21}^{\infty}\delta s - J_{22}^{\infty}\delta p. & (1.5) \end{aligned}$$

where the J_{ij}^{∞} are real numbers giving the instantaneous response to the input fields. If pressure does not vary, $\delta p = 0$, then

$$\frac{T}{c_p} \equiv \left(\frac{\delta T}{\delta s}\right)_p = \gamma_1 \left(\frac{\delta\varepsilon}{\delta s}\right)_p + J_{11}^{\infty}, \tag{1.6}$$

and likewise

$$-\frac{1}{\beta_S} \equiv \left(\frac{-\delta V}{\delta s}\right)_p = \gamma_2 \left(\frac{\delta\varepsilon}{\delta s}\right)_p + J_{21}^{\infty}. \tag{1.7}$$

Since the J_{ij}^{∞}'s are real numbers we get

$$\frac{\gamma_1}{\gamma_2} = \frac{\left({}^{T_0}/_{c_p}\right)''}{\left({}^{1}/_{\beta_S}\right)''}. \tag{1.8}$$

On the other hand, if $\delta s = 0$, we have

$$\frac{1}{\beta_S} = \left(\frac{\delta T}{\delta p}\right)_S = \gamma_1 \left(\frac{\delta\varepsilon}{\delta p}\right)_S - J_{21}^{\infty}, \tag{1.9}$$

and

$$\kappa_S \equiv \left(\frac{-\delta V}{\delta p}\right)_S = \gamma_2 \left(\frac{\delta\varepsilon}{\delta p}\right)_S - J_{22}^{\infty}, \tag{1.10}$$

Again, the glass response is a given by real numbers and we get

$$\frac{\gamma_2}{\gamma_1} = \frac{(\kappa_S)''}{(1/\beta_S)''}. \tag{1.11}$$

Multiplying Eq. 1.8 with Eq. 1.11 we get the dynamic PD-ratio equal to unity.

1.0.1 Strongly Correlating Liquids (SCL) - approximately single internal parameter liquids

An example of a liquids where the dynamic PD-ratio is close to unity is given by the class of liquids discussed in a number of papers published by members of the Glass and Time group, at Roskilde liquid University (see for example [27] or companion Paper C.2). These liquids are termed "strongly correlating liquids", a term refering to the strong correlations exhibited between their constant-volume equilibrium fluctuations of the potential energy U and virial $W \equiv -1/3 \sum_i \boldsymbol{r}_i \cdot \boldsymbol{\nabla}_{\boldsymbol{r}_i} U(\boldsymbol{r}_1, \ldots, \boldsymbol{r}_N)$, where $\boldsymbol{r}_i$ is the position of particle i. Recall that, if p is the pressure, V the volume, N the number of particles, and T the temperature, the average virial $\langle W \rangle$ gives the configurational contribution to the pressure [28]:

$$pV = Nk_BT + \langle W \rangle. \tag{1.12}$$

If Δ denotes the instantaneous deviations from equilibrium mean values, the WU correlation is quantified by the correlation coefficient R defined by

$$R \equiv \frac{\langle \Delta W \Delta U \rangle}{\sqrt{\langle (\Delta W)^2 \rangle \langle (\Delta U)^2 \rangle}} \tag{1.13}$$

Perfect correlation gives $R = 1$; strongly correlating liquids are defined [27] by $R \geq 0.9$ for fluctuations monitored in the NVT ensemble, i.e., at constant volume and temperature. In the Ph.D. thesis of Ulf R. Pedersen [29] and in [24] it was shown that a perfectly correlating liquid is described by a single internal parameter. If the correlations are "just" strong, the correlation coefficient R is, to a good approximation given by the (VT) version of the PD-ratio (see for example [29]), i.e.,

$$R_{WU} \simeq \frac{1}{\sqrt{\Pi_{VT}^{lin}}}. \tag{1.14}$$

The simulations of Reference 1 in companion Paper C.2 showed that van der Waals type liquids and metallic liquids are generally strongly correlating, whereas in contrast, liquids composed of molecules whose interactions have competing or directional interactions are generally not strongly correlating. The latter classes of liquids include the hydrogen-bonded liquids, the covalently bonded liquids, and the (strongly) ionic liquids. With these findings in mind, and the relation suggested by Eq. 1.14, you thus have an indication of which kind of liquids that are good candidates for being approximate single internal parameter liquids. The choise of liquid in Part II of this thesis was guided by the above observations, and the fact that it is a van der Waals type liquid.

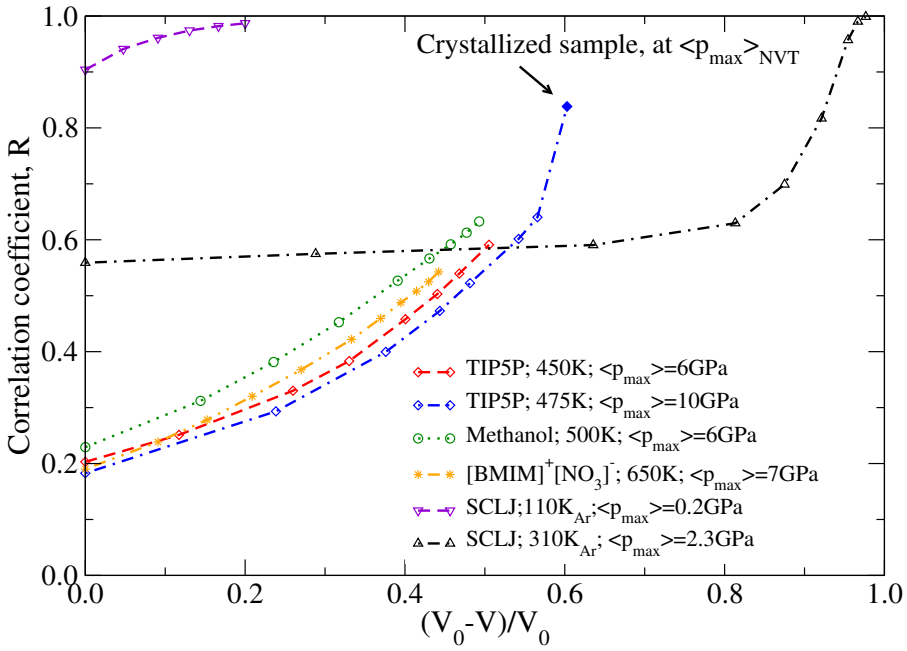

Figure 1.2 The correlation coefficient R plotted against the volume decrease relative to the volume V0 at the lowest pressure of the given isotherm. Data were taken from 10 ns of simulations of each liquid. The higher density isotherm (450 K) of TIP5P water shows stronger correlation than its less dense counterpart (475 K) at the same pressure.

A final remark to be made on the strongly correlating liquids is the following. The range of papers refered to in Reference 1 of companion Paper C.2 indicated that the correlation coefficient R tends to increase at increasing pressure, but no systematic studies had been carried out of the effect of pressure on the correlation. The question whether all liquids become strongly correlating at sufficiently large pressure was studied in companion Paper C.2.

Figure 1.2 shows the the correlation coefficient as a function of volume decrease relative to the volume V_0 at the lowest pressure of a given isotherm. Given the relation between the correlation coefficient and the linear PD-ratio, that figure indicates an increasing number of constraints on the internal parameters [30]. Extrapolated to even higher pressures (if crystallization is avoided) one could then speculate that a single internal parameter description becomes valid, in all types of systems, regardless of competing interactions or directional bonding.

Bibliography

[1] F. Simon and F. Lange. On the question of entropy of amorphic substances. *ZEITSCHRIFT FUR PHYSIK*, 38:227–236, 1926.

[2] G. Adams and J. H. Gibbs. On the temperature dependence of cooperative relaxation properties in glass-forming liquids. *Journal of Chemical Physics*, 43(1):139–146, 1965.

[3] F. H. Stillinger and P. G. Debenedetti. The Kauzmann paradox revisited. *Journal of Physical Chemistry B*, 105:11809–11816, 2001.

[4] I. Prigogine and R. Defay. *Chemical Thermodynamics*. Longmans, London, 1954.

[5] R. O. Davies and G. O. Jones. The irreversible approach to equilibrium in glasses. *Proc. R. Soc.*, 217:26, 1952.

[6] R. O. Davies and G. O. Jones. Thermodynamic and kinetic properties of glasses. *Adv. Phys.*, 2:370, 1953.

[7] M. Goldstein. 39:3369, 1963.

[8] M. Goldstein. *J. Phys. Chem.*, 77:667, 1973.

[9] P. K. Gupta and C. T. Moynihan. Prigogine-defay ratio for systems with more than one order parameter. *Journal of Chemical Physics*, 65(10):4136, 1976.

[10] Th. de Donder and P. van Rysselberghe. *Thermodynamic Theory of Affinity*. Stanford University Press, Stanford, 1936.

[11] E. A. DiMarzio. *J. Appl. Phys.*, 45:4143, 1974.

[12] E. A. DiMarzio. Comments on a paper entitled: "prigogine-defay ratio for systems with more than one order parameter". *J. Chem. Phys.*, 67(5):2393, 1977.

[13] P. K. Gupta and C. T. Moynihan. Reply to dimarzio's comments. *J. Chem. Phys.*, 67(5):2395, 1977.

[14] M. Goldstein. *Macromolecules*, 10(6):1407, 1977.

[15] E. A. DiMarzio. Some insights into the order parameter theory of glasses. a response to a comment by goldstein. *Macromolecules*, 10(6):1407, 1977.

[16] S. Brawer. *Relaxation in Viscous Liquids and Glasses*. Columbus OH: American Ceramic Society, 1985.

[17] G. W. Scherer. Volume relaxation far from equilibrium. *Journal of American Ceramic Society*, 69:374–381, 1986.

[18] I. Gutzow and J. Schmelzer. *The vitreous state: Thermodynamics, Structure, Rheology, and Crystallization*. Springer, Berlin, 1995.

[19] P. K. Gupta and J. W. Haus. The prigogine-defay ratio for inhomogeneous systems with a single internal parameter. *Journal of Non-Crystalline Solids*, 24:291–295, 1977.

[20] J. W. P. Schmelzer and I. Gutzow. The prigogine-defay ratio revisited. *J. Chem. Phys.*, 125:184511, 2006.

[21] N. P. Bailey, T. Christensen, B. Jakobsen, K. Niss, N. B. Olsen, U. R. Pedersen, T. B. Scrøder, and J. C. Dyre. Glass-forming liquids: one or more 'order' parameters? *Journal of Physics: Condensed Matter*, 20:244113, 2008.

[22] R. J. Roe. Thermodynamics of glassy state with multiple order parameters. *J. Appl. Phys.*, 48:4085, 1977.

[23] C. T. Moynihan and P. K. Gupta. Order parameter model for structural relaxation in glass. *J. Non-Cryst. Solids*, 29:143, 1978.

[24] N. L. Ellegaard, T. Christensen, P. V. Christiansen, N. B. Olsen, U. R. Pedersen, T. B. Schröder, and J. C. Dyre. Single-order-parameter description of glass-forming liquids: A one-frequency test. *Journal of Chemical Physics*, 126:074502, 2007.

[25] T. Christensen, N. B. Olsen, and J. C. Dyre. Conventional methods fail to measure $c_p(\omega)$ of glass-forming liquids. *Physical Review E*, 75:041502, 2007.

[26] T. Christensen and J. C. Dyre. Solution of the spherically symmetric linear thermoviscoelastic problem in the inertia-free limit. *Physical Review E*, 78:021501, 2008.

[27] U. R. Pedersen, T. Christensen, T. B. Schøder, and J. C. Dyre. Feasibility of a single-parameter description of equilibrium viscous liquid dynamics. *Physcial Review E*, 77:011201, 2008.

[28] M. P. Allen and D. J. Tildesley. *Computer Simulation of Liquids*. Oxford University Press, 1987.

[29] U. R. Pedersen. *Long-time simulations of viscous liquids - from strong correlations to crystallization*. PhD thesis, Roskilde University, 2009.

[30] M. Goldstein. volume 3. Butterworths Scientific, London, 1964.

Part I

Cooling by heating

2 Introduction

This part of the thesis concerns a little known and until now poorly understood phenomenon of thermoelasticity; as you transfer heat from the surroundings into a spherical system through its boundary, the temperature initially decreases in its interior - I call it *cooling by heating* (or heating by cooling). In my view it constitutes an amazing example of how theories, as well established as the theory of thermoelasticity, can reveal new interesting phenomena. Historically, thermoviscoelasticity is an important engineering subject, as it is of paramount importance in the design of knew products, that one is able to model and predict the thermoelastic behavior of the product, before investing huge amounts of money to build the first prototype. In fact there is even a specialized journal called "Journal of thermal stresses" whose emphasis "*is placed on new developments in thermoelasticity, thermoplasticity, and theory and applications of thermal stresses.*" [1]. In this light it might seem strange that a counter-intuitive phenomenon like cooling by heating has not been exposed to much attention. The reason for this is probably related to the fact that it is a signature of a subtle thermo(visco)elastic coupling that is highly suppressed, except for in the highly viscous state of a liquid close to the glass transition.

Until now I have only encountered two works dealing with phenomena that could be related to the effect discussed here. The first is a publication [2] whose authors are heating one end (50mm) of a 310mm long copper bar with a cross section of 5mm$\times$5mm by placing it into an oven raising the temperature to 150℃. To measure the temperature of the cold end they use a chromel-alumel thermocouple, of diameter 0.1mm. When steady state is achieved the cold end of the bar has a temperature of 75℃, after which they remove the hot end from the oven and shortly hereafter submerge it in room temperature water of depth 70mm. The transient temperature distribution in the cold end was recorded using a chart recorder, and temperature measurement error was estimated to be about $\pm$0.5℃. What they found is shown in figure 2.1. As the hot end of the bar is submerged in the room temperature water (indicated by the arrow) the temperature of the cold end initially (at about 1sec) decreases about 1℃, after which the temperature increases with about 4℃.

The authors offer the following explanation:

"*The sudden cooling of the hot end causes it to contract rapidly. This contraction produces an elastic wave which propagates towards the cold end. This wave, under certain conditions, may trigger the sequence of events described in [Aleshin, G.Ya., Int. Comm. Heat and Mass Transfer, v.24, No 4, pp.497-505 (1997)], which are responsible for the release of energy in the media. Consequently, the reported experimental results*

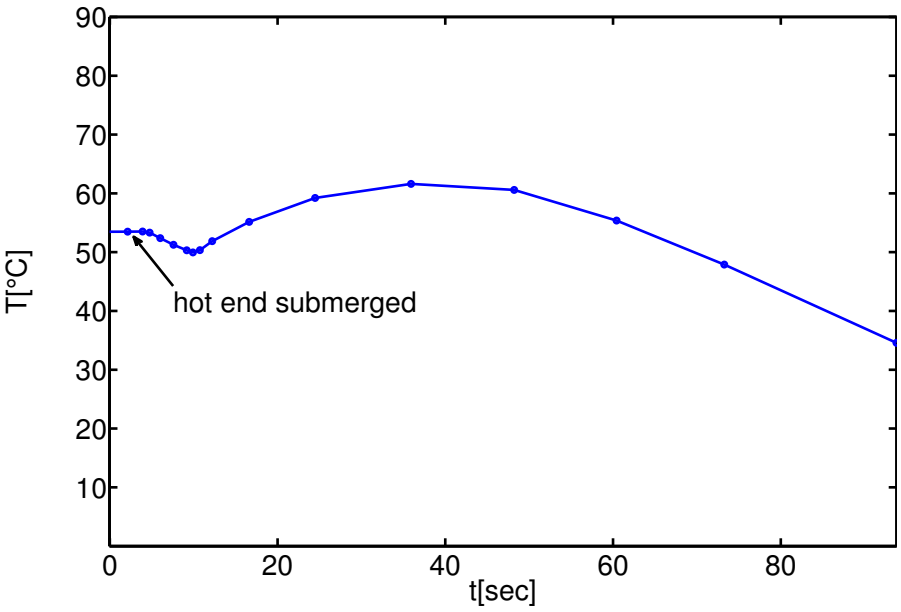

Figure 2.1 Transient temperature response of a copper bar's cold end as its hot end is rapidly cooled. The arrow indicates the point in time when the hot end is submerged in room temperature water. Data taken from [2].

corroborate the working hypothesis of a "steam explosion".".

The reference they invoke in [2] concerns a hypothesis regarding an explanation of a process called a "steam explosion" in an ionic liquid. In essence, it suggests that the interaction of a water jet with a melt inside a cylindrical vessel produces elastic waves which propagates within the melt. This triggers phase transitions (crystallization) and energy redistribution (uptake of heat from the vessel) with the final stage being a sudden release of energy (explosion) after the elastic wave is reflects at the end of the vessel and moving back with a phase shift, causing violent cooling [3].
The aim in [2] is then to examine if a release of energy, similar to that described in [3] can be observed in other states of matter, such as a solid rod (of copper), if an elastic wave could be generated within the solid media - thus indicating a structural phase transition in the solid body.

The second encounter with a phenomenon like cooling by heating was in my master's thesis [4]. The aim was to use in-house equipment - the piezoelectric bulk modulus gauge (PBG), which is described in chapter 7, in a new way. The PBG is basically a piezoelectric spherical shell polarized in the radial direction and coated on both sides with electrodes thus acting as a capacitor. Normally an alternating electric field is applied resulting in deformation of the ceramic, thus changing the volume inside the shell. A liquid is introduced inside the shell, and opposes the deformation of the ceramic, thus changing the measured capacitance. Comparing to the capacitance measured on the empty shell, you can deduce the adiabatic bulk modulus of the liquid. A very nice and exhaustive documentation of this use of the PBG is given in the Ph.D-thesis [5] of

Tina Hecksher.
The novelty in the approach of my master's thesis was to use the pyroelectric nature of the ceramic in the PBG. Instead of applying an alternating electric field to the liquid filled PBG shell, a temperature step was made with the cryostat in which the PBG is inserted. The capacitance was then measured and the data was analyzed with the objective to deduce the pressure coefficient. In the process of modeling the thermo-viscoelastic behavior of the liquid and the interaction with the ceramic, we solved the coupled thermoviscoelastic equations numerically. The resulting temperature profile we obtained is shown in figure 2.2.

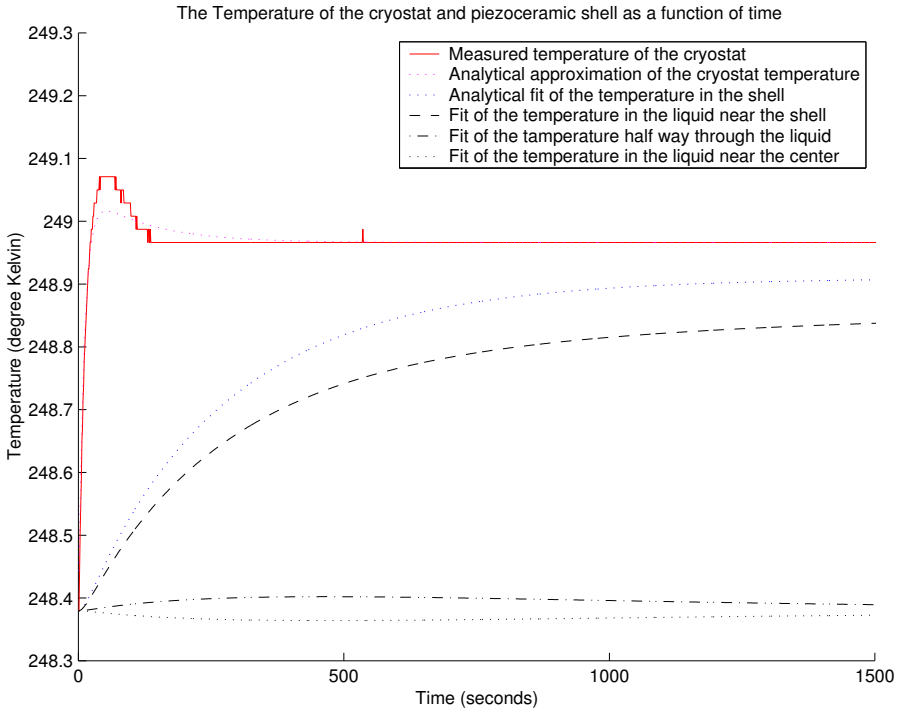

Figure 2.2 The temperature evolution of the shell and different regions of the liquid after a temperature rise from 248 K to 249 K.

In my thesis we made the following comment to figure 2.2:
"*In that figure it is illustrated how the very low diffusivity of the liquid will inhibit heat to even reach the center of the sphere in the time frame of the measurement, instead temperature changes according to the mechanical pressure changes that travel much faster than the heat.*"

The comment is referring to the last curve in 2.2 showing the temperature evolution close to the center of the sphere. Our only explanation was that as heat is added at the surface of the PBG the temperature drops in the center of the sphere due to a thermoelastic effect. At that point we did not explore this further, as it was not possible for us to actually measure the temperature inside the PBG. In fact, at that time, we did ascribe the effect to numerical artifacts, and it was only later that Nils Boye Olsen pointed out that there might be more to it than just numerical problems. Tage

Christensen, presented to this finding, suggested that the effect might even be present in the absence of the PBG. This is the actual topic of this part of the thesis.

Before I go into the details of the phenomenon, I will make a last detour to literature. It concerns the work of my supervisor in the two papers [6, 7] in which he and his coauthors, Jeppe Dyre and Niels Boye Olsen, investigate the implications of thermoelastic coupling in the determination of the frequency dependent specific heat in thermal effusion methods. Their conclusion is:

By solving the full one-dimensional thermoviscoelastic problem analytically it is shown that, because of thermal expansion and the fact that mechanical stresses relax on the same time scale as the enthalpy relaxes, the plane thermal-wave method does not measure the isobaric frequency-dependent specific heat $c_p(\omega)$. This method rather measures a "longitudinal" frequency-dependent specific heat, a quantity defined and detailed here that is in between $c_p(\omega)$ and $c_V(\omega)$. This result means that no reliable wide-frequency measurements of $c_p(\omega)$ on liquids approaching the calorimetric glass transition exist[6].

In the second paper [7] they deduce the solution to the full thermoviscoelastic spherically symmetric problem in terms of the transfer matrix formalism [8]. My modeling is based on this solution, and in fact the modeling described in part II of this thesis, where I measure a complete set of thermoviscoelastc constitutive quantities, is also based on the the work done in [7].

The conclusion in [6, 7] is clear: Measuring the isobaric frequency-dependent specific heat over a large frequency range of a liquid approaching its calorimetric glass transition is not that easy, in fact what is measured is another quantity - the longitudinal specific heat (defined in next chapter), which may differ dynamically from the isobaric specific heat. For now I will just point out that the longitudinal specific heat reflects the fact that the experimental conditions restricts the thermal expansion to take place in one direction only (e.g. the radial direction). What is not clear from the analysis in [6, 7] is: To what extent do the isobaric- and longitudinal specific heats differ? In the following I show that the phenomenon of cooling by heating is a direct consequence of the difference between the two specific heats, as it can only be present when the two specific heats differ.

3 Theoretical investigation of a thermoviscoelastic effect

Studying our problem basically comes down to accounting for the coupling of scalar quantities; pressure, volume, entropy and temperature, as well as the coupling between the traceless parts of stress and strain with temperature through some constitutive relation. In appendix A I have derived the equations that describe the time evolution of the displacement field and temperature. The result is stated in Eq. 3.1 which basically is newtons second law applied on an infinitesimal volume, and Eq. 3.2 which describes the diffusion of heat.

$$M_T \boldsymbol{\nabla}(\boldsymbol{\nabla} \cdot \mathbf{u}) - G\boldsymbol{\nabla} \times (\boldsymbol{\nabla} \times \mathbf{u}) - \beta_V \boldsymbol{\nabla}\delta T = \rho_0 \frac{\partial^2 \mathbf{u}}{\partial t^2}, \tag{3.1}$$

$$c_V \frac{\partial \delta T}{\partial t} + T_0 \beta_V \frac{\partial}{\partial t}(\boldsymbol{\nabla} \cdot \mathbf{u}) = \lambda \boldsymbol{\nabla}^2 \delta T. \tag{3.2}$$

Here ρ_0 denotes the average mass density, while the deviations from equilibrium are given by the displacement field $\boldsymbol{u}(\boldsymbol{r}, t)$ and temperature $\delta T(\boldsymbol{r}, t) = T(\mathbf{r}, t) - T_0$. The longitudinal modulus is given by $M_T = K_T + \frac{4}{3}G$, where G is the shearmodulus and $K_T \equiv -V\left(\frac{\partial p}{\partial V}\right)_T$ is the isothermal bulk modulus. The coupling between the two equations is given by the isochoric pressure coefficient $\beta_V = \alpha_p K_T$ with $\alpha_p \equiv \frac{1}{V}\left(\frac{\partial V}{\partial T}\right)_p$ being the isobaric expansion coefficient coefficient. λ is the heat conductivity as defined by Fourier's law and $c_V \equiv \frac{T}{V}\left(\frac{\partial S}{\partial T}\right)_V$ is the isochoric specific heat per volume .

In the rest of this chapter I will only be concerned with the limit where I ignore acoustic waves - the inertia-free limit, where accelerations are so small they can be ignored, i.e., when the wavelength, $1/\omega$ is much larger than the size of the sample (at the frequencies of interest). Taking the speed of sound to be $3 \cdot 10^3$m/s, then for a spherical sample of diameter of 10^{-2}m, the typical acoustic frequency will be situated in the kilohertz regime. For lower frequencies it is therefor safe to assume that only thermal waves are present and quasi-static elastic conditions to apply. Eq's 3.1 and 3.2 are then reduced to

$$M_T \boldsymbol{\nabla}(\boldsymbol{\nabla} \cdot \mathbf{u}) - G\boldsymbol{\nabla} \times (\boldsymbol{\nabla} \times \mathbf{u}) - \beta_V \boldsymbol{\nabla}\delta T = 0, \tag{3.3}$$

$$c_V \frac{\partial \delta T}{\partial t} + T_0 \beta_V \frac{\partial}{\partial t}(\boldsymbol{\nabla} \cdot \mathbf{u}) = \lambda \boldsymbol{\nabla}^2 \delta T. \tag{3.4}$$

3.1 Some general observations

What kind of information can be extracted by looking at Eq's. 3.3 and 3.4. First of all, as mentioned above, the two equations couple whenever the expansion coefficient is non-zero, i.e. the temperature distribution depends on the state of deformation. For example, if the expansion coefficient is zero, $\alpha_p = 0$, Eq. 3.1 reduces to the ordinary elastic equation and Eq. 3.2 reduces to the isochoric version of the heat equation. On the other hand, if for some reason, pressure is constant, (trace of stress tensor equal to zero), Eq. A.23, which relates the relative volume change $\frac{\delta V}{V_0} = \boldsymbol{\nabla} \cdot \mathbf{u}$ to pressure and temperature,

$$\boldsymbol{\nabla} \cdot \mathbf{u} = -\frac{1}{K_T}\delta p + \alpha_p \delta T. \tag{3.5}$$

is simplified since now the first term on the right hand side vanishes. Combining this with a thermodynamic identity $T_0 \beta_V \alpha_p = (c_p - c_V)$, Eq. 3.4 reduces to the heat equation under isobaric conditions

$$\frac{\partial \delta T}{\partial t} = \frac{\lambda}{c_p}\boldsymbol{\nabla}^2 \delta T. \tag{3.6}$$

Now you might ask: When is it the case that isobaric conditions apply, or, how does the mechanical boundary conditions come into play? To answer this we consider the case where the shear modulus is zero, $G = 0$, as in a liquid at zero frequency (or high temperature). The Duhamel-Neumanns relation, Eq. A.30 reads, where δ_{ij} is the Kronecker delta,

$$\sigma_{ij} = K_T \boldsymbol{\nabla} \cdot \mathbf{u}\delta_{ij} + 2G\left(\varepsilon_{ij} - \frac{1}{3}\boldsymbol{\nabla} \cdot \mathbf{u}\delta_{ij}\right) - \beta_V \delta T \delta_{ij}. \tag{3.7}$$

If $G = 0$ and you impose a stress-free boundary condition, $\sum_j \sigma_{ij} n_j = 0$ where n_j is a unit normal vector, then Eq. 3.7 gives, on the boundary, that $0 = \sum_j \sigma_{ij} n_j = (K_T \boldsymbol{\nabla} \cdot \mathbf{u} - \beta_V \delta T)\, n_i$. Since this is valid for all n_i, you have that on the boundary

$$\boldsymbol{\nabla} \cdot \mathbf{u} - \alpha_p \delta T = 0. \tag{3.8}$$

This is then used to determine the (time dependent) integrationconstant $b(t)$ that comes out of integration of Eq. 3.3 (with $G = 0$):

$$b(t) = \boldsymbol{\nabla} \cdot \mathbf{u} - \alpha_p \delta T = 0. \tag{3.9}$$

This is valid for all $\boldsymbol{r}$. Substituting $\boldsymbol{\nabla} \cdot \mathbf{u} = \alpha_p \delta T$ into Eq. 3.4 you again obtain Eq. 3.6. This is a result valid in general, that is, if the shear modulus is zero, then for a mechanically non-clamped boundary, isobaric (and of course hydrostatic) conditions apply. This means you can use the "isobaric" version of the heat diffusion equation in the description of temperature. This is not the case when the shear modulus is non-zero, as discussed in [6, 7], and we will see, exotic phenomena may follow due to the subtle thermomechanical coupling that arise with a non-zero shear modulus.

3.2 The spherically symmetric case

The spherically symmetric case, which constitutes a simple case, both computationally and experimentally, is obtained when you perturb a spherical system uniformly at the boundary. In this case the displacement field becomes a function of radius and time only: $\mathbf{u} = u(r,t)\mathbf{r}$. This means that the curl of the displacement field becomes zero, $\boldsymbol{\nabla} \times \mathbf{u} = 0$, and Eq. 3.3 reduces to

$$\boldsymbol{\nabla} \left(M_T \boldsymbol{\nabla} \cdot \mathbf{u} - \beta_V \delta T \right) = 0. \tag{3.10}$$

This can again be integrated to give

$$M_T \boldsymbol{\nabla} \cdot \mathbf{u} - \beta_V \delta T = b(t). \tag{3.11}$$

Expressing the rr-component of stress in terms of Duhamel-Neumanns relation, Eq. 3.7 (now $G \neq 0$), you get, after some rearranging, that

$$\sigma_{rr} = M_T \boldsymbol{\nabla} \cdot \mathbf{u} - \frac{4G}{3} \frac{u}{r} - \beta_V \delta T. \tag{3.12}$$

If the boundary of the sphere is mechanically non-clamped, i.e. at radius R, $\sigma_{rr}(R,t) = 0$, then, combining the boundary condition with Eq. 3.12 you find that the unknown constant $b(t)$ is given by

$$b(t) = \frac{4}{3} G \frac{u(R,t)}{R}. \tag{3.13}$$

That is, the relative volume change is given by

$$\boldsymbol{\nabla} \cdot \mathbf{u}(r,t) = \frac{\beta_V}{M_T} \delta T(r,t) + \frac{4}{3} \frac{G}{M_T} \frac{u(R,t)}{R}. \tag{3.14}$$

The change in volume of an infinitesimal region in the sphere thus depends on the temperature, *locally*, and the amount of displacement of the surface of the sphere.

Likewise, the component of stress, $\sigma_{rr}(r,t)$ is easily found to be given by the difference of the local displacement and the displacement of the surface:

$$\sigma_{rr}(r,t) = \frac{4}{3} G \left(\frac{u(R,t)}{R} - \frac{u(r,t)}{r} \right). \tag{3.15}$$

That is, if the shear modulus is non-zero, the "radial" component of pressure, σ_{rr} may vary, even when the surface of the sphere is mechanically non-clamped. This means that the thermodynamic pressure may also vary, and isobaric conditions could be violated. If on the other hand, $G = 0$, then the pressure doesn't change, and isobaric conditions apply, as argued above in section 3.1. So, mechanically, the shear modulus determines the local state of deformation, but if you turn to thermal quantities, a more subtle relation appears.

The change in entropy in an infinitesimal region, which is given by

$$\delta S = \frac{c_V}{T_0}\delta T + \beta_V \boldsymbol{\nabla}\cdot\mathbf{u}, \tag{3.16}$$

can also be expressed in terms of $b(t)$. Substituting 3.14 in Eq. 3.16 gives

$$\delta S(r,t) = \frac{c_l}{T_0}\delta T(r,t) + \frac{4}{3}\frac{G}{M_T}\frac{u(R,t)}{R}\beta_V. \tag{3.17}$$

Here a knew quantity enters: the *longitudinal* specific heat, defined as

$$c_l = c_V + T_0\frac{\beta_V^2}{M_T}. \tag{3.18}$$

Two conclusions can be drawn. First of all, if the expansion coefficient is zero, i.e. $\beta_V = \alpha_p K_T = 0$, then isochoric conditions apply, as argued in the section above (3.1). Second, if the expansion coefficient is non-zero, then it is the vanishing (or not) of the shear modulus that becomes decisive. So if the expansion coefficient is non-zero but the shear modulus vanishes, then, through the thermodynamic relation $T_0\beta_V\alpha_p = c_p - c_V$, isobaric conditions apply. If both expansion coefficient and shear modulus is non-vanishing, Eq. 3.17 tells us that if the surface of the sphere is displaced outwards (due to thermal expansion) and at the same time no heat is transported into a region, i.e., $\delta S = 0$, then temperature of that region decreases adiabatically. This provides the physical understanding of the phenomenon cooling by heating. When the mechanically non-clamped surface of a sphere is heated, it expands, causing an adiabatic cooling of the interior of the sphere.

The fact that the longitudinal specific heat enters, represents the longitudinal character of expansion that is imposed by the geometry of the problem. Finally this is carried on to the description of temperature; substituting Eq. 3.11 into Eq. 3.4 gives the following heat diffusion equation, which involves the longitudinal specific heat.

$$c_l\frac{\partial\delta T}{\partial t} + T_0\beta_V\frac{\partial}{\partial t}\left(b(t)\right) = \lambda\boldsymbol{\nabla}^2\delta T. \tag{3.19}$$

In terms of the adiabatic and isothermal longitudinal moduli $M_S = K_S + 4/3\,G$ and $M_T = K_T + 4/3\,G$, the longitudinal specific heat may be expressed by [7]

$$c_l = \frac{M_S}{M_T}c_V \tag{3.20}$$

This should be compared to the well known relation

$$c_p = \frac{K_S}{K_T}c_V \tag{3.21}$$

A difference between c_l and c_p only occurs when two conditions are met simultaneously. First, shear modulus should be non-vanishing compared to bulk modulus and second, the adiabatic and isothermal bulk moduli should differ significantly. The effect may be dynamic since shear modulus near the glass transition increases with frequency.

As argued above the difference between the c_p and c_l expresses a subtle thermomechanical coupling as compared to the coupling that is trivially present when the expansion coefficient differs from zero. The relative difference between c_p and c_v is given by the identity

$$a \equiv \frac{c_p - c_V}{c_p} = \frac{T_0 \alpha_p^2 K_T}{c_p}. \tag{3.22}$$

Combining Eq's. (3.20) and (3.21) gives the longitudinal coupling constant a_l defined as

$$a_l \equiv \frac{c_p - c_l}{c_p} = \frac{4}{3} \cdot \frac{G}{M_T} \cdot a \tag{3.23}$$

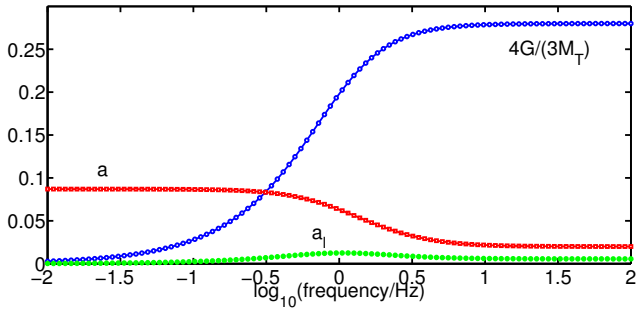

Figure 3.1 Sketch of the two factors in the definition of c_l. The curves show the absolute values.

It follows from Eq. (3.23) that $|a_l| \leq 1$. Also, note that even if the trivial coupling is present ($a \neq 0$) one can still have an $a_l = 0$ if the ratio between the moduli in Eq. (3.23) is vanishing. In the glass transition region where upon increasing frequency the first factor $[G/M_T]$ increases while the second $[(c_p - c_v)/c_p]$ decreases. As I will show later (section 3.4) modeling suggests that exactly in the glass transition region the coupling constant becomes large. Still, it is in general not clear how the different quantities compare, a situation that is illustrated in the *sketch* in Figure 3.1. To set the levels I used Glucose data for the isobaric specific heat, isothermal compressibility, and isobaric expansion coefficient taken from Davies and Jones [9] and Shear modulus data from [10]. Davies and Jones however notes that the data, being sparse, is collected from the work of different groups, and are probably encumbered with large error. In [7] the authors estimate the size of the coupling constant in Glycerol and they reach an upper bound on a_l of as much as 0.15. That is the isobaric and longitudinal specific heat may differ up to 15%. In any case, experimental data to produce a plot like the one in Figure 3.1, would require the measurement of a complete set of thermoviscoelastic response functions, as well as the shear modulus. This is not a simple task at all (see Part II of this thesis), and it would be preferable to have another method to asses the difference between the two specific heats. To investigate this further I will model a simple (ideal) experimental situation. This is done in the following section.

3.3 Thermoelastic problem illustrating the difference between c_l and c_p: Heat supplied at mechanically free boundary

Consider the case when a periodically varying heat $\delta Q(t) = \mathbf{Re}\left\{\delta Q e^{i\omega t}\right\}$ is supplied at the surface of a massive sphere of radius R. The surface is assumed to be mechanically non-clamped, i.e., the sphere is free to expand. This translates into the boundary condition that the rr-component of the stress tensor is zero at the surface at all times, $\sigma_{rr}(R,t) = 0$. We wish to calculate how temperature and displacement fields vary throughout the sphere, i.e., to calculate the complex amplitudes of temperature $\delta T(r)$ and radial displacement field $u(r)$, from which the stress components σ_{rr}, etc, may be calculated.

Denote the cyclic angular frequency by ω, and assume a heat conductivity λ that is not dependent on frequency. Denote the complex frequency-dependent isothermal bulk and shear moduli by $K_T(\omega)$ and $G(\omega)$, the complex frequency-dependent isobaric thermal expansion coefficient and isochoric specific heat by $\alpha_p(\omega)$ and $c_V(\omega)$. Then Eq.'s 3.3 and 3.4 become the fundamental coupled thermoviscoelastic equations to be solved are in the inertia-free limit [7].

$$\boldsymbol{\nabla}\left(\left(K_T(\omega)+\frac{4}{3}G(\omega)\right)\boldsymbol{\nabla}\cdot\mathbf{u}-\alpha_p(\omega)K_T(\omega)\delta T\right) = 0 \tag{3.24}$$

$$(i\omega)c_V(\omega)\delta T+(i\omega)T_0\alpha_p(\omega)K_T(\omega)\boldsymbol{\nabla}\cdot\mathbf{u}-\lambda\nabla^2\delta T = 0\,. \tag{3.25}$$

Here δT and u are the complex frequency- and radius-dependent amplitudes of the periodic variations of temperature and displacement field, respectively. The boundary conditions of the problem are:

1. No displacement at the center: $u(0) = 0$
2. No temperature gradient at the center: $\frac{\partial \delta T}{\partial r}(0) = 0$
3. No radial stresses at the surface: $\sigma_{rr}(R) = 0$
4. The heat supply boundary condition at the surface: $\lambda\frac{\partial \delta T}{\partial r}(R) = i\omega\frac{\delta Q}{4\pi R^2}$

Dropping for simplicity the explicit indication of frequency dependence, the solutions to Eq.'s. (3.24) and (3.25) can be found by using the transfer matrix formulation [7] of the general solution of the thermoviscoelastic problem in a spherically symmetric case. Including the radial stress field and the time-integrated heat-current density that are related to the temperature and displacement fields, the authors of [7] end up with an inhomogeneous system of four ordinary differential equations to solve. The solution is summarized in the general form of a transfer matrix $\mathbf{T}(r_j, r_i)$ that links the dimensionless complex amplitudes of the fields at the boundaries r_i with those at r_j:

$$\begin{pmatrix}\delta p_r\\ \delta T\\ \delta V\\ \delta S\end{pmatrix}_j = \mathbf{T}(j,i)\begin{pmatrix}\delta p_r\\ \delta T\\ \delta V\\ \delta S\end{pmatrix}_i$$

Here δS, δV, δT, and δp_r are the complex amplitudes of entropy, volume, temperature and radial component of pressure ($\delta p_r = -\sigma_{rr}$) respectively. The elements of the

transfer matrix are given in reference [7]. From this general solution one can work out different cases pertaining to different combinations of boundary conditions, like the one we handle here. The boundary condition on $r_1 = 0$, giving net flux of heat through the center of the sphere, is set equal to zero, $\delta S_1 = 0$, since heat is supplied uniformly across the surface r_3 giving a spherically symmetric case. For the same reason, $\delta V_1 = 0$ and at the mechanically free outer boundary r_3 the heat supplied, δS_3, is given and $\delta p_{r,3} = 0$. Letting $r = r_2$ be an intermediate radius between r_1 and r_3 one has

$$\begin{pmatrix} \delta p_r \\ \delta T \\ \delta V \\ \delta S \end{pmatrix}_2 = \mathbf{T}(2,1) \begin{pmatrix} \delta p_r \\ \delta T \\ 0 \\ 0 \end{pmatrix}_1 . \tag{3.26}$$

Writing out the components of the matrix $\mathbf{T}(2,1)$, using the boundary conditions at radii 1 and 2, Eq. 3.26 is reduced to

$$\begin{pmatrix} \delta p_r \\ \delta T \\ \delta V \end{pmatrix}_2 = \begin{pmatrix} T_{11}(2,1) & T_{12}(2,1) \\ T_{21}(2,1) & T_{22}(2,1) \\ T_{31}(2,1) & T_{32}(2,1) \end{pmatrix} \begin{pmatrix} \delta p_r \\ \delta T \end{pmatrix}_1 . \tag{3.27}$$

Likewise the transfer matrix connecting the quantities at radii 3 and 1 is reduced to

$$\begin{pmatrix} 0 \\ \delta T \\ \delta V \\ \delta S \end{pmatrix}_3 = \mathbf{T}(3,1) \begin{pmatrix} \delta p_r \\ \delta T \\ 0 \\ 0 \end{pmatrix}_1 . \tag{3.28}$$

From Eq. 3.28 one has that $\delta p_{r,1} = -\frac{T_{12}(3,1)}{T_{11}(3,1)}\delta T_1$, or $\delta T_1 = -\frac{T_{11}(3,1)}{T_{12}(3,1)}\delta p_{r,1}$, whereby $\delta S_3 = (T_{42}(3,1) - \frac{T_{41}(3,1)T_{12}(3,1)}{T_{11}(3,1)})\delta T_1 = (T_{41}(3,1) - \frac{T_{42}(3,1)T_{11}(3,1)}{T_{12}(3,1)})\delta p_{r,1}$.

Solving for temperature and pressure at radius 1 one obtains

$$\delta T_1 = \frac{T_{11}(3,1)}{T_{42}(3,1)T_{11}(3,1) - T_{41}(3,1)T_{12}(3,1)})\delta S_3 \tag{3.29}$$

$$\delta p_{r,1} = \frac{T_{12}(3,1)}{T_{41}(3,1)T_{12}(3,1) - T_{42}(3,1)T_{11}(3,1)})\delta S_3 \tag{3.30}$$

Inserting this into Eq. (3.27) one finally arrives at

$$\delta p_{r,2} = \frac{T_{11}(2,1)T_{12}(3,1) - T_{12}(2,1)T_{11}(3,1)}{T_{41}(3,1)T_{12}(3,1) - T_{42}(3,1)T_{11}(3,1)})\delta S_3 \tag{3.31}$$

$$\delta T_2 = \frac{T_{21}(2,1)T_{12}(3,1) - T_{22}(2,1)T_{11}(3,1)}{T_{41}(3,1)T_{12}(3,1) - T_{42}(3,1)T_{11}(3,1)})\delta S_3 \tag{3.32}$$

$$\delta V_2 = \frac{T_{31}(2,1)T_{12}(3,1) - T_{32}(2,1)T_{11}(3,1)}{T_{41}(3,1)T_{12}(3,1) - T_{42}(3,1)T_{11}(3,1)})\delta S_3 \tag{3.33}$$

These equations is to be evaluated in the limit of $r_1 \to 0$. The displacement field u is found as $u(r_2) = \frac{1}{r_2^2}\delta V_2$ and finally the difference between the stress components are found using

$$\sigma_{rr} - \sigma_{\theta\theta} = \frac{3}{2}(\delta p - \delta p_r) = G\left(2r^{-2}\frac{\partial \delta V}{\partial r} - 6r^{-3}\delta V\right) \tag{3.34}$$

Inserting the elements of the transfer matrix found in [7] into Eq.'s 3.31 to 3.34 one obtains the following solutions for temperature, displacement field and stress in a sphere.

$$\begin{aligned}
\frac{\delta T(r)}{\delta Q} &= \frac{1}{c_p V_0} \times \\
&\left\{\frac{a_l}{a_l - 1} + \frac{1}{1 - a_l}\frac{(kR)^3}{kR\cosh(kR) - \sinh(kR)}\frac{\sinh(kr)}{kr}\right\} && (3.35)\\
\frac{u(r)}{\delta Q} &= \frac{i\omega\alpha_s}{4\pi\lambda} \times \\
&\left\{\left(\frac{c_l}{c_V} - 1\right)\frac{(kR)\cosh(kr) - \sinh(kr)}{(kR)\cosh(kR) - \sinh(kR)} + a_l\left(\frac{r}{R}\right)^3\right\} && (3.36)\\
\frac{\sigma_{rr}(r)}{\delta Q} &= \frac{1}{\alpha_p T_0 V_0}\frac{a_l}{1 - a_l} \times \\
&\left\{1 - \left(\frac{R}{r}\right)^3 \frac{kr\cosh(kr) - \sinh(kr)}{kR\cosh(kR) - \sinh(kR)}\right\} && (3.37)\\
\frac{\sigma_{\theta\theta}(r)}{\delta Q} &= \frac{1}{\alpha_p T_0 V_0}\frac{a_l}{1 - a_l} \times \\
&\left\{1 + \frac{1}{2}\left(\frac{R}{r}\right)^3 \frac{kr\cosh(kr) - (1 + (kr)^2)\sinh(kr)}{kR\cosh(kR) - \sinh(kR)}\right\} && (3.38)
\end{aligned}$$

Here V_0 is the sphere volume, k the complex frequency-dependent thermal wave vector $k = \sqrt{i\omega c_l(\omega)/\lambda}$, while α_s is short-hand notation for $\alpha_s = \frac{c_p}{T_0\alpha_p K_S}$. If one evaluates Eq. 3.35 for $r = 0$ and set the value of the coupling constant to $a_l = 0.091$ the response $c_p V_0 \frac{\delta T(r=0)}{\delta Q}$ will look like the plot in Figure 3.2. It illustrates why (compare [6, 7]) the measurement of the high-frequency isobaric specific heat is problematic. At zero (low) frequency, the ratio between complex amplitudes of temperature at the center and heat supplied at the surface, gives the isobaric specific heat while at high frequencies one measures $\frac{1}{c_p V_0}\frac{a_l}{a_l - 1}$ and not $\frac{1}{c_p V_0}$.

In principal we can understand the effect of cooling by heating in terms of Eq.'s 3.14, 3.15, 3.17, as an example of adiabatic cooling. But in order to gain more insight into the cooling by heating effect and show the relevance of the longitudinal coupling constant a_l in controlling the effect I have solved Eq.'s 3.35, 3.37 and 3.38 in the thermoelastic case, i.e. for a solid where the constitutive properties are frequency independent. If a delta

function heat flux is applied at $t = 0$, the heat supplied at the surface is a Heaviside step-function, $\delta Q(R,t) = \delta Q H(t)$; in this case calculating the inverse Laplace (Stieltje) transform by the standard residue calculus leads to the following expressions for the temperature, stresses, and pressure as functions of time after $t = 0$. These calculations are not shown here and the reason for this is two-fold. First of all they are really lengthy and a check can be done by inspection. Secondly it would risk boring the reader, while a truly interested reader would be able to do the calculations on their own. I advise you to do that, it is almost like magic how this mathematical tool can be used to solve such involved problems analytically. Nevertheless, the results are as follows:

$$\begin{aligned}
\delta T(r,t) &= \frac{\delta Q}{c_p V_0} \times \\
&\quad \left\{ 1 + \frac{1}{1-a_l} \frac{2}{3} \sum_{n=1}^{\infty} \frac{R}{r} \frac{\sin(\frac{r}{R} x_n)}{\sin(x_n)} e^{-x_n^2 t/\tau} \right\}, \qquad (3.39) \\
\sigma_{rr}(r,t) &= \frac{-2\delta Q}{\alpha_p T_0 V_0} \frac{a_l}{1-a_l} \left(\frac{R}{r} \right)^3 \times \\
&\quad \sum_{n=1}^{\infty} \frac{\sin(\frac{r}{R} x_n) - \frac{r}{R} x_n \cos(\frac{r}{R} x_n)}{x_n^2 \sin(x_n)} e^{-x_n^2 t/\tau}, \qquad (3.40) \\
\sigma_{\theta\theta}(r,t) &= \frac{\delta Q}{\alpha_p T_0 V_0} \frac{a_l}{1-a_l} \left(\frac{R}{r} \right)^3 \times \\
&\quad \sum_{n=1}^{\infty} \frac{[1 - (\frac{r}{R} x_n)^2] \sin(\frac{r}{R} x_n) - \frac{r}{R} x_n \cos(\frac{r}{R} x_n)}{x_n^2 \sin(x_n)} e^{-x_n^2 t/\tau}, \qquad (3.41) \\
\delta p(r,t) &= \frac{2\delta Q}{3\alpha_p T_0 V_0} \frac{a_l}{1-a_l} \times \\
&\quad \sum_{n=1}^{\infty} \frac{R}{r} \frac{\sin(\frac{r}{R} x_n)}{\sin(x_n)} e^{-x_n^2 t/\tau}. \qquad (3.42)
\end{aligned}$$

Here $\tau = R^2 c_l/\lambda$ is the characteristic heat diffusion time, and $x_1 < x_2 < ...$ are the positive roots of the transcendental equation $x = \tan(x)$ given by $x_n = \sqrt{(n\pi + \frac{\pi}{2})^2 - 2}$. Clearly, when $a_l = 0$ there are no induced stresses, but how can we see that there is no cooling-by-heating effect in this case? In the limit where $r \to 0$ the terms inside the sum in Eq. 3.39 becomes $\sum_{n=1}^{\infty} \frac{x_n)}{\sin(x_n)} e^{-x_n^2 t/\tau}$. This is an alternating sum, where the sequence of numerical values of the terms in the sum converge to zero as n goes to infinity. This makes the sum convergent. For $t >> \tau$ the sum converges to zero, while for $t << 0$ it converges to $-\frac{3}{2}$. Therefor, for $t \to 0$ the temperature will drop instantaneously to a value given by $\frac{1}{c_p V_0} \left(1 - \frac{1}{1-a_l} \right) = \frac{1}{c_p V_0} \left(\frac{a_l}{a_l - 1} \right)$. Using the liquid value of the specific heat around T_g of Glucose, $c_p = 2.13 \cdot 10^6 {}^{\mathrm{J}}/_{\mathrm{m^3 K}}$ [9], and assuming a value of the coupling constant $a_l = 0.091$, then for a sphere of radius 9mm the drop in temperature would be $16^{\mathrm{mK}}/_{\mathrm{J}} \cdot \delta Q$. In Figure 3.3 we plot the scaled temperature change $c_p V_0 {}^{\delta T}/_{\delta Q}$ for several radii r/R as given by Eq. (3.39). Time is given in units of the characteristic heat diffusion time τ, and the coupling constant is here fixed to $a_l = 0.091$

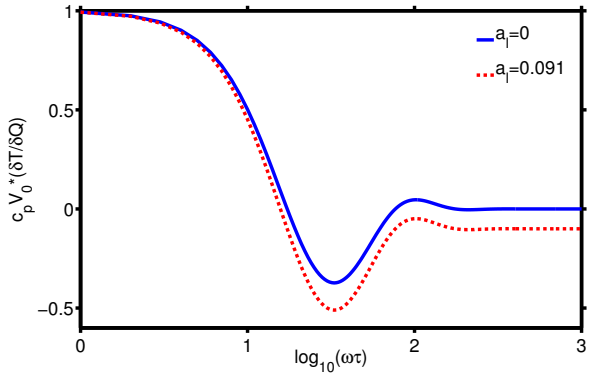

Figure 3.2 At zero frequency, you measure the isobaric specific heat, while at high frequencies one measures a combination of c_p and c_l, namely $\frac{1}{c_p V_0}\frac{a_l}{a_l - 1}$.

Figure 3.3 clearly shows the cooling-by-heating effect. Since a finite amount of heat was added at the surface at $t = 0$, the surface temperature initially diverges (it is infinitely thin). The interior of the sphere, independent of radius, even close to the surface, instantaneously cools to a common temperature determined by the value of the coupling constant $\frac{a_l}{a_l - 1}$. The expansion of the surface is immediately felt in the interior, and since no heat has yet arrived by diffusion, it cools adiabatically. This initial response is followed by a complicated evolution in time where the temperatures of the different parts of the sphere finally converge to a temperature determined by the volume and specific heat of the sphere $c_p V_0$, and eventually equilibrate .

Consider the components of stress given by Eqs. 3.40 and 3.41, respectively. In Fig. 3.4 the σ_{rr} component of the stress tensor is plotted. As the surface receives heat and expands, an immediate traction is felt in the interior of the sphere giving a negative contribution to pressure that persists until equilibrium is reached.

The other stress component $\sigma_{\theta\theta}(r, t)$, is shown in Fig. 3.5. For all the radii shown one notices an immediate, uniform increase of $\sigma_{\theta\theta}(r, t)$ throughout the sphere. This is then followed by a transient where initially $\sigma_{\theta\theta}$ is positive contributing negatively to the pressure. At some point it shifts sign and oppose the expansion, giving a positive contribution to pressure that persist until the systenm is equilibrated. The resulting pressure $\delta p(r) = -\frac{1}{3}(\sigma_{rr} + 2\sigma_{\theta\theta})$ is shown in Fig. 3.6. Comparing with temperature in Fig. 3.3 we see that the temporal evolution of temperature basically follows that of the pressure. In fact, multiplying Eq. 3.42 with the inverse of the adiabatic pressure coefficient times the coupling constant a_l , $(a_l \beta_s)^{-1} = T_0 \alpha_p / c_p$, and adding a factor $\delta Q/(c_p V_0)$, one arrives at Eq. 3.39.

3.4 Thermoviscoelastic case of cooling by heating

This section considers a case that is more likely to be found in an experimental situation where temperature instead of heat current is controlled at the surface. The surface is still free to move and otherwise the boundary conditions are the same as in the preceding sections. Also we restrict ourselves to find the temperature at the center of

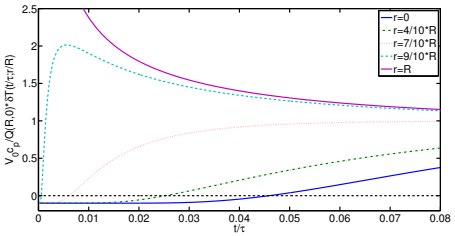

Figure 3.3 The temperature response of the sphere as function of time scaled by the volume and specific heat $c_p V_0$. After addition of heat at the surface, the temperature drops instantaneously throughout the sphere to a temperature given by $\frac{a_l}{a_l - 1}$, thus showing adiabatic cooling. The time scale is given by the characteristic heat diffusion time, $\tau = R^2 c_l/\lambda$ and the coupling constant was here chosen to be $a_l = 0.091$.

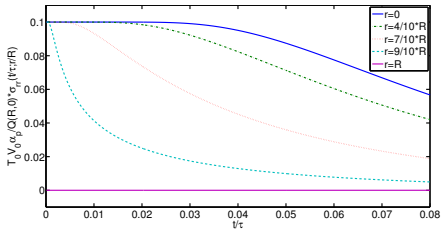

Figure 3.4 The rr-component of stress tensor throughout the sphere as a function of time. After the addition of heat at the surface, $\sigma_{rr}(t/\tau; r/R)$ throughout the sphere immediately increases, giving a negative contribution to the pressure that persists until equilibrium is eventually reached.

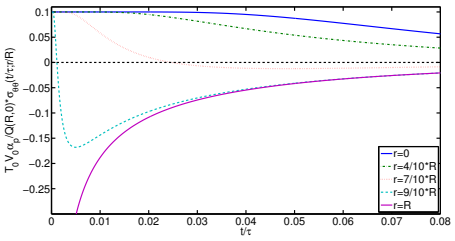

Figure 3.5 The $\theta\theta$-component of stress in the sphere as a function of time. After an adiabatic step up in $\sigma_{\theta\theta}(t/\tau; r/R)$ in the interior of the sphere follows a complicated evolution in time.

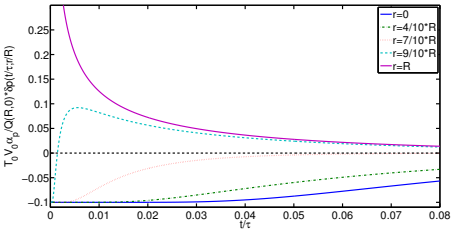

Figure 3.6 The pressure in the sphere as a function of time. Scaling and shifting the pressure with $(a_l \beta_s)^{-1} = \frac{T_0 \alpha_p}{c_p}$ and $\frac{\delta Q}{V_0 c_p}$ one gets the temperature shown in Fig. 3.3.

the sphere and set $r = 0$. In this case, if $x \equiv \sqrt{i\omega\tau}$, where $\tau = {}^{R^2 c_l}/_{\lambda}$, the solution in the frequency domain is given by:

$$\begin{aligned} \delta T(0,s) &= \Phi(s)\delta T(R,s) \\ &= \left(1 - \frac{x^3 - x^2\sinh(x)}{3a_l[x\cosh(x) - \sinh(x)] - x^2\sinh(x)}\right) \cdot \delta T(R,s) \end{aligned} \tag{3.43}$$

One could go on and find an analytical solution in the time domain, but here we wish to study the response of a thermoviscoelastic sphere instead of a solid sphere. According to the discussion in section 3.2 (see for example Figure 3.1), around the glass transition region, the coupling constant may be dynamically larger than otherwise expected. In order to examine this possibility one has to take into account that the constitutive parameters become complex frequency-dependent quantities. Thus it is no longer possible to find an analytical solution of the problem and one must resort to numerical

methods. To do that we need to make a model that can express the constitutive parameters of the linear thermoviscoelastic response of a differential volume element V_0, that is, the elements of the compliance matrix, **J**:

$$\begin{pmatrix} \delta S \\ \delta V \end{pmatrix} = V_0 \begin{pmatrix} \frac{1}{T_0} c_p(\omega) & \alpha_p(\omega) \\ \alpha_p(\omega) & \kappa_T(\omega) \end{pmatrix} \begin{pmatrix} \delta T \\ -\delta p \end{pmatrix} = \mathbf{J} \begin{pmatrix} \delta T \\ -\delta p \end{pmatrix} \tag{3.44}$$

Here δS, δV, δT and δP denotes the complex amplitudes of harmonically varying perturbations of entropy, volume, temperature and pressure. Note that the products of conjugated variables gives the energy transferred into the system from the surroundings thus expressing the First law of thermodynamics of a differential volume.

3.4.1 Linear network model

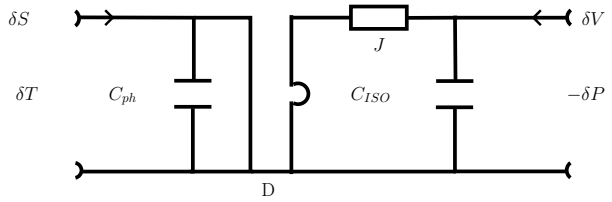

Figure 3.7 Electrical equivalent diagram of the interaction of a volume element with the surroundings through two ports. The thermal side where entropy displacement and temperature (corresponding to charge displacement and voltage) can be controlled, and the mechanical port where volume displacement and negative pressure can be controlled. C_{ph} represents the instantaneously stored vibrational energy as temperature is increased and C_{iso} represents the potential energy stored as the average distance between the molecules change with an instantaneous volume response. Displacement and Voltage is transformed in the transducer D connecting the two ports. J represents the structural deformation and it is the only frequency dependent element in the model.

In order to make it simple I have chosen to use a model where the relaxing part of all the constitutive parameters are the same. The model is reticulated in the electrical equivalent diagram shown in figure 3.7. The interaction with the small volume takes place at the two ports. The thermal energy bond consists of temperature as the effort variable and entropy as the displacement variable. The arrow indicates in which direction the generalized displacement is taken as positive. The mechanical bond consists of the negative pressure and volume and the two ports are connected by the transformer ratio D with units $^{\mathrm{J}}/_{\mathrm{m}^3\mathrm{K}}$. On each side of the transformer there are some elements representing physical properties. The capacitances on each side models the instantaneous response to variations in the different fields; C_{ISO} gives the instantaneous elastic change in volume and C_{ph} gives the instantaneous change in temperature. Both elements represent ways to store energy - by isostructural deformation or increasing vibrational energy. The last element, J is not specified yet, but it will contain the dissipative elements of the model and represents the structural part of the thermoviscoelastic response. The aim now is to express the elements of the compliance matrix in terms of the elements of the model. When this is done we can express the two parameters that goes into Eq. 3.43, a_l and τ in terms of the model. A final comment about the model is in place as it is a very simple model. Consider the placement of the elements and assume the

mechanical port is short-circuited ($\delta p = 0$). Imposing a temperature variation in the thermal port in this case leads to the displacement of volume:

$$-\delta V = J \cdot D\delta T \Leftrightarrow V_0\alpha_p = J_{21} = -JD \tag{3.45}$$

It is clear that if we then use a model for the relaxing function J which goes to zero at high frequencies, the model predicts an isobaric expansion coefficient that is zero in that limit. This is not quite true to the known phenomenology of viscous liquids but it actually serves a purpose, as I will show below.

Element J_{11} of the compliance matrix is found by short-circuiting the mechanical port. Imposing a temperature variation δT the displacement of entropy δS is

$$\delta S = \left(C_{ph} + D^2 J\right)\delta T \Leftrightarrow V_0\xi_p = J_{11} = C_{ph} + D^2 J \tag{3.46}$$

where $\xi_p = c_p/T_0$. If the thermal port is short-cicuited $\delta T = 0$ and a pressure is imposed, the volume displacement will be

$$\delta V = (C_{ISO} + J)(-\delta p) \Leftrightarrow V_0\kappa_T = J_{22} = C_{ISO} + J \tag{3.47}$$

Finally J_{12} can be found by imposing a pressure variation when the thermal port is short-circuited.

$$-\delta S = D \cdot J(-\delta p) \Leftrightarrow J_{12} = J_{21} = -DJ \tag{3.48}$$

Note that this linear network (energy bond) model obeys Onsager's reciprocity principle making the compliance matrix symmetric. The five other parameters are also given in terms of the elements in the model.

$$\beta_V = \frac{\alpha_p}{\kappa_T} = \frac{-D \cdot J}{C_{ISO} + J} \tag{3.49}$$

$$\beta_S = \frac{\xi_p}{\alpha_p} = -\frac{C_{ph} + D^2 J}{DJ} \tag{3.50}$$

$$V_0\kappa_S = C_{ISO} + \frac{C_{ph}J}{C_{ph} + D^2 J} \tag{3.51}$$

$$V_0\alpha_S = -\frac{C_{ph}C_{ISO} + C_{ph}J + C_{ISO}D^2 J}{DJ} \tag{3.52}$$

$$V_0\xi_V = V_0\frac{c_V}{T_0} = C_{ph} + D^2\frac{C_{ISO}J}{C_{ISO} + J} \tag{3.53}$$

$$\tag{3.54}$$

We wish to ascribe a numerical value to the elements of the model based on data that can be found in the literature. Denote the difference in a parameter between two frequencies as $\Delta x = x(\omega_2) - x(\omega_1)$. Then the transformer ratio is given by

$$\frac{\Delta\alpha_p}{\Delta\xi_p} = -\frac{1}{D} = \frac{\Delta\kappa_T}{\Delta\alpha_p} = \gamma_{Tp} \tag{3.55}$$

The indecis indicate that the transformer ratio is found by combining constitutive parameters obtained in an experiment where you control temperature and pressure. Also the fact that the model operates with only one relaxing function makes it a model of a single internal parameter liquid; pairs of constitutive parameters become proportional, and the linear Prigogine-Defay ratio becomes unity:

$$\Pi_{TP} = \frac{\Delta c_p \Delta\kappa_T}{T_0 \left(\Delta\alpha_p\right)^2} = 1. \tag{3.56}$$

There is no explicit reference to the glassy state, any two frequencies can do, and also, the relaxing function need not be exponential for the above to apply.

The other elements are given by

$$\begin{aligned} -\frac{\Delta 1/\alpha_S}{\Delta 1/\xi_V} &= -\frac{C_{ph}}{DC_{ISO}} = -\frac{\Delta 1/\kappa_S}{\Delta 1/\alpha_S} = \gamma_{SV} \\ -\frac{\Delta 1/\beta_S}{\Delta 1/\xi_p} &= -\frac{1}{V}\frac{C_{ph}}{D} = \frac{\Delta\kappa_S}{\Delta 1/\beta_S} = \gamma_{Sp} \\ -\frac{\Delta\beta_V}{\Delta\xi_V} &= \frac{V}{DC_{ISO}} = \frac{\Delta 1/\kappa_T}{\Delta\beta_V} = -\gamma_{TV} \end{aligned} \tag{3.57}$$

It follows that certain relations between the γ_{XY}'s apply, namely

$$\gamma_{Sp}\gamma_{TV} = \gamma_{Tp}\gamma_{SV} \tag{3.58}$$

and the parameters of the model are given by

$$\begin{aligned} \frac{-1}{D} &= \gamma_{Tp} \\ C_{ph} &= V\frac{\gamma_{Sp}}{\gamma_{Tp}} \\ C_{IS0} &= V\frac{\gamma_{Tp}}{\gamma_{TV}} \end{aligned} \tag{3.59}$$

Now we can express the longitudinal specific heat c_l that goes into the characteristic time τ in Eq. 3.43:

$$\begin{aligned} c_l &= (1-a_l)\,c_p = \frac{T}{V}(1-a_l)\left(C_{ph} + D^2 J\right) \\ &= (1-a_l)\left(\gamma_{Sp} + j_b\right)\frac{T}{\gamma_{Tp}} \end{aligned} \tag{3.60}$$

where $j_b = \frac{J}{V\gamma_{Tp}}$. The coupling constant is given by $a_l = \frac{4}{3}\frac{G}{K_T + {}^4/_3 G}\frac{c_p - c_V}{c_p}$. Using the relation $\xi_p - \xi_V = {}^{\alpha_p^2}/_{\kappa_T}$ we can write the coupling constant as

$$a_l = \frac{\kappa_T}{\kappa_T + \frac{3\gamma_{Tp}}{4} j_{sh}} \frac{\alpha_p^2}{\kappa_T} \tag{3.61}$$

where $j_{sh} = {}^{J_{sh}}/_{\gamma_{Tp}}$ is the scaled shear compliance. Combining Eq. 3.58 and Eq. 3.59 and inserting into Eq. 3.61 the coupling constant becomes

$$a_l = \frac{j_b^2}{(\gamma_{Sp} + j_b)\left(\frac{1}{\gamma_{TV}} + \frac{3}{4} j_{sh} + j_b\right)} \tag{3.62}$$

3.4.2 Parametrizing the model

The only thing that is missing is to put in a model for the two functions j_{sh} and j_b. The shear compliance I choose to model by a Maxwell element (capacitor and resistance in parallel): $\gamma_{Tp} j_{sh} = \frac{1}{G_\infty} + \frac{1}{i\omega\eta_{sh}}$, where G_∞ is the infinite shear modulus and η_{sh} is the shear viscosity. For the bulk compliance j_b I will use two different models. The first model is a Voigt element (capacitor and resistance in series):

$$\text{Model} \quad 1: \quad \gamma_{Tp} V j_b = \frac{1}{K_0 + i\omega\eta_b} \tag{3.63}$$

Taking the limit of $\omega \to 0$ and combining Eq.'s 3.47 and 3.59 we have for the inverse capacitance $K_0 = \frac{1}{\kappa_T(\omega\to 0) - \frac{\gamma_{Sp}}{\gamma_{SV}}}$. Note that Model 1 forces the coupling constant to be zero in the glass ($\omega \to \infty$) as $\alpha_p = \frac{J}{\gamma_{Tp}}$ goes to zero in this limit.

The other model, Model 2, allows the isobaric expansion coefficient to be non-zero also in the glass. It is constructed by putting a capacitance in series with a Maxwell element. The two models are listed together with the parameters in Table 3.4.2

	$\gamma_{Tp} V j_b =$	K_0	K_∞
Model 1	$\frac{1}{K_0 + i\omega\eta_b}$	$\frac{1}{\kappa_T(\omega\to 0) - \frac{\gamma_{Sp}}{\gamma_{SV}}}$	NaN
Model 2	$\frac{1}{K_0 + (K_\infty - K_0)\frac{\frac{i\omega\eta_b}{(K_\infty - K_0)}}{1 + \frac{i\omega\eta_b}{(K_\infty - K_0)}}}$	$\frac{1}{\kappa_T(\omega\to 0) - \frac{\gamma_{Sp}}{\gamma_{SV}}}$	$\frac{1}{\kappa_T(\omega\to \infty) - \frac{\gamma_{Sp}}{\gamma_{SV}}}$

Table 3.1 The two models used to create Figure 3.9 and Figure 3.8.

The final assumption is that the bulk viscosity equals the shear viscosity, i.e. $\eta = \eta_b = \eta_{sh}$. To parametrize the two models I chose to use Glycerol data. In reference [11, p. 165] my supervisor fits viscosity data on Glycerol from reference [12] with the fitting function $\ln\eta = a + \frac{b}{T^3}$ proposed by [13]. The data by Meissner [12] were taken over 4 decades from 233K to 333K. The fitted parameters were found to be $a = -6.32$ and $b = 2.26 \cdot 10^8 \mathrm{K}^3$. Extrapolated to 184K the viscosity becomes $\eta = 10^{12}\mathrm{Pa} \cdot \mathrm{s}$. The data for isobaric specific heat, c_p, isobaric expansion coefficient, α_p and isothermal compressibility κ_T are taken from Davies and Jones [9], while the infinite shear modulus G_∞ is found in reference [14]. The thermal conductivity is assumed to be independent of frequency and the data used is found in reference [15].

Now that the parametrization of the model is in place equation 3.43 is inverted numerically. The algorithm for the inverse Laplace transform is an improved version of de Hoog's quotient difference method [16] developed and implemented in Matlab by [17].

3.4.3 Numerical results

Figure 3.8 shows the results based on Model 2 and Figure 3.9 shows the result based on Model 1. In both cases a step up in temperature of size $\Delta T = 1$K has been applied at the free surface of the sphere. The radius of the sphere is set to $r = 10$mm. This is done for a range of temperatures below and above $T_g \approx 184$K, from 150K deep in the glass, up to 210K in the liquid.

Figure 3.8 shows that the effect of the thermomechanical coupling is non-present at high temperature. But as temperature is decreased and the liquid gets more and more viscous, a dip in temperature emerges. Going further down in temperature the effect of cooling by heating reaches a maximum slightly above T_g. Even further down in temperature, in the glassy state, the effect dies away.

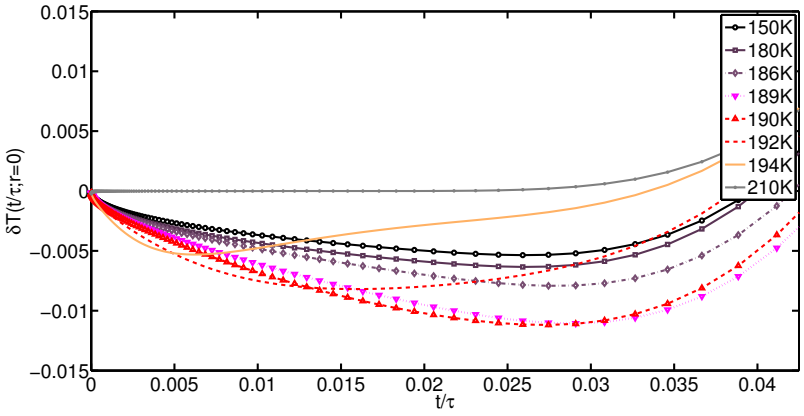

Figure 3.8 The change in temperature, δT as function of time scaled by the characteristic diffusion time τ, at the center of a sphere, after a temperature step of $\Delta T = 1K$ has been applied at the surface. Radius is set to $r = 10$mm and parameters are determined by glycerol data. The result is based on Model 2 where we allow $c_p \neq c_V$, corresponding to a more realistic case where the expansion coefficient is non zero in the solid. The maximum occurs just above T_g (presumably around 184K in glycerol. Close to T_g a detectable change in temperature at the center of the sphere is on the order of 10mK The maxima occurs after 0.03τ, which in this case is approximately 30 seconds.

Figure 3.9 shows the result based on Model 2, which is the case where we force the coupling constant to be zero in the glass. Even in this case is the phenomenon present, thus showing that cooling by heating is an effect that is characteristic of liquids close to the glass transition.

These two results strengthens the conjecture that the phenomenon is a fingerprint of the glass transition, as suggested in section 3.2. Also, based on Figure 3.8, there is a (presumably) measurable change around 10mK with a time window of approximately 0.03τ, which in the case of a sphere with radius $r = 10$mm is around 30 seconds using a typical value of the characteristic diffusion time of a viscous liquid.

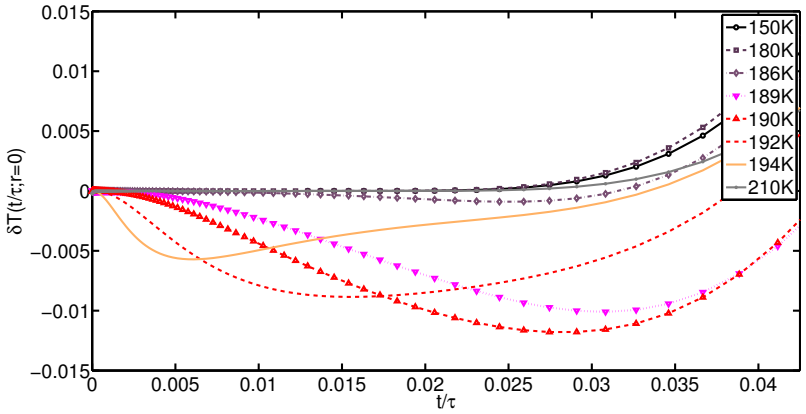

Figure 3.9 The change in temperature, δT as function of time scaled by the characteristic diffusion time τ, at the center of a sphere, after a temperature step of $\Delta T = 1$ has been applied at the surface. The parameters are the same as used in Figure 3.8 except that here we force $a_l = 0$ for $\omega \to \infty$ (Model 1); This figure shows that effect of cooling by heating is expected to be present even in the case when the volume expansion of the solid is negligible. The maximum occurs just above T_g (presumably around 184K in glycerol).

The lesson to be learned from all this is the following. The phenomenon of cooling by heating is a fingerprint of a liquid being close to the glass transition. It establishes the difference between the longitudinal and isobaric specific heats as it can only be present when the two differ. The reason for this is that in this temperature range, the shear modulus is non-vanishing compared to the bulk modulus, simultaneously with the isothermal and adiabatic bulk moduli being significantly different. The question is, how large is the effect, and can it be measured? This is the topic of next chapter.

4 Cooling by heating - experimental proof of concept

This chapter gives a brief account on the experiment and choice of liquid as well as the modeling done to guide us in the setup of the experiment. The results are presented in the end, while the procedure to mold the samples is described in Appendix B.

The prediction of the phenomenon of cooling by heating was based on analytical and numerical results pertaining to the spherically symmetric case. To prove the existence of the phenomenon we thus set out to do measurements on a spherical sample. The idea was to use existing in-house equipment - a cryostat to make temperature steps, and a multimeter to measure the change in temperature using a semiconductor, which has a temperature dependent resistance, as a thermometer. This should be done without the need to construct new machinery or indulging in other time-consuming preparations. The following criteria were chosen.

- *The liquid should have a calorimetric glass transition around room temperature.* The reason for this is that in our lab, the molding of the sphere has to be done outside the cryostat that is used to perform the experiment. That is, if a liquid with a calorimetric glass transition temperature much below room temperature was to be used, a number of problems would occur. First of all, since the strategy was to mold a sphere, we needed a liquid that could retain it's shape long enough to have time to move it from the molding device to the cryostat where the measurement is performed. If not, since we cannot do the experiment on a space station, molding would have to be done in a cold environment, something which would give rise to new problems; the process of transporting the sample from the molding environment, mounting on the pre-cooled holder of the measuring cell, and insertion into the pre-cooled thermostat, would need to be done fast, in order to prevent the sample from warming up and deform. Also, it would be very difficult to avoid formation of ice which would make it impossible to fit the holder back into the cryostat.
- *The liquid should not crack upon cooling*
- *The liquid should have a large expansion coefficient.* Eq. 3.23 tells us that the coupling constant a_l goes as α_p^2, that is, the higher an expansion coefficient, the greater the chances of seeing the effect we are looking for.
- *The liquid should be inexpensive.* Since we wanted to mold a sphere with a radius of approximately 10mm (roughly the size of the cryostat chamber) and we expected to need many attempts to mold a sphere before finding the best method, the price of the substance should not be to large.

The obvious choice was to look into the naturally occurring sugars. They are not that

expensive, and they all have a relatively large expansion coefficient around $4.5{\cdot}10^{-4}$. We experimented with Fructose, Saccharose, Glucose, Maltose, and binary mixtures here of. The final choice fell on Glucose, or to be more precise, α-D-Glucose, bought from Sigma. When melted, this liquid has a calorimetric glass transition around 38°C[18–21], it doesn't crack unless you cool it too fast, it's cheap, and it turns out to be easy to work with, with respect to avoiding caramellization and formation of air-bubbles.

4.1 Experimental setup and calibration of NTC-thermistor bead

The basic procedure of the experiment was the following. Place a spherical sample of Glucose inside a cryostat, make a temperature step with the cryostat, and measure the change in temperature in the center of the sphere. This is illustrated in figure 4.1.

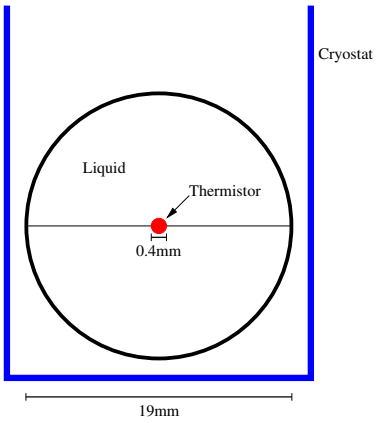

Figure 4.1 A sketch of the experimental setup. The liquid is molded into a sphere, in which a small NTC-thermistor bead is placed in the center, connected to wires that lead to a multimeter that performs resistance measurements. The sphere is inserted into the cylindrical chamber of a cryostat.

4.1.1 NTC-thermistor bead

The Negative-Temperature-Coefficient thermistor bead (NTC) is a semi conductor with temperature dependent electrical resistance. Contrary to normal its resistance increases when temperature decreases. Measuring the resistance thus provides a way to measure temperature. The NTC is used heavily in Part II later in this thesis, so for now I will restrict myself to the most simple use of it - to measure temperature.

The resistance measurement is done with an HP3458A Multimeter, which passes a known current through the NTC and measures the voltage over it to determine the resistance. The measured value is given as the mean over 4 power-line cycles corresponding to a measuring time of 80 milliseconds for a 50Hz power-line. The current I choose to put through the NTC is 50μA giving a resolution of about 10mΩ. This corresponds to a temperature change of 0.2mK.

The temperature dependence of the NTC is due to the fact that in a semiconductor the number of charge carriers in the conduction-band depends on temperature. This

is assumed to be an activated process so the resistance is written in the following exponential form:

$$R_{NTC} = R_\infty e^{\frac{E_a}{k_b T}} = R_\infty e^{\frac{k_b T_A}{k_b T}} = R_\infty e^{\frac{T_A}{T}}, \tag{4.1}$$

where T_A is the thermal activation temperature, T is the actual temperature of the NTC and R_∞ is the limiting high temperature resistance of the NTC. Taking the logarithm of Eq. 4.1 we get a linear relation that can be fitted to resistance data collected on the NTC in a range of temperatures

$$\ln(R_{NTC}) = \ln(R_\infty) + \frac{T_A}{T}. \tag{4.2}$$

The result of such a fitting procedure is shown in Figure 4.2. For this specific bead the change in resistance with temperature is around $50\text{m}\Omega/\text{m}K$. This means that a temperature change of $2\text{m}K$ will give a change in resistance of about $100\text{m}\Omega$ - the error would then be around 10% given the resolution when a current of 50μA is used.

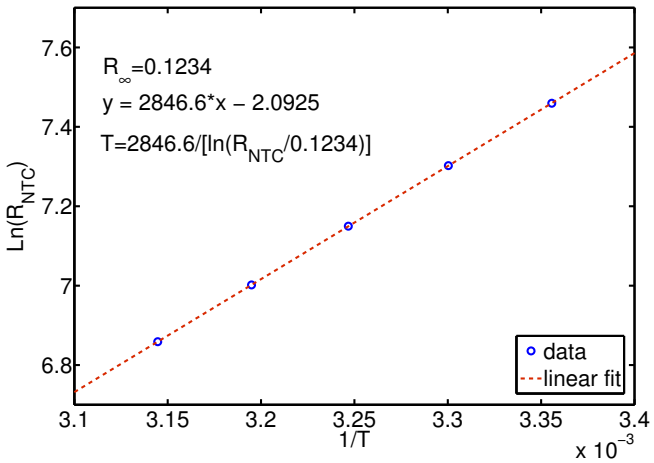

Figure 4.2 The log of the resistance of the NTC plotted against inverse temperature. The line is a fit to Eq. 4.2. The values of the fitted parameters are $R_\infty = 0.1234$ and $T_A = 2846.6$

4.1.2 The cryostat - Critically damped temperature "step"

In next section (4.2) I model how the temperature changes inside a sphere as the response to a Heaviside step in temperature at the walls of a cavity in which the sphere resides. This is to mimic the experimental setup (sphere inside cryostat) that I am using. In reality, the cryostat is not capable of doing such an instantaneous step in temperature. Also, since one of the possible developments of this experiment is to Laplace transform the data, the knowledge of the functional form of the temperature

of the cryostat makes it possible to isolate the response function using the convolution theorem for Laplace transforms. This way one could in principle analyze the transformed data in the frequency domain using Eq. 4.9 to determine the frequency dependent coupling constant $a_l = \frac{c_l - c_p}{c_p}$.

The temperature function of the cryostat, $\delta T_C(t)$, is a complicated function. The cryostat will approach the new temperature level via a PID method (proportional, integral, and derivative control) with the purpose of finding the fastest change between two temperature levels.

The cryostat is made from a cold liquid nitrogen fueled bath and a heater. The PID method controls the temperature in the experimental stage by means of balancing the heat outflow to the cold bath, $w_{out}(t)$, with the heat effect of the heater, $w(t)$, measured in W, such that the heat load on the experimental stage, $w_L(t)$, will approach or be kept at an almost constant level:

$$\bar{w}(t) + \bar{w}_L(t) = \bar{w}_{out}(t), \tag{4.3}$$

where $\bar{w}(t)$ represents the time average of $w(t)$. In the standard PID method the heater output, $w(t)$, is determined by [22]

$$w(t) = I\frac{1}{\Delta t}\int_{t-\Delta t}^{t} w(t')dt' - P(T(t) - T_{aim}) - D\frac{dT}{dt}, \tag{4.4}$$

where T_{aim} is the temperature level to approach or maintain, and P, I, D, Δt are constant parameters of the method.

However, it is not necessary to use the complicated equations above to describe/model the temperature in the cryostat, as long as the temperature steps are small. For small steps the cryostat temperature can be well approximated by the following function:

$$\delta T(t) = \Delta T - \Delta T\left(Ae^{-k_1 t} + (1-A)e^{-k_2 t}\right), \tag{4.5}$$

where A is a number larger than one, k_1 and k_2 are time-constants, and ΔT is the difference between the end temperature, T_{end}, and the starting temperature T_0. Note that constants in this equation can be chosen in a way that makes the resulting graph resemble that of a damped system; a quick look at the temperature of the cryostat plotted against time makes this approximation reasonable. If one ask the cryostat to perform a 2K jump in temperature, one would get something that looks the way it does in figure 4.3.

As seen from figure 4.3 it is fairly easy to get a good fit to the function given in equation 4.5.

4.2 Modeling of experiment - heating through a heat resistance

The analysis in the preceding sections was concerned with a number of examples, but only one of them investigated the spatial dependence of temperature in the sphere. In

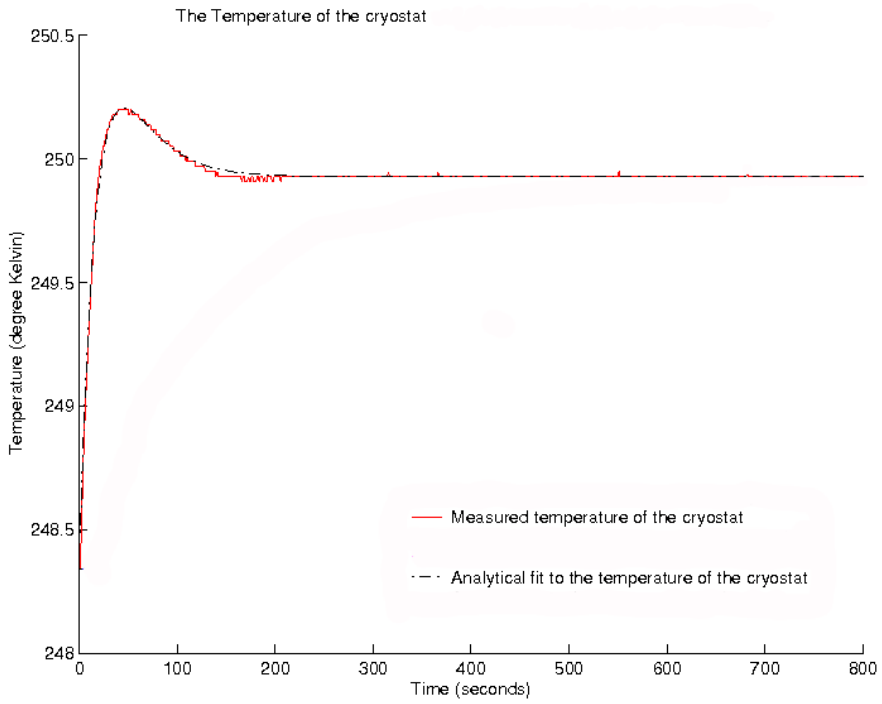

Figure 4.3 The temperature of the cryostat walls after it is asked to make a step of about 2K. Shown is also a fit to a function that normally describes a damped oscillation (4.5).

that case we considered the problem where a varying complex heat amplitude is given as the boundary condition on the surface of the sphere, whereas in the experiment we wanted to perform, we control temperature. So the prior results, showing that there is an instantaneous drop in temperature, common for the whole interior of the sphere, may in fact not be the case. As shown below, when you control temperature instead of heat current, the magnitude of cooling by heating depends on the distance from the center of the sphere. The first aim of this modeling was therefore to find out how precise you need to be in placing the "thermometer" in the center of the sphere.

Moreover, the fact that we are controlling the temperature of the walls of a cryostat, and heat then has to be transferred through air on its way to the sphere, leads to the question of how temperature in the sphere is affected by the heat resistance of the medium between the sphere and the walls of the cryostat.

To investigate this I consider the same case as the one in section 3.3, where a periodically varying heat $\delta Q(t) = \mathrm{Re}\left\{\delta Q e^{i\omega t}\right\}$ is supplied at the surface of a massive sphere of radius R. The boundary conditions used there were:

1. No displacement at the center: $u(0) = 0$
2. No temperature gradient at the center: $\frac{\partial \delta T}{\partial r}(0) = 0$
3. No radial stresses at the surface: $\sigma_{rr}(R) = 0$
4. The heat supply boundary condition at the surface: $\lambda \frac{\partial \delta T}{\partial r}(R) = i\omega \frac{\delta Q}{4\pi R^2}$

The solution was found to be given by

$$\frac{\delta T(r)}{\delta Q} = \frac{1}{c_p V_0}\left\{\frac{a_l}{a_l - 1} + \frac{1}{1 - a_l}\frac{(kR)^3}{kR\cosh(kR) - \sinh(kR)}\frac{\sinh(kr)}{kr}\right\} \tag{4.6}$$

Here V_0 is the sphere volume, k the complex frequency-dependent thermal wave vector $k = \sqrt{i\omega c_l(\omega)/\lambda}$ and a_l is the complex frequency-dependent dimensionless "longitudinal" coupling constant defined in Eq. 3.23.

To model the experimental conditions in our experiment, I will change boundary condition number 4 in the above list. I consider a case where we change the temperature of a spherical cavity (representing the walls of the cryostat) at a given distance from the surface of the sphere, and heat is then transferred through a heat resistance (air) into the surface of the sphere. Fouriers law of heat conduction in spherical geometry is given by

$$\frac{\delta Q}{r^2} = \frac{\lambda_s 4\pi}{i\omega}\frac{\partial \delta T}{\partial r}, \tag{4.7}$$

where λ_s is the thermal conductivity of the surroundings. Integrating from the radius of the sphere, R to the walls of the cavity, R_C, the heat supply boundary condition above can be changed to

$$\delta Q(R) = \frac{\lambda_s}{i\omega}\frac{3V_0}{R^2}\frac{b}{b-1}\left(\delta T_C - \delta T(R)\right), \tag{4.8}$$

where $b = \frac{R_C}{R}$ is the ratio of cavity to sphere radii, and δT_C is the temperature variation of the cavity. Substituting this into the solution given by Eq. 4.6, one obtains, after some algebra,

$$\frac{\delta T(r)}{\delta T_C} = \frac{\frac{(kR)^3}{kR\cosh(kR)-\sinh(kR)}\frac{\sinh(kr)}{kr} - 3a_l}{B(kR)^2 + \frac{(kR)^3}{kR\cosh(kR)-\sinh(kR)}\frac{\sinh(kR)}{kR} - 3a_l}, \tag{4.9}$$

where $B = \frac{\lambda}{\lambda_s}\frac{b-1}{b}$. From this it is possible to study the radial dependence of temperature, the influence of the coupling constant, a_l, and the effect of a varying heat resistance of the surrounding medium parametrized by B. Since I wanted to model a sphere of glucose I chose to fix the ratio of thermal conductivities, λ/λ_s in B, and instead vary b to investigate the B-dependence of the effect. For λ_s I used the thermal conductivity of air; the larger a thermal conductivity of the surrounding medium the better - a large heating rate at the surface induces a larger expansion rate. Likewise the smaller a thermal conductivity of the sphere, the longer time it takes the heat to reach the center of the sphere, and cancel the phenomenon we are looking for.

Restricting myself to the thermoelastic case (solid, where the constitutive properties are frequency independent), I calculate the temperature in the sphere as a response to a Heaviside step in temperature at the walls of the cavity, $\delta T_C(t) = \Delta T H(t)$. Note that this is not the actual case. The temperature changes in the cryostat is shown in Figure 4.3. This can of course be incorporated in the model, but for now I assume a Heaviside type step in temperature at the walls of the cavity. Making an inverse Laplace(-Stieltje)

transform by the standard residue calculus, the solution in the time-domain is found to be

$$\delta T(r,t) = \Delta T \left(1 + \sum_{n=1}^{\infty} R_n e^{-x_n \frac{t}{\tau}} \right), \tag{4.10}$$

where $\tau = R^2 c_l/\lambda$ is the characteristic diffusion time, $R_n = 2\frac{\frac{R}{r}\frac{\sin\left(\frac{r}{R}x_n\right)}{\sin(x_n)}\left(Bx_n^2+3a_l\right)-3a_l}{(B-1)x_n^2+9a_l-(Bx_n^2+3a_l)^2}$ are the residues and the x_n's are the roots of the transcendental equation given by $x\cot(x) = \frac{(B-1)x^2+3a_l}{Bx^2+3a_l}$.

4.2.1 Results of the modeling

Here I present the results of the modeling pertaining to the questions asked above. Since the choice of Glucose as the system to study, we fix the ratio of thermal conductivities based on literature values; for glucose - $\lambda = 8.23$cal/cm/s/K [23], and for air - $\lambda_s = 0.60$cal/cm/s/K. In all the figures below, I use a value of the coupling constant $a_l = 0.05$. That is, the relative difference between the longitudinal specific heat and the isobaric ditto is 5%. As the size of the temperature step I use $\Delta T = 5$K

Distance from sphere to cryostat walls

Regarding the distance from the surface of the sphere to the walls of the cryostat, we a priori expect the best result if they are closely spaced, which would make the parameter B smaller. In figure 4.4 we plot the minimum temperature reached (cooling by heating) at the center of the sphere as a function of time scaled by the characteristic diffusion time τ, which for a sphere of radius 1cm is about 1000 seconds.

To parameterize the curves I used the relative difference in radii, $B_b = \frac{R_C-R}{R_C} = \frac{b-1}{b}$. The figure shows that the dependence on B_b is not trivial, but as expected, it shows that the closer the surface of the sphere is to the walls of the cryostat, the larger the temperature dip due to cooling by heating. In the end we chose a diameter of the sphere of Glucose to be 19.1mm, corresponding to a $B_b = 0.045$. This was the largest sphere we could use without risking electrical contact between the wires and the walls of the cryostat. With this choice of B_b the minima in temperature occurs about $0.038\tau \approx 38$sec after the temperature step has been applied, giving enough time to do the measurement.

Centering the thermometer

In Figure 4.5 I have plotted the change in temperature, δT as a function of time in units of the characteristic diffusion time, τ, and again the coupling constant is set to $a_l = 0.05$, $B_b = 0.045$ and the temperature step is of size $\Delta T = 5$K. The different curves represent the temperature at different distances from the center of the sphere. The figure shows that there is room for placing the NTC-bead a bit off-center. When molding the sphere of glucose, we can place the NTC-bead within 1.5mm from the center of the sphere, which more or less corresponds to the red curve with cruxes with $r = 0.2R$ in Figure 4.5. For the parameter values chosen to make the plot in this figure,

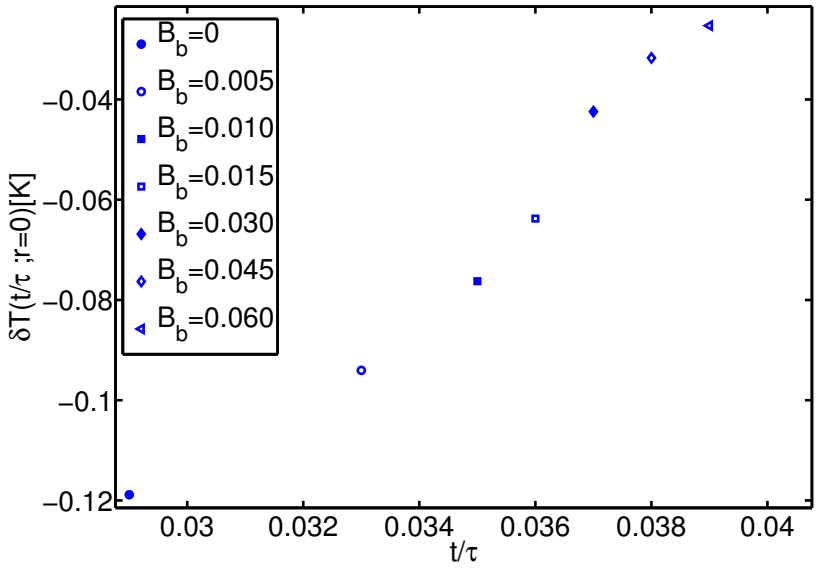

Figure 4.4 Figure showing the magnitude and position (in time) of the dip in temperature due to cooling by heating as $B_b = \frac{R_C - R}{R_C}$ is varied. The coupling constant was chosen to be $a_l = 0.05$ and the temperature step was taken to be $\Delta T = 5$K. The figure shows that the larger the distance from the spere to the walls of the cryostat (larger B_b), the smaller an effect of cooling by heating (in the thermoelastic case) in the center of the sphere as expected.

misplacing the NTC by that amount would mean measuring a temperature dip 15% smaller than the largest possible dip.

4.3 The measurements

Going through the steps in the molding scheme described in Appendix B, you end up with a sphere of Glucose in the glassy state, like the one shown in Figure 4.6. Even though you cannot see the NTC inside the sphere (since the sphere is partially crystallized), the photo shows clearly the wires that leads into the sphere, connecting the NTC to the terminals in the peek-plate shown in the photo. When mounted on a holder, the terminals get connected to the Multimeter that will do the resistance measurements.

Measuring scheme

Before doing a measurement, I followed the following procedure:

1. Bring down the temperature to the desired starting level.
2. Wait for the temperature to equilibrate. This is monitored by measuring the resistance every 5'th minute. The typical waiting time for my samples are 18

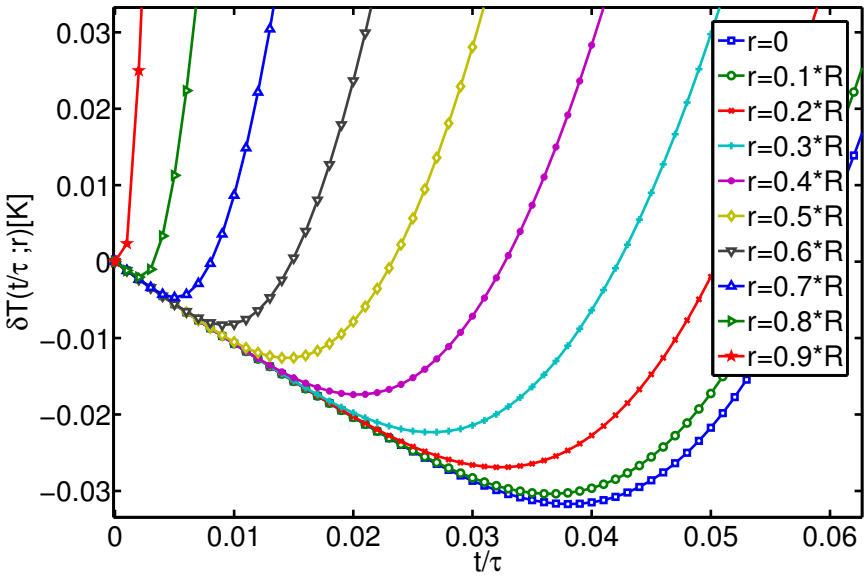

Figure 4.5 Temperature change as a function of time scaled by the characteristic diffusion time for different positions in the sphere. Here $B_b = 0.045$ is used together with a $a_l = 0.05$ and a temperature step of size $\Delta T = 5$K. The figure tells us that there is room for not being perfectly exact placing the NTC-bead. The red curve, $r = 0.2R$, would in our case ($R = 9.5$mm) correspond to the temperature 1.9mm from the center of the sphere.

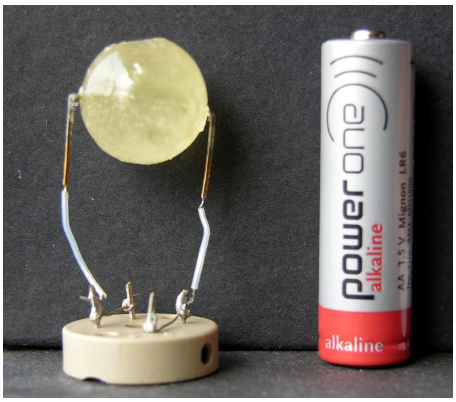

Figure 4.6 A photo of one of the spheres used in the measurements. At the time of the photo shoot (1 month after molding) the sample is no longer transparent - it has crystallized.

hours.

3. After the initial waiting time, I increase the sampling rate of the Multimeter to about 5 data points per minute. This is done for 1 hour to get a baseline like the one in Figure 4.7.

4. Make a temperature step of size 5K and continue the sampling of data for another 10 minutes with a sampling rate of 15 data points per minute..

Limitations and reproducibility

Below I present the results of the measurements. To be frank, the results are not entirely what I had hoped for. This is due to an annoying reproduction-problem. The first measurement on a newly molded sphere was always done at room temperature, giving a result like the one presented below. But after going through the steps 2-4 listed above, in order to do a measurement at the final temperature of the preceding jump, the phenomenon would either be reduced to almost within the noise level of the baseline, or not be detected at all. Even if I went back in temperature to do the measurement that just succeeded, did the situation not change. Only with a fresh sample could the phenomenon be reproduced. This leads me to the following hypothesis of what ruins the signal.

As described in Appendix B the spheres are made by "gluing" to half-spheres together. This could lead to the following problems:

- *Air bubbles:* When the two half-spheres are joined to produce the sphere, air is trapped forming small bubbles of air in the region where the two half sphere meet. If the bubbles accumulate on the NTC under the temperature jump, then the thermal contact to the sample is ruined. This I detected using a microscope, after one successful measurement that could not be reproduced with the same sample.
- *Cracks:* After one successful measurement that could not be reproduced, I registered a crack in the plane where the to halves of the sphere are "glued" together.

4.3.1 The results

In Figure 4.7 you see the temeprature measured by the NTC during a measurement with a step from 298K to 303K. You see the baseline that extends for 1 hour and then you see the characteristic dip in temperature. The size of the dip is 7.3 ± 0.2mK and is reached 36 seconds after the step is made.

I repeated the experiment on three different samples. The first measurement done on each sample, at the same temperature is summarized in Figure 4.8. Each marker represents lowest temperature reached in one measurement. They are plotted against time after the step is initiated with the cryostat.

4.4 Summary

Given the results of the measurements I conclude the following. There is a huge problem of reproducibility in the sense that the phenomenon of cooling by heating can only be detected measuring on a fresh sample. Above I suggested two causes for the vanishing of the signal: Formation of air bubbles and cracks. An other possibility could be that the sample starts to crystallize; even though it is a bit more speculative reason the phenomenon of cooling by heating itself points out a plausible explanation.

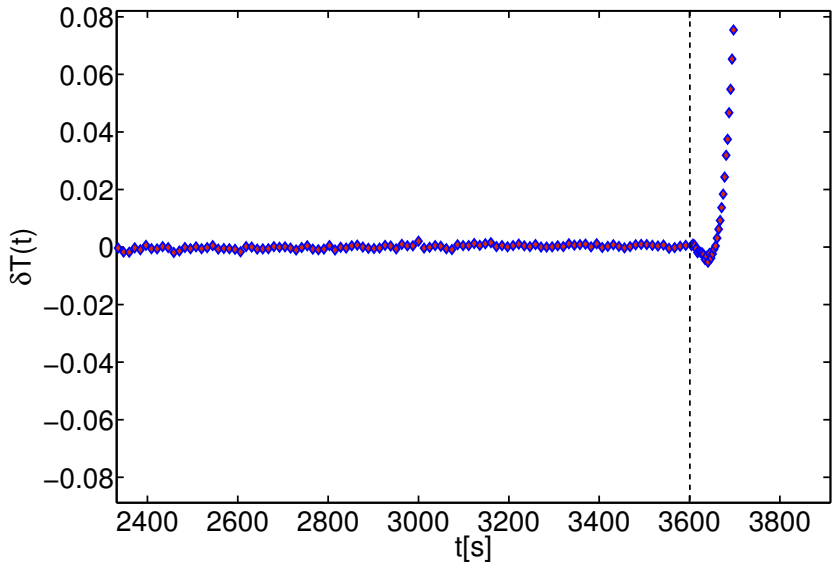

Figure 4.7

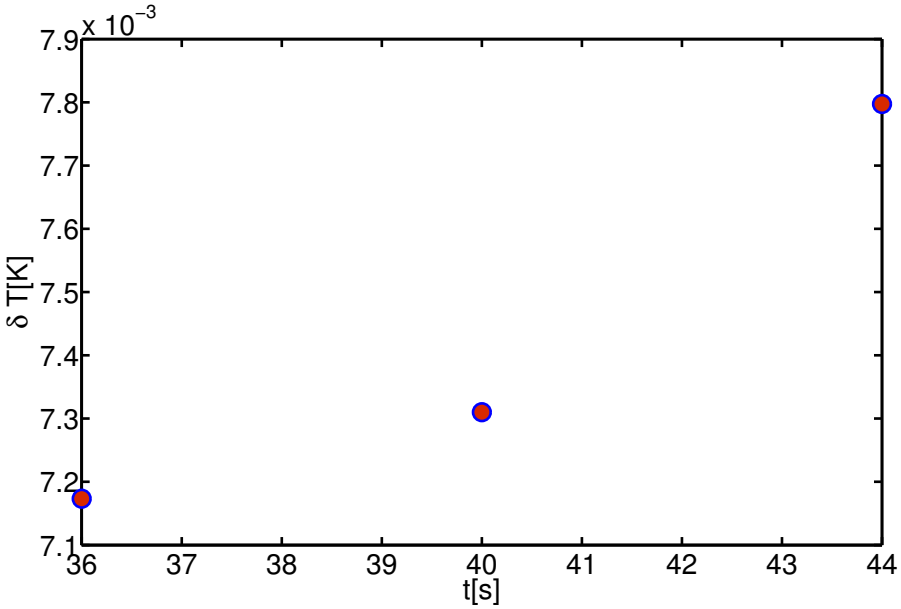

Figure 4.8

The phenomenon is the result of a decreasing pressure (density), which in principle increases the mobility of the molecules. In turn an increasing mobility could facilitate crystallization, starting in the center of the sphere.

Given the unfortunate situation I have to seek comfort in the systematic nature of the

problems reproducing the measurements, and attempt to analyze the results anyway. The measurements done on the fresh samples seem to give a drop in temperature with a magnitude about the same size in the three samples that all had the same thermal history, see Figure 4.8. The difference between them can be accounted for if you compare with the finding in the modeling section, i.e. Figure 4.5. That is, if the NTC was placed at different distances from the center in the three samples, the measured change in temperature would not be the same. The position of the minima also indicates that this could be the case.

A comparison with the modeling section should also be made, and two points of critique can be made: The first is that I model a solid sphere of glucose, placed in a spherical cryostat. This is certainly not the case - it is cylindrical. The second point is that I assume a Heaviside step in temperature at the walls of the cryostat. This is also not the case - it is more like a critically damped oscillation like in Figure 4.3. Therefor it would not make sense to fit the measured curves to Eq. 4.10 in order to extract a value of the coupling constant.

If I were to include the real temperature profile on the walls of the cryostat it would give a smaller temperature drop in the sphere. Likewise the cylindrical geometry of the cryostat cavity, can as a first approximation be modeled by setting the radius of the spherical cavity in the model a bit larger than the radius of the cylindrical cryostat. This would reduce the temperature drop further. Therefore, the value chosen for the coupling constant in the modeling section, $a_l = 0.05$ might not be to far off after all.

Regardless of the reproducibility question, the following conclusion can be made. The experiments shows, that there is a non-negligible difference between the longitudinal specific heat and isobaric specific heat in glassy Glucose, as the existence of the phenomenon of cooling by heating is not possible otherwise.

5 Cooling by heating - a molecular dynamics study

The motivation for this work is the following. The experimental results presented in the preceeding Chapter 4 were the result of measurements on a glassy sphere of glucose. A Molecular Dynamics (MD) study of the phenomenon would complement the preceding results proving the existence of the phenomenon of cooling by heating, also in the liquid state. Also, this gives the opportunity to investigate how the phenomenon of cooling by heating is affected when you shrink your system. When going down in size, letting the characteristic length of your system approach the molecular scale, the length of acoustic and thermal wave vectors become comparable. The acoustic wave vector is given by $q^2 = \frac{s^2}{c_s}$ where s is the Laplace frequency ($s = i\omega$) and c_s the speed of sound. The thermal wave vector is given by $k^2 = \frac{s}{D}$, where D is the heat diffusion constant. Inserting values typical for the two quantities - $c_s \sim 3 \cdot 10^3 {}^{\mathrm{m}}/_{\mathrm{sec}}$ and $D = 10^{-7} {}^{\mathrm{m}^2}/_{\mathrm{sec}}$, you get the following estimate for the ratio of the squared length of the wave vectors

$$\frac{q^2}{k^2} = 10^{-14} \cdot 2\pi f \approx 10^{-13} \cdot f, \tag{5.1}$$

where $f = {}^{\omega}/_{2\pi}$. Taking the system to be a sphere with a radius $r = 10^{-8}$m, its characteristic acoustic frequency, $f = \frac{c_s}{\pi r} \approx 10^{11}$Hz, gives a ratio $\frac{q^2}{k^2} \approx 10^{-2}$. This means that for a system this size, only a factor 10 separates the lengths of the thermal and acoustic wave vectors.This separation could easily be reduced with a slight change in the values used for the speed of sound and heat diffusivity. So for a nano sized object, one is moving close to a situation where the distinction between acoustic and thermal waves starts to become blurred. Further more, for nano-sized objects, the assumption that acoustic waves propagate adiabatically begins to break down. The upper bound on the frequency that will assure adiabatic propagation is found by comparing the distance heat can travel (given by the diffusivity) during half a period of the acoustic wave. Doing this, using the above values of the speed of sound and diffusivity, you find that the adiabatic assumption reads

$$f \ll \frac{c_s^2}{2\pi^2 D} \approx 10^{12}\text{Hz}. \tag{5.2}$$

This corresponds to a bound on the timescale in the picosecond range, $\tau \gg 1$ps - the typical time scale studied in MD simulations. The above observations should also be compared to the fact that the assumption used in the two preceding chapters - the assumption of being in the inertia-free limit, begins to break down. Therefor it is interesting to see if the phenomenon of cooling by heating is also present in a very

small object, like the ones you can study with MD simulations. Also such a study could give yet another proof of concept of the phenomenon, which is not clouded by problems of reproducibility. The following gives a brief presentation of what you find when simulating the heating of a spherical nano sized droplet on its mechanically non-clamped surface.

5.1 Preparing the simulations

Almost all MD-simulations [1] of supercooled systems are performed with the Kob-Andersen binary mixture of Lennard-Jones particles (KABLJ) [25]. This system consist of 80% A-particles and 20% smaller B-particles in a strong exothermic mixture, which makes it very resistant against crystallization [26]. The glas transition temperature, T_g is estimated to be $T_g = 0.438$ [25] for a uniform system of $N = N_{\mathrm{A}} + N_{\mathrm{B}} = 1000$ Lennard-Jones (LJ) particles at a density, $\rho = 1.2$. A droplet of only one thousand particles is, however, much too small to establish the effect. For this reason we created a droplet of N=500.000 particles. The reason for choosing such a big number is to make sure that there is time enough to measure an effect of thermomechanical coupling before everything is washed out by the diffusion of heat, and to secure the separation of acoustic and thermal waves.

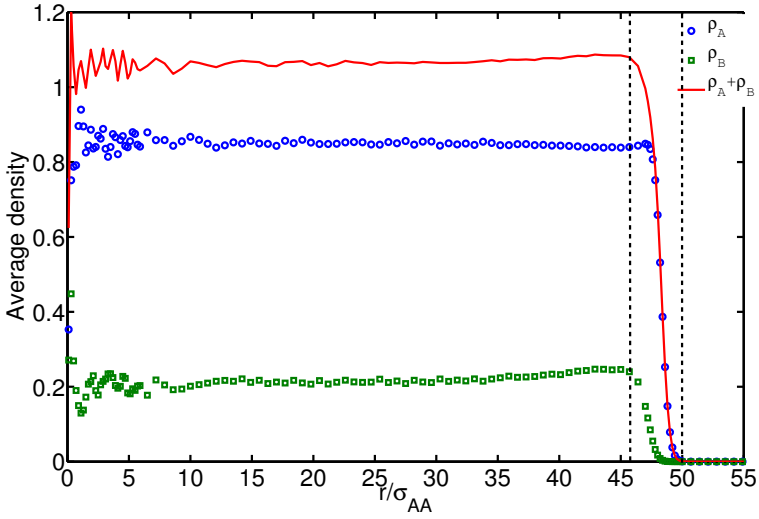

Figure 5.1 Density profile, $\rho(r)$, averaged over a short equilibrium run. Shows the density as a function of the distance r from the center in the droplet before the thermal wave was created. The KABLJ droplet consists of solvent A-particles and solute B-particles. The droplet is later heated up in the surface shell at $r \approx 50$, marked by the vertical lines

A droplet of $N = 500.000$ KABLJ particles was created in the following way: A KABLJ

1 For MD details see [24]. Unit length, energy and time is σ_{AA}, ϵ_{AA} and $\sigma_{\mathrm{AA}}\sqrt{m_{\mathrm{A}}/\epsilon_{\mathrm{AA}}}$, where σ_{AA} and ϵ_{AA} is the length and the energy parameters in the Lennard-Jones (LJ) potential $u_{\mathrm{AA}} = 4\epsilon_{\mathrm{AA}}[(\sigma_{\mathrm{AA}}/r)^{-12} - (\sigma_{\mathrm{AA}}\ /r)^{-6})$.

system of $N = 1000$ particles was calibrated at a density of $\rho = 1.2$ and temperature $T = 0.40$. A number of copies of the system were then fused into a huge system, from which a spherical droplet consisting of 500.000 particles was cut out. The droplet was then placed in a container with a box-side length 10 times larger than the radius of the droplet [27]. Droplets were then equilibrated at 3 temperatures: $T = 0.38, 0.40, 0.42$, all below the glass-temperature.

Figure 5.1 shows the density profile of a droplet at the temperature $T = 0.40$ where the density of the bulk is approximately $\rho = 1.07$. I took the relaxation time, τ_α of the systems to be given by the time when the AA incoherent intermediate scattering function in a KABLJ is equal to $1/e$ (at wave vector $q = 7.25(\rho/1.2)^{1/3}$ [28]). Then simulations were run at the three state points, dumping configurations separated by $2\tau_\alpha$, creating an ensemble consisting of 300 droplets with uncorrelated start configurations at each state point.

5.2 Simulation details

In the production runs I thermostated the particles in a concentric shell containing the surface of the droplet, keeping track of all the particles during the whole run. The particles in the shell were defined as those that are situated in an interval of radii from the center shown by vertical lines in figure 5.1. These particles were thermostated by a Nose-Hoover thermostat (NHT) [24]. The NHT thermostat consists of a "friction therm" in the classical equations of motion and the thermostat has a relaxation parameter τ_T which controls the heat flow into and out of the system. A big value of τ_T results in big and slow oscillations of the temperature T around the target temperature whereas a small value of τ_T results in small and quick oscillations [2]. The NHT thermostated particles are not accelerated (heated) or damped (cooled) by particle collisions, but by the dynamic friction parameter in the equations of motion, by which you in general can avoid thermal waves in the system if all particles are coupled to the thermostat. In the present simulations however, I wanted to create a thermal wave by heating only the particles at the surface.

The thermal wave was started by increasing the thermostate temperature with $\delta T = 0.04$, for particles in the surface shell. This was done in the following way. First I used a big value of τ_T for a short time creating “Heaviside-like” step change in temperature. At the time where the temperature reached the desired value, I switched to a smaller value of τ_T which immediately stabilized the temperature at the new target temperature $(T + \delta T)$ in the surface shell. The NHT thermostating with the small value of τ_T then continued for the rest of the production run, lasting in all 12000 time steps. The temperature evolution in the surface shell of one droplet is shown in figure 5.2 for the step done from $T = 0.40$ to $T = 0.44$.

In order to calculate the local quantities, like density and temperature I divided the system into concentric shells, with some given thickness. In all the figures shown in

2 A natural time unit for a MD thermostat is the mean collision time τ_c of the thermostated particles. A small value of the thermostats relaxation time, τ_T, corresponds to $\tau_T \approx \tau_c$

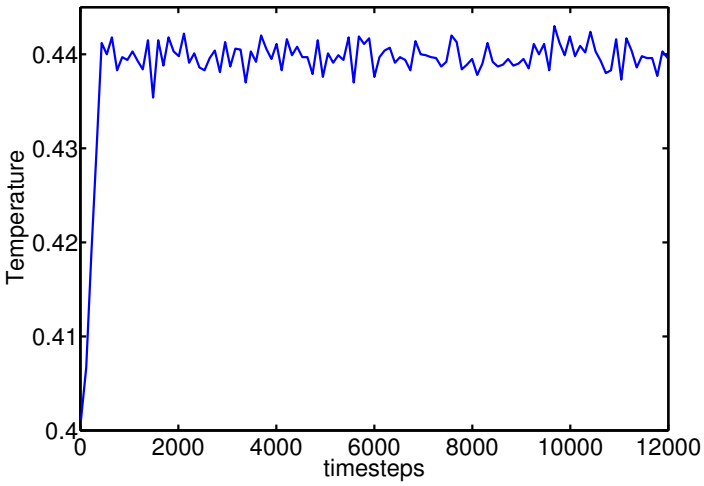

Figure 5.2 Temperature evolution in the thermostatted shell (surface) indicated by the vertical dashed lines in Figure 5.1. After a short heating of 390 time steps with a big value of τ_T, the shell was calibrated the rest of the production run with a $\tau_T \approx \tau_c$, at $T = 0.44$

this work I chose to divide the droplets into 10 shells. This number is based on a compromise to secure good enough statistics, especially in the innermost shells, but still get a good enough resolution in order to study the evolution of the temperature in the shells.

5.3 Results

The evolution of temperature and displacement fields were analyzed in the preceding chapter. The analysis included the evolution of stresses and pressure after a spherical system had been perturbed thermally at its surface. However, only addition of heat, or jumps up in temperature at the surface of the sphere were considered, while the effect of a removal of heat, or jump down in temperature was not. In the thermoelastic case (solid) where one can ignore memory effects and the influence of temperature on relaxation properties of the system, one would expect the phenomenon to be symmetric with respect to the direction of heat transfer.

Figure 5.3 shows the temperature of two sections, r_6 and $r_7 > r_6$, of the droplet. They are located about half-ways in to the droplet after a step up, $\Delta T > 0$, and a step down, $\Delta T < 0$, in temperature has been applied at the surface of the droplet, on the same starting configuration, at a temperature $T = 0.42$. The plot is quite busy, but shows the following. During the first 500 time steps or so, the evolution is identical for the two temperature steps. The next 1000 time steps show a change in temperature due to an acoustic wave that is induced by the temperature step at the surface. After this the evolution in temperature differs in the two shells. In the outermost shell, r_7,

the diffusion of heat kicks in immediately, while in r_6, cooling by heating is seen; the thermal expansion of the surface causes an adiabatic cooling/heating of the interior of the droplet. Eventually, after yet another 2500 time steps or so, diffusion of heat gives an increase/decrease in this region as well. The figure also shows, that clearly, the phenomenon of cooling by heating exists in a nano-sized object, and that it is symmetric with respect to the sign of the applied temperature step.

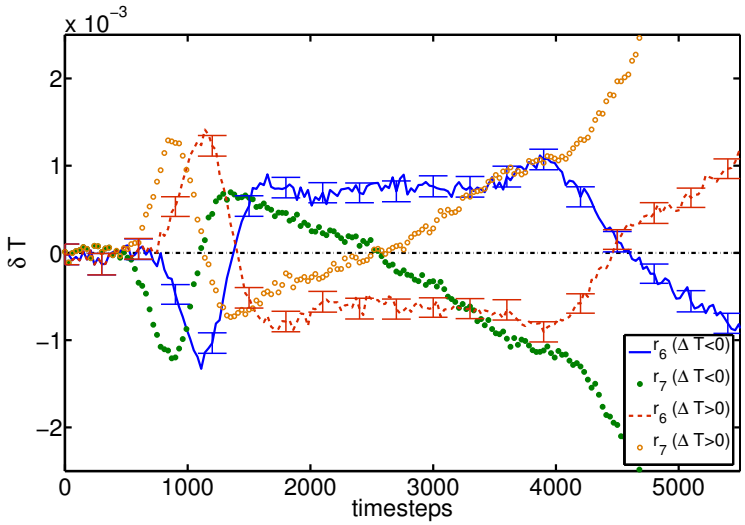

Figure 5.3 Temperature change, δT as function of time steps in two shells at radii r_6 and $r_7 > r_6$ after steps up, $\Delta T > 0$, and down $\Delta T < 0$, in temperature on the surface of the droplet at time $t = 0$, starting at temperature $T = 0.42$. The error-bars, giving the error on the ensemble mean, is shown for the innermost shell, r_6, which has worse statistics than in r_7. An interpretation of this busy figure is given in the text, but besides that, this figure shows that the evolution in temperature is symmetric with respect to the sign of the temperature step applied on the surface.

Figure 5.4 shows the temperature as a function of time for a number of concentric shells in the droplet. When the temperature at the surface is increased from $T = 0.40$ to $T = 0.44$, it induces an acoustic wave which travels in towards the center of the sphere and results in an increase in temperature due to the thermomechanical coupling. In the outermost shells this is followed by an increase in temperature due to heat diffusing in to these regions. In regions closer to the center, this is not the case. Instead you see a decrease in temperature due to cooling by heating, an effect which becomes more pronounced the closer you get to the center of the sphere. This was anticipated by the modeling done in Chapter 4. In Figure 5.4 I have left out the innermost shell. The reason for this is twofold. First of all, since the number of particles in the shells - they all have the same thickness, decreases as one gets closer to the center of the droplet, the noise increases as there are fewer particles to average over, resulting in large error bars. An other interesting thing that takes place is the focusing of the acoustic wave in the center of the droplet. The figure shows how the energy of the acoustic wave, when distributed in smaller and smaller regions, results in larger temperature changes. Curves r_2 and r_3 shows how the reflected acoustic wave (phase shifted) is giving an

additional decrease in temperature overlapping the effect of cooling by heating. The reflected wave propagates outwards giving the complicated evolution in temperature shown. For example the curves representing the innermost parts of the sphere seem to cross in a systematic manner at approximately 3500 time steps.

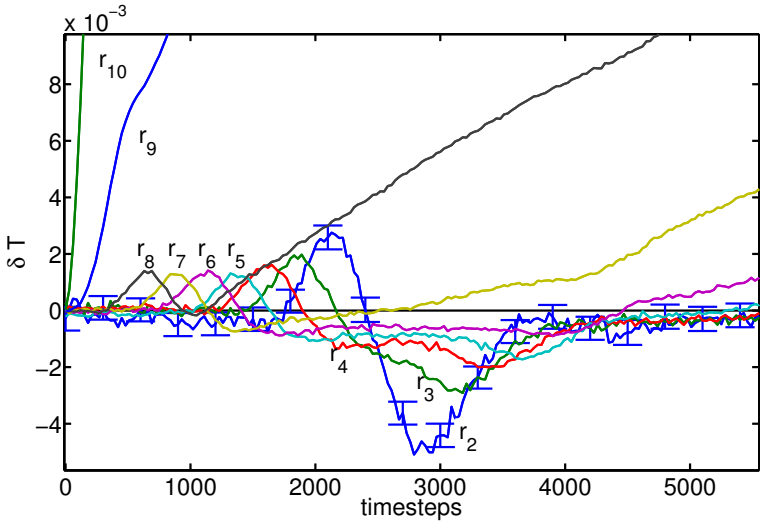

Figure 5.4 The temperature change as a function of time for a number of radii after a temperature step from $T = 0.40$ to $T = 0.44$ has been applied at the surface of the droplet. The uppermost curve represents the temperature of the thermostated surface. The curve below refers to a radius a bit closer to the center of the droplet, and so on. For all radii one first sees the elastic wave that is induced by the step in temperature on the surface of the droplet. In the outermost parts of the droplet, this is followed by an increasing temperature due to the diffusion of heat. However, for the innermost parts of the droplet the elastic wave is followed by the phenomenon of cooling by heating. The figure shows that the size of the effect increases the closer you get to the center of the droplet, as anticipated in Chapter 4. The error bars represent the error of the mean taken over an ensemble consisting of 300 droplets. On the other curves, the error is much smaller, since the number of particles increases with increasing radius giving better statistics as radius is increased.

This crossing of the curves is difficult to explain, but I have found more than one member of the ensemble which crystallizes from the center and outwards. A plausible explanation could be that the drop in density that accompanies the temperature drop, which is the largest in the center, increases the mobility of the particles, thus facilitating crystallization. I have not looked into this yet, since it requires many hours of looking at an enormous number of huge configurations to make proper statistics. However, it would be interesting to calculate a crystallization rate and compare with the crystallization rate found in equilibrium simulations of the same type of system (but smaller) at corresponding temperatures and densities.

5.4 Summary

In this chapter I have shown that the phenomenon of cooling by heating exists also in a nano-sized object, which is not fully described by the set of equations used to model the phenomenon in the preceding chapters. The results complement the previous results where experimental difficulties made it impossible to (re)produce a whole set of measurements on one sample.

Bibliography

[1] Aims & scope of journal of thermal stresses, apr 2011.

[2] G. Ya. Aleshin, J. C. Mollendorf, and J.D. Felske. The temperature response of a metallic rod near a s̈tream explosion: *Int. Comm. Heat Mass Transfer*, 26(4):509–512, 1999.

[3] G. Ya. Aleshin. New working hypothesis of the s̈team-explosionp̈henomenon. *Int. Comm. Heat Mass Transfer*, 24(4):497–505, 1997.

[4] J. Papini and J. Heebøll-Christensen. Pyroelectricity-a new application for the piezoelectric bulk transducer. Master's thesis, Roskilde University, 2008.

[5] T. Hecksher. *Relaxation in supercooled liquids.* PhD thesis, Roskilde University, 2011.

[6] T. Christensen, N. B. Olsen, and J. C. Dyre. Conventional methods fail to measure $c_p(\omega)$ of glass-forming liquids. *Physical Review E*, 75:041502, 2007.

[7] T. Christensen and J. C. Dyre. Solution of the spherically symmetric linear thermoviscoelastic problem in the inertia-free limit. *Physical Review E*, 78:021501, 2008.

[8] H. S. Carslaw and J. C. Jaeger. *Conduction of Heat in Solids.* Clarendon, Oxford, 1959.

[9] R. O. Davies and G. O. Jones. Thermodynamic and kinetic properties of glasses. *Adv. Phys.*, 2:370, 1953.

[10] H. H. Meyer and John D. Ferry. Viscoelastic properties of glucose glass near its transition temperature. *TRANSACTIONS OF THE SOCIETY OF RHEOLOGY*, 9:2:343–350, 1965.

[11] T. Christensen. personal communication.

[12] W. Z. Meissner. *Z. Angew. Phys.*, 75(1-2), 1948.

[13] T. A. Litovitz. Temperature dependence of the viscosity of associated liquids. *Journal of Chemical Physics*, 30(7):1088–1089, 1952.

[14] Yoon H. Jeong. Frequency-dependent shear modulus of glycerol near the glass transition. *Physical Review A*, 36(2):766–773, 1987.

[15] Shulz. *Kolloid Zeitschrifft 138*, 138:75, 1954.

[16] F. R. de Hoog, J. H. Knight, and A. N. Stokes. An improved method for numerical inversion of laplace transforms. *S.I.A.M. J. Sci. and Stat. Comput.*, 3:357–366, 1982.

[17] K. J. Hollenbeck. Invlap.m: A matlab function for numerical inversion of laplace transforms by the de hoog algorithm, January 2011.

[18] S. Vyazovkin and I. Dranca. Comparative relaxation dynamics of glucose and maltitol. *Pharmaceutical Research*, 23(9):2158–2164, 2006.

[19] L.-M. Wang, C. A. Angel, and R Richert. Fragility and thermodynamics in nonpolymeric glass-forming liquids. *Journal of Chemical Physics*, 125:074505, 2006.

[20] R. Wungtanagorn and S. J. Schmidt. Phenomenological study of enthalpy relaxation of amorphous glucose, fructose, and their mixtures. *Thermochimica Acta*, 369:95–116, 2001.

[21] J.-A. Seo, J. Oh, H. K. Kim, Y.-H. Hwang, Y. S. Yang, and S. J. Kim. Study of glass transition temperatures in sugar mixtures. *Journal of the Korean Physical Society*, 46(3):606–609, 2005.

[22] A. Hoshino, K. Shinozaki, Y. Ishisaki, and T. Mihara. *Nuclear Instruments and Methods in Physics Research A*, 558:536–541, 2006.

[23] E. S. Greene and G. S. Parks. Xvii. the thermal conductivity of glassy and liquid glucose. *Journal of Chemical Physics*, 9:262–265, 1941.

[24] S. Toxvaerd. Algorithms for canonical molecular dynamics simulations. *Mol. Phys.*, 72:159, 1991.

[25] W. Kob and H. C. Andersen. *Phys. Rev. E*, 51:4626, 1993.

[26] S. Toxvaerd, U. R. Pedersen, T. Schrøder, and J. C. Dyre. *J. Chem. Phys.*, 130:224501, 2009.

[27] S. Toxvaerd. *J. Chem. Phys.*, 117:10303, 2002.

[28] U. R. Pedersen, T. B. Schøder, and J. C. Dyre. *Physcial Review Lett*, 105:157801, 2010.

Part II

Complete triple of thermoviscoelastic response functions

6 Introduction

In the Roskilde Glass and Time group there has been a long tradition of measuring thermoviscoelastic response functions [1–8]. Among these the most well established technique, along side the measurement of the frequency dependent shear modulus, is the method to determine the adiabatic bulk modulus. The measuring cell used to do these measurements is the piezoelectric bulk modulus gauge (PBG) [2]. The PBG is basically a piezoelectric spherical shell polarized in the radial direction and coated on both sides with electrodes. Applying an alternating electric field to it results in deformation of the ceramic, thus changing the volume inside the shell. If a liquid is introduced in the interior of the shell, it will oppose the deformation of the ceramic, thus changing the measured capacitance. Comparing the capacitance measured on the liquid filled PBG to the capacitance measured of the empty shell, one deduces the frequency dependent adiabatic bulk modulus of the liquid. This technique covers up to 6 decades in frequency in the range 10mHz − 10kHz.

Another method which has been documented just recently [8] is the measurement of the frequency dependent longitudinal specific heat in spherical geometry. The method employs thermal waves that effuse radially out from the surface of a spherical thermistor bead that acts both as a heat generator and thermometer. A nice thing with this method compared to other effusivity measurements is that the spherical geometry of the setup introduces an extra characteristic length scale (radius of the thermistor) besides that of the heat diffusion length. This makes it possible to extract both the thermal conductivity and specific heat from the measured signal independently. On the other hand the frequency range of the method becomes limited to cover only $2-3$ decades between 10mHz − 10Hz.

The introduction of this thesis presented the concept of internal parameters and the consequence of having a single internal parameter that determines the structural relaxation of a liquid. In [9] members of the Glass and Time group gave a rigorous reformulation of the classical PD-ratio test of "single parameterness" for equilibrium liquids in terms of (four) dynamic PD-ratios. The one most easily accessible from an experimental viewpoint is Λ_{sp} defined by:

$$\Lambda_{sp}(\omega) = -\frac{\left(T/c_p(\omega)\right)'' \kappa_s''(\omega)}{\left[\left(1/\beta_s(\omega)\right)''\right]^2}, \tag{6.1}$$

It contains the complex frequency-dependent specific heat $c_p(\omega)$, adiabatic compressibility $\kappa_s(\omega)$ and the adiabatic pressure coefficient $\beta_S(\omega) \equiv (\delta p(\omega)/\delta T(\omega))_S$. As mentioned above we can measure $\kappa_s(\omega) = 1/K_S(\omega)$ with the PBG. Mounting a thermistor

bead in the center of the PBG we can measure $c_l(\omega)$ under identical conditions on the very same sample. The setup is illustrated in Figure 6.1.

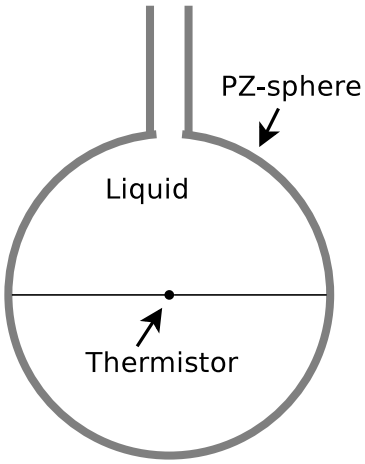

Figure 6.1 Thermistor bead inside the PBG - the setup of the triplet experiment.

This part of the thesis explores the possibility of combining the two censors in order to measure the third quantity that goes in to the dynamic PD-ratio, namely $\beta_S(\omega)$. In companion paper C.1 in the appendix of this thesis we deduce how the expansion of the liquid upon heating in the center affects the measured capacitance of the PBG. The rest of this chapter concerns the theoretical basis of these experiments.

Before exploring this a final note should be made in relation to the PD-ratio. As mentioned we do not measure the isobaric specific heat needed to calculate the PD-ratio given by Eq. 6.1. Instead we measure the longitudinal specific heat c_l, which was defined in Part I of this thesis. There we discussed the consequences of the longitudinal specific heat not being equal to the isobaric specific heat. However, the results obtained by measurements on Glucose in Chapter 4 indicate that the two specific heats differ only by a small amount. In any case, lets say that a series of measurements produce the set of complex frequency-dependent parameters c_l, κ_s and β_s. Then using the definition of the longitudinal specific heat:

$$c_l = \frac{\frac{1}{\kappa_s} + \frac{4}{3}G}{\frac{1}{\kappa_T} + \frac{4}{3}G} c_V, \tag{6.2}$$

where G is the shear modulus, together with the identities [10]

$$\frac{c_p}{c_V} = \frac{\kappa_T}{\kappa_S} \qquad \text{and} \qquad \kappa_T - \kappa_S = \frac{c_p}{T_0 \beta_S^2}, \tag{6.3}$$

the deviation between the longitudinal and isobaric specific heat may be expressed by

$$\frac{1}{c_p} = \frac{1}{c_l} - \frac{1}{T_0 \beta_S^2} \frac{\frac{4}{3}G}{1 + \frac{4}{3}G\kappa_S}. \tag{6.4}$$

This gives c_p in terms of the three quantities measured in the triplet experiment. One only has to supplement with a measurement of the shear modulus G, which is experimentally accessible by the Piezoelectric Shear modulus Gauge (PSG) developed by Tage Christensen and Niels Boye Olsen in the Glass and Time group [5].

To sum up we have an experimental setup that in principle can be used to measure a complete set of thermoviscoelastic response functions. The force of this approach is the fact that the measurements are done on the same sample, in the same cryostat under the same conditions. If the measurement of the pressure coefficient can be developed to a fully operational method, an unprecedented determination of the dynamic PD-ratio will be possible. This would constitute a reliable test of "single parameterness" of real liquids not seen so far. The following section gives the theoretical basis for the triplet experiment.

6.1 The transfer matrix of a spherical system

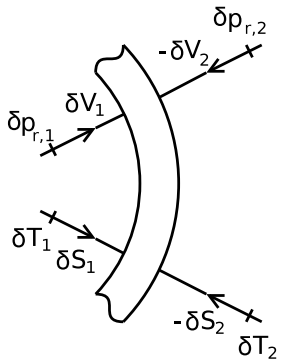

Figure 6.2 Depiction of the four thermal and mechanical interactions at the boundaries r_1 and r_2 of a spherical system.

The interaction of a spherical system with its surroundings is depicted in Figure 6.2 in terms of four thermal and mechanical bonds at the boundaries r_1 and r_2. In the experiments we will do the thermistor interacts with the liquid through the bonds at r_1, while the interaction of the liquid with the PBG takes place at the bonds at r_2. The different measurements in the triplet experiment is realized by combining different inputs and outputs. The situation can be simplified a bit by assuming that the volume of the thermistor bead is constant during the measurement. This is a reasonable assumption corresponding to no displacement of volume in the mechanical bond at r_1. In the measurement of the bulk modulus, the lowest frequency of operation is roughly 10mHz. The corresponding heat diffusion length is given by $|l_D| = |\sqrt{\frac{D}{i\omega}}|$ and using a value of $D = 0.1^{\mathrm{mm}^2}/_{\mathrm{s}}$, typical of liquids, the heat diffusion length is around 1.3mm. This should be compared to the inner radius of the transducer which is $r_2 = 9$mm, meaning that the bulk modulus is measured under adiabatic conditions. Likewise, when generating a heat current at r_1 by joule heating, the thermal wave created at the lowest frequency is damped out after $|l_D| = 4$mm. So in all three experiments of the triplet we can neglect the thermal boundary condition at r_2.

The combined response to the thermal stimuli at r_1 and mechanical stimuli at r_2 has been solved in [10] and is given in terms of the transfer matrix

$$\begin{pmatrix} \delta T \\ i\omega\delta S \end{pmatrix}_1 = \begin{pmatrix} i\omega T_0 Z_{th} V_2 \kappa_S \beta_S & T_0 Z_{th} \beta_S \\ i\omega V_2 \kappa_S \beta_S & \beta_S \end{pmatrix} \cdot \begin{pmatrix} \delta p_r \\ i\omega\delta V \end{pmatrix}_2 \tag{6.5}$$

Here $V_2 = \frac{4\pi}{3} r_2^3$ and Z_{th} is the thermal impedance

$$Z_{th}(\omega) = \frac{1}{4\pi r_1 \left(1 + \sqrt{i\omega r_1^2 c_l(\omega)/\lambda}\right)}. \tag{6.6}$$

Besides the thermal conductivity λ we see that the c_l enters the thermal impedance. The determinant of 6.5 is zero although a transfer matrix relating proper conjugated variables should have determinant 1. The reason for this is that we are studying a limiting case $|i\omega Z_{th} T_0 V_2 \kappa_S \beta_S^2| \gg 1$. The simplified transfer matrix can be represented by the equivalent diagram shown in Figure 6.3. The equivalent diagram is a more correct description since it leads to a transfer matrix deviating from Eq. 6.5 only with a negligible term $1/\beta_S$ in the 11-component of the matrix. However, the equivalent diagram has a determinant of 1 and is used later in the modeling of the combined experiment leading to β_S.

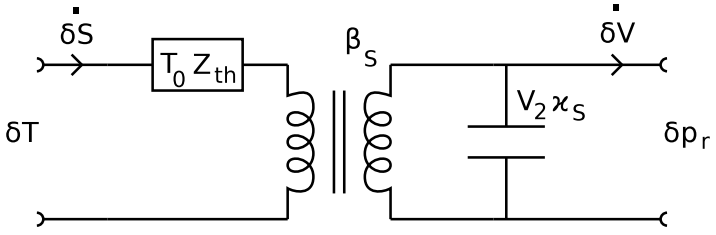

Figure 6.3 Equivalent diagram of the liquid representing Eq. 6.5.

The solution given by Eq. 6.5 infers three results. The normal stress response to compression at r_2 becomes

$$-V_2 \left(\frac{\delta p_r}{\delta V}\right)(r_2) = K_S, \tag{6.7}$$

the adiabatic bulk modulus. The temperature response on the inner surface to a thermal current of amplitude $P_{th} = i\omega T_0 \delta S$ becomes

$$\left(\frac{\delta T}{P_{th}}\right)(r_1) = Z_{th}. \tag{6.8}$$

Finally one has

$$P_{th}(r_1) = i\omega T_0 V_2 \kappa_S \beta_S \delta p_r(r_2) + i\omega T_0 \beta_S \delta V(r_2). \tag{6.9}$$

This means that the relation between thermal current at r_1 and volume displacement and negative normal stress at r_2 is not affected by any kind of thermal diffusion.

In order to measure κ_S, c_l and β_S we need to model the two devices in the setup, i.e. we need the corresponding transfer matrices - or equivalent diagrams, for the thermistor bead and PBG respectively.The two auto response functions (connecting conjugated variables of the same bond), κ_S and c_l, constitute a prerequisite for the measurement of the cross response function (connecting conjugated variables of different bonds), β_S. As mentioned above the methods to measure the auto responses are well established techniques, that I will only cover briefly in the next chapter (Chapter 7).

7 Bulk modulus and specific heat

The PBG with thermistor mounted in the center of the cavity is sketched in Figure 7.1. The liquid to be measured on is inserted in the cavity using a syringe. The pipe on top of the hole is there to contain excess liquid that can be sucked in to the cavity as temperature is lowered and the liquid contracts.

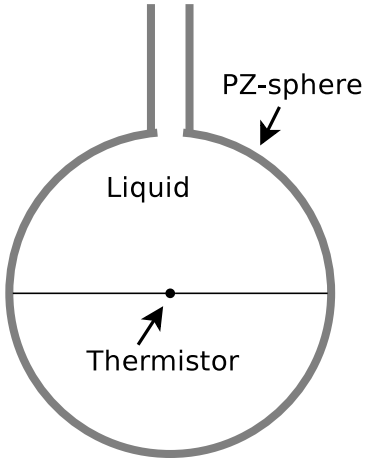

Figure 7.1 Thermistor bead inside the PBG - the setup of the triplet experiment.

Going down in temperature to reach the relaxation region, one has to be careful. If cooling to much the sample may crack and destroy the PBG. The liquid I have studied here is a vacuum diffusion pump oil called DC705 (1,3,5-trimethyl-1,1,3,5,5-pentaphenyltrisiloxane). It never crystallize and the Glass and Time group has gained quite a lot of experience measuring on this liquid. Its glass transition temperature has been determined by dielectric measurements using the temperature where the dielectric loss peak is at 1mHz - this gives a $T_g = 230K$.

7.1 Bulk modulus

In Figure 7.2 I have shown the real part of the measured capacitance of the empty transducer (full lines) and the liquid filled transducer (dots) for temperatures ranging from 300K − 237K. The spectrum of the empty transducer shows a resonance at the high end of the spectrum (around 100kHz. In the liquid-filled spectrum there is a resonance at lower frequencies. This is due to the liquid flowing in the hole and as the liquid gets more viscous lowering the temperature, the resonance moves to lower frequencies.

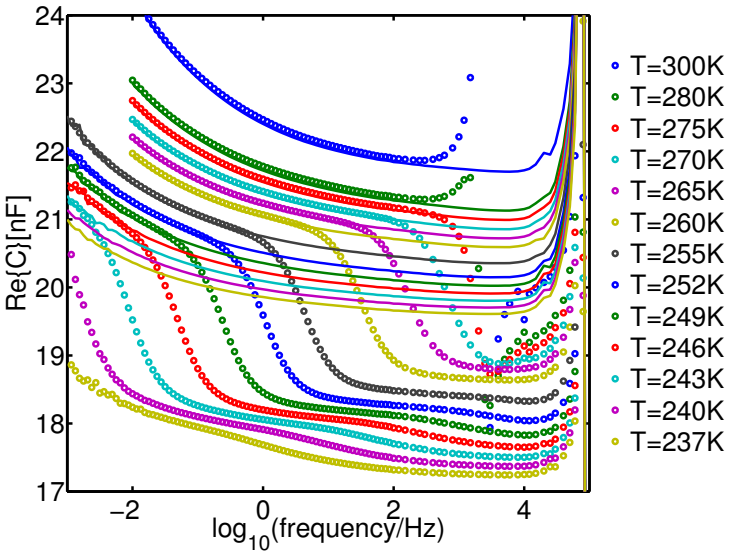

Figure 7.2 The measured capacitance of the empty and liquid filled PBG. The lines are the measured capacitance of the empty PBG. The dots are the measured capacitance of the liquid filled PBG. The two sets give a reasonable match at low frequencies where the curves should overlap.

Modeling the PBG

When the bulk transducer is supplied with an electrical potential it acts like a complicated capacitor. The electric field of the capacitor will deform the ceramic via the piezoelectric effect. Under this deformation the ceramic shell responds in several ways. Firstly it will create an opposing force by means of Hooke's law; when a material is deformed it creates an opposing force proportional to the deformation. Secondly the deformed material has mass and will respond with inertia. Finally some energy is dissipated during the deformation.

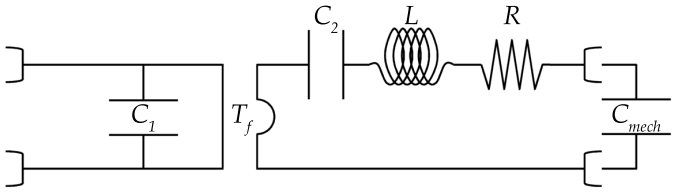

Figure 7.3 An electric network analogue of the bulk transducer. An electric potential input is supplied through the gates at the left and is stored in the capacitor, C_1, or transformed to a force through the transformer, T_f. The right side of the transformer is the so called mechanical side, the force deforms the piezo-ceramic that reacts with a Hooke's opposing force, C_2, inertia, L, and dissipation, R. The capacitance C_{mech} describes inverse stiffness from the inner cavity and changes if it is empty or filled with liquid.

Typically this is illustrated with an electric network analogue as shown in figure 7.3. The model has an electrical side to the left and the mechanical properties to the right. The transducer T_f models the conversion of electric charge and potential, to displacement of volume and pressure. The capacitor on the mechanical side, C_2, represent the elastic properties of the ceramic. The inertia and friction in the ceramics are modeled by an inductance, L and a resistor, R. The two sides are connected in parallel as seen from the electrical side; at high frequencies the ceramic becomes mechanically clamped but charge can still accumulate at the electrodes, meaning that placing the electric capacitance in series with the mechanical side would not make sense. The elements on the mechanical side (including the mechanical stiffness of the liquid, $1/C_{mech}$) are placed in series as they are all subject to the same displacement of volume.

The model signified by the network in figure 7.3 can be described with a response function of charge to electric potential - the electric compliance J:

$$J(\omega) = C_1 + \frac{T_f^2}{\frac{1}{C_2} - \omega^2 L - i\omega R + \frac{1}{C_{mech}}}. \tag{7.1}$$

At high frequencies the transducer becomes mechanically clamped and Eq. 7.1 is reduced to

$$C_{cl} = J_\infty = C_1 \tag{7.2}$$

while at low frequencies the “free“ compliance becomes

$$C_{fr} = J_0 = C_1 + T_f^2 C_2. \tag{7.3}$$

The main resonance shown in Figure 7.2 stems from the RCL part of the network, and defines the resonance frequency $\omega_0 = \sqrt{\frac{1}{LC_2}}$. This together with the quality factor $Q = \frac{1}{R}\sqrt{\frac{L}{C_2}}$ makes it possible to rewrite Eq. 7.1:

$$C_m^{\text{mech}} = C_{c1} + \frac{C_{fr} - C_{cl}}{1 + i\frac{\omega}{\omega_0}\frac{1}{Q} - \left(\frac{\omega}{\omega_0}\right)^2 + \frac{C_2}{C_{mech}}} \tag{7.4}$$

where the superscript ”mech” will change depending on the mechanical stiffness $1/C_{mech}$ of whatever is inside the cavity of the transducer. If the transducer is empty we have

$$C_m^{\text{emp}} = C_{c1} + \frac{C_{fr} - C_{cl}}{1 + i\frac{\omega}{\omega_0}\frac{1}{Q} - \left(\frac{\omega}{\omega_0}\right)^2} \tag{7.5}$$

A fit of Eq. 7.5 to the data obtained with the empty PBG determines the parameters of the model. An example of such a fit is shown in Figure 7.4.

In Eq. 7.4 the stiffness of the liquid $1/C_{mech}$ is normalized by the stiffness of the PBG, $1/C_2$. This parameter is given by the $1/C_2 = L\omega_0^2$, so in order to fix this parameter we have to determine the inertance, L of the PBG. The inertance is taken as a temperature

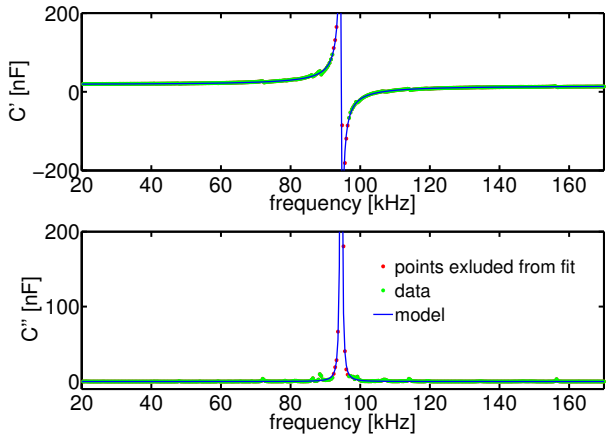

Figure 7.4 Fit to to the empty transducer

independent quantity that relates generalized potential (pressure variation δp) to the derivative of generalized current (volume acceleration $\delta\ddot{V}$). By Newtons Second law the pressure is given by $\delta p = m\ddot{u}_r/A$. For small displacements the volume change is approximated by $\delta V \approx Au_r$. The inertance is then given by

$$L = \frac{\delta p}{\delta \ddot{V}} \approx \frac{m\ddot{u}_r}{A^2\ddot{u}_r} = \frac{m}{A^2}. \tag{7.6}$$

The transducer has been weighed and measured giving an inertance of

$$L = (3.8 \pm 0.2) \cdot 10^3 \frac{\text{kg}}{\text{m}^4}. \tag{7.7}$$

Now the stiffness of the liquid can be expressed in terms of the fitted parameters and C_2:

$$S_{\text{liq}}(\omega) = \frac{1}{C_{liq}(\omega)} = \frac{1}{C_2}\left\{\frac{1}{F} - 1 - i\frac{\omega}{\omega_0}\frac{1}{Q} + \left(\frac{\omega}{\omega_0}\right)^2\right\}, \tag{7.8}$$

where $F = \frac{C_m^{\text{liq}}(\omega) - C_{cl}}{C_{fr} - C_{cl}}$.

Dispersion in the ceramics

Looking closer at the measured capacitance in Figure 7.2 one will see that at low frequencies the free capacitance increases. In order to get around the problem of this dispersion we assume that the frequency dependence of C_{fr} and C_{cl} is the same:

$$\frac{C_{fr}(\omega)}{C_{cl}(\omega)} = \frac{C_{fr}^*}{C_{cl}^*} \tag{7.9}$$

Then we can write

$$F = \frac{C_m^{\text{liq}}(\omega)/C_{fr}(\omega) - C_{cl}^*/C_{fr}^*}{1 - C_{cl}^*/C_{fr}^*} \tag{7.10}$$

Now, if the capacitance of the empty PBG and the capacitance of the liquid filled PBG overlap at low frequencies, we can assume that the frequency dependence of C_{fr} is the same in both measurements. Figure 7.2 indicate that this is indeed the case. The stiffness of the liquid is then given by

$$S_{\text{liq}}(\omega) = \frac{1}{C_2}\left\{\frac{1 - C_{cl}/C_{fr}}{C_m^{\text{liq}}(\omega)/C_m^{\text{emp}}(\omega) - C_{cl}/C_{fr}} - 1 - i\frac{\omega}{\omega_0}\frac{1}{Q} + \left(\frac{\omega}{\omega_0}\right)^2\right\}, \tag{7.11}$$

where the superscript $(*)$ has been omitted.

The bulk modulus

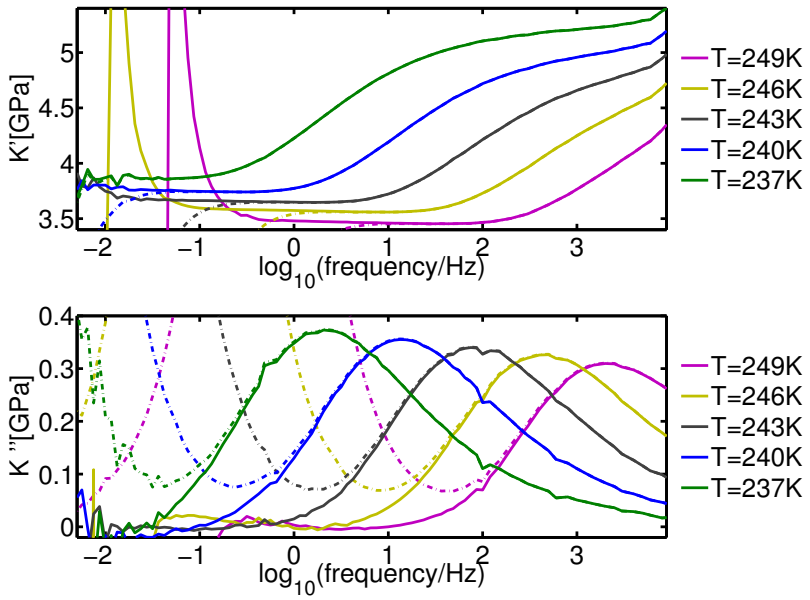

Figure 7.5 Real and imaginary part of bulk modulus at low temperatures. The broken lines are the data found based on Eq. 7.11, while the full lines are found by modeling of the (Poiseuille) flow of liquid in the hole of the PBG.

The bulk modulus is related to the stiffness by [2]:

$$S(\omega) = \frac{1}{V}\left\{K_S - M_S\left(1 + \frac{1}{3}\frac{(k_l r)^2\sin(k_l r)}{k_l r\cos(k_l r) - \sin(k_l r)}\right)\right\}, \tag{7.12}$$

where K_S and M_S are the adiabatic bulk and longitudinal moduli respectively. $k_l = \sqrt{\frac{\rho}{M_S}}\omega$ is the longitudinal wave vector and ρ the density. At high frequencies the stiffness depends both on K_S and M_S where longitudinal waves are excited, but at low frequencies it is simply given by:

$$S(\omega) = \frac{1}{V}K_S \tag{7.13}$$

Combining this with Eq. 7.11 we deduce the measured bulk modulus. It is shown in Figure 7.5. The broken lines are the data found based on Eq. 7.11, while the full lines are found by modeling of the (Poiseuille) flow of liquid in the hole of the PBG. In practice this is done by placing a resistance in parallel with the stiffness of the liquid in the model. The details of this is straight forward, but will be skipped here. However, the interested reader can consult an excellent account of how to do it in the Ph.D. thesis of Tina Hecksher [11].

In next chapter we will use the inverse of the bulk modulus, the compressibility $\kappa_s(\omega)$ and the fitted parameters of the network model in order to get the pressure coefficient $\beta_S(\omega)$.

7.2 Longitudinal specific heat

Detecting the glass transition of a liquid is often done by performing a measurement of the specific heat. An example of such a measurement was shown in Figure 1.1 in the introduction of this thesis. It shows that the specific heat is lower in the glass than in the liquid phase. This being the case, one would suspect that the specific heat becomes frequency dependent when approaching the glass transition. In 1985 Birge and Nagel [12] and Christensen [13] confirmed this measuring the frequency dependent specific heat of Glycerol independently, and in 1996, Nielsen and Dyre derived a fluctuation-dissipation theorem for the specific heat.

The method of Birge and Nagel, which covered a larger frequency range than that of Christensen, is based on the $3\omega_e$-technique and measures the so-called thermal effusion of a liquid. A thin metal film is deposited on a plane slab of glass and is immersed in a liquid. The metal film has a resistance and an applied electric current of angular frequency ω_e generates Joule heating at double frequency $\omega = 2\omega_e$. The generated heat current "effuses" as thermal waves into the liquid and the glass plate supporting the metal film. As a result the temperature changes, depending on the specific heat and thermal conductivity (the effusivity $\sqrt{c\lambda}$) of the liquid . Since the electrical resistance of the metal film is temperature dependent, the resistance varies with the changing temperature at a frequency $2\omega_e$. By Ohms law the measured voltage (given by the product of current and resistance) thus contains a $3\omega_e$ component. By solving the heat-diffusion equation Birge and Nagel found the following formula to relate the complex amplitudes of temperature, $\delta T(\omega)$ and heat current, $j(\omega)$ through the thermal impedance Z:

$$Z \equiv \frac{\delta T(\omega)}{j(\omega)} = \sqrt{i\omega c\lambda}. \tag{7.14}$$

If the thermal conductivity is frequency independent (this was confirmed by [14]), the method gives the frequency dependent specific heat. However, in 2007 Christensen et. al. [15] showed that the plane-plate experiment does not measure the isobaric specific heat, but the longitudinal ditto. The temperature perturbation induces stresses and the high shear modulus makes the relaxation of the deviatoric part of the stress tensor slow down, causing non-isobaric conditions. However, the results in Part I of this thesis indicate that the deviation from isobaric conditions is not that large.

It is not only the plane-plate experiment that gives the longitudinal specific heat; also the method used in this thesis measures the longitudinal specific heat. It is also based on the $3\omega_e$-technique, but compared to the plane-plate experiment, it covers a narrower frequency range. The method is, like that of Birge and Nagel, an effusion method and it was documented by Jakobsen and Christensen in 2010 [8]. Instead of using a thin metal film, the thermal power, P is generated in a small thermistor bead, just like the one used in the measurement of the cooling by heating effect described in Part I of this thesis.

The details of how to measure the thermal impedance is given in reference [8]. Once the measured impedance Z is found one can use it to deduce the thermal impedance of the liquid, Z_{liq}.

Thermal impedance of the liquid

To this end we consider a liquid confined between two radii r_1 and r_2. In a spherical geometry, if the outer radius is much larger than the thermal diffusion length, $|l_D(\omega)| \ll r_2$ the liquid thermal impedance Z_{liq}, at the inner radius r_1 is given by [8]:

$$Z_{liq} = \frac{\delta T(r_1)}{P(r_1)} = \frac{1}{4\pi\lambda r_1(1+\sqrt{i\omega r_1^2 c_l/\lambda})}. \tag{7.15}$$

Note that being in the "thermally thick" limit in spherical geometry ensures that the thermal impedance is independent of mechanical boundary conditions (see Eq. 6.8 in previous chapter or [10]). However, it turns out not to be enough to use the simple expression for the impedance of spherical effusion given by Eq. 7.15. Instead one need to model the thermal interaction of the thermistor bead and the liquid. The bead consists of a core of semiconducting material with radius r_0 at which the actual temperature δT is measured, and the heat current P is generated. This core is covered by a glass capsule of outer radius r_1, at which the thermal contact with the liquid is established. This is depicted in Figure 7.6

The heat flow $P(r_1)$ out through the surface at r_1 is in general different from the heat flow $P(r_0)$ at the surface r_0. Also the temperatures may differ. The thermal impedance of the liquid,

$$Z_{liq} = \frac{\delta T(r_1)}{P(r_1)} \tag{7.16}$$

is in general not equal to the measured impedance

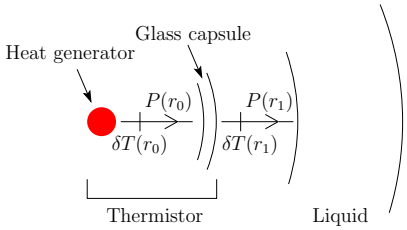

Figure 7.6 Schematic picture of the thermal interaction between thermistor and liquid. The actual measured impedance $Z = \frac{\delta T(r_0)}{P(r_0)}$ is found at the radius r_0 while the impedance of the liquid is given by $Z_{liq} = \frac{\delta T(r_1)}{P(r_1)}$.

$$Z = \frac{\delta T(r_0)}{P(r_0)}. \tag{7.17}$$

The glass capsule has a thermal conductivity λ_b and a specific heat c_b. The bead is a solid, so we assume the difference between isochoric and isobaric specific heat is negligible, i.e we ignore any thermomechanical coupling in thermistor. In that case the heat diffusion is well described by a thermal transfer matrix whose elements are given in reference [10]:

$$\begin{pmatrix} \delta T(r_1) \\ P(r_1)/i\omega \end{pmatrix} = \mathbf{T}^{th}(\lambda_b, c_b, r_1, r_0) \cdot \begin{pmatrix} \delta T(r_0) \\ P(r_0)/i\omega \end{pmatrix} \tag{7.18}$$

This implies that the thermal impedance $Z_{lic} = Z_{r_1}$ is transformed to the thermal impedance Z_{r_0} via

$$Z_{r_0} = \frac{1}{i\omega} \frac{T_{12}^{th} - T_{22}^{th} i\omega Z_{liq}}{T_{11}^{th} - T_{21}^{th} i\omega Z_{liq}}. \tag{7.19}$$

Some of the power generated at r_0 is used to raise the temperature of the core of the bead, whose heat capacity is taken to be $C_0 = 4/3\pi r_0^3 c_b$. The thermal impedance is thus given by

$$\frac{1}{Z} = \frac{1}{i\omega C_0} + \frac{1}{Z_{r_0}}. \tag{7.20}$$

The longitudinal specific heat

The combined model - Eq.'s 7.15, 7.19 and 7.20, is fitted to the measured impedance Z. The full model involves six frequency independent parameters if the fit is done at high temperature where c_l can be considered frequency independent: r_1, r_2, λ_b, λ, c_b and c_l. It turns out that only five parameters can be determined independently from the fit and the last one has to be found by other means. The five parameters used in the fit here are:

$$\tau_l = r_1^2 \frac{c_l}{\lambda}, \quad \tau_b = r_1^2 \frac{c_b}{\lambda_b}, \quad \tilde{r} = \frac{r_0}{r_1}, \quad \tilde{c} = \frac{c_l}{c_b}, \quad Z_{liq,0} = \frac{1}{4\pi\lambda r_1}. \tag{7.21}$$

Note that only $\tilde{c} = \frac{c_l}{c_b}$ mix bead and liquid properties. The parameters found in a least-squares fit to the measured thermal impedance is shown in Figures 7.7 to 7.12. The red symbols are the temperatures used to extrapolate the values of the parameters to lower temperatures.

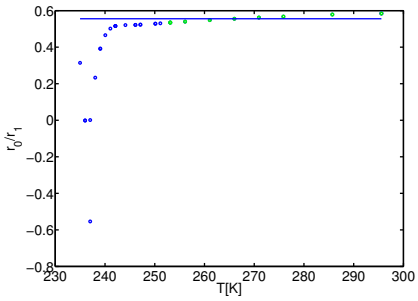

Figure 7.7 Fitted parameter $\tilde{r} = r_0/r_1$

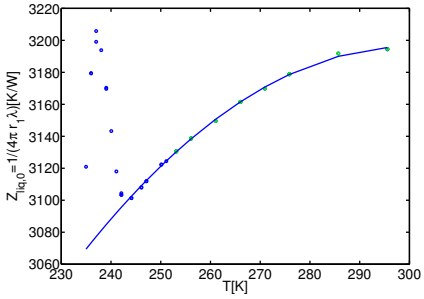

Figure 7.8 Fitted parameter $Z_{liq,0} = {}^1/_{4\pi\lambda r_1}$

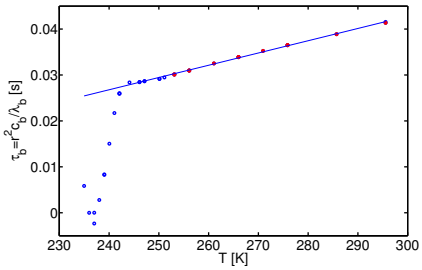

Figure 7.9 Fitted parameter $\tau_b = r_1^2 \frac{c_b}{\lambda_b}$

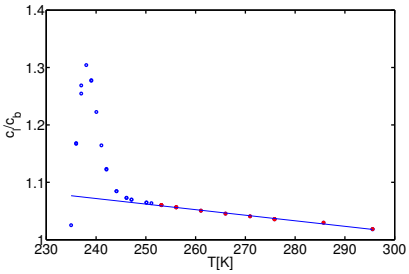

Figure 7.10 Fitted parameter $\tilde{c} = \frac{c_l}{c_b}$

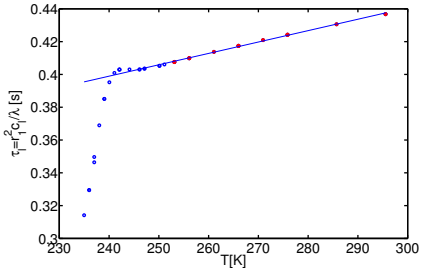

Figure 7.11 Fitted parameter $\tau_l = r_1^2 \frac{c_l}{\lambda}$

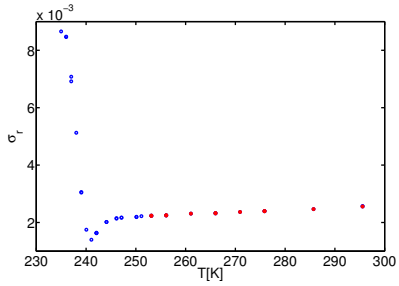

Figure 7.12 Relative error from least squares fit.

One thing to be noted is the temperature dependence of the parameter $\tilde{r} = r_0/r_1$ in Figure 7.7. It turns out that the fitted value of this parameter depends strongly on the frequency range used in the fit. The wider the range of frequency, the larger (and unphysical) a temperature dependence one finds. I have not explored this, but it deserves to be investigated further. Figure 7.13 shows the real and imaginary part of the measured impedance Z as blue and red dots respectively. Also the fit of the model is shown in full lines. The temperature used is 285K and it is seen that the model fits the data fairly well.

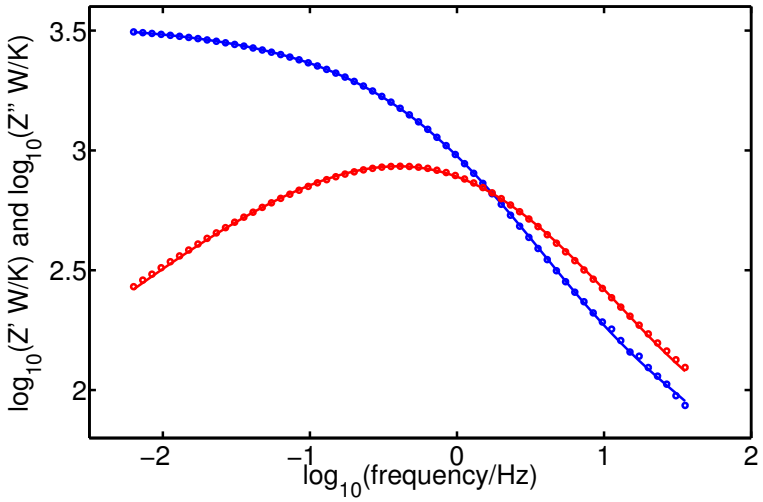

Figure 7.13 The measured impedance at 285K together with prediction of the full model for Z (Eq.'s 7.15, 7.19 and 7.20).

From the thermal impedance we can find the thermal conductivity of the liquid by noting that the admittance Y_{liq} is the reciprocal quantity of the impedance. At low frequency, where c_l reaches it's non-complex equilibrium value, we can cancel the square-root term by taking the difference between Y'_{liq} and Y''_{liq}:

$$\lambda = \frac{Y'_{liq} - Y''_{liq}}{4\pi r_1}. \tag{7.22}$$

The values found for λ can then be used to find the frequency dependent specific heat from Eq. 7.15. In order to find the absolute value of λ and c_l one needs to specify one of the two radii r_0 and r_1. We have measured r_1 and the value found is

$$r_1 = 0.195\text{mm}. \tag{7.23}$$

Unfortunately I have not been able to find a value of the specific heat of DC705 in the literature in order to see if the measured r_1 gives the right value to c_l. Still, based on that value of r_1 we find the thermal conductivity and longitudinal specific heat. These are shown for temperatures in the range 241K-235K in Figure 7.14 and Figure 7.15 respectively. For some of the temperatures there are two curves; one going down in temperature, and one going up.

Even though the absolute value of the specific heat may be a bit wrong, it turns out that it does not affect the measured value of the pressure coefficient. In next chapter we show that the pressure coefficient β_S is determined by the thermal impedance of the liquid, and not the specific heat itself. Likewise, it will be the normalized stiffness that enters from the measurement of the bulk modulus. Of course, in the end, if one wants to calculate the PD-ratio, the absolute values become important.

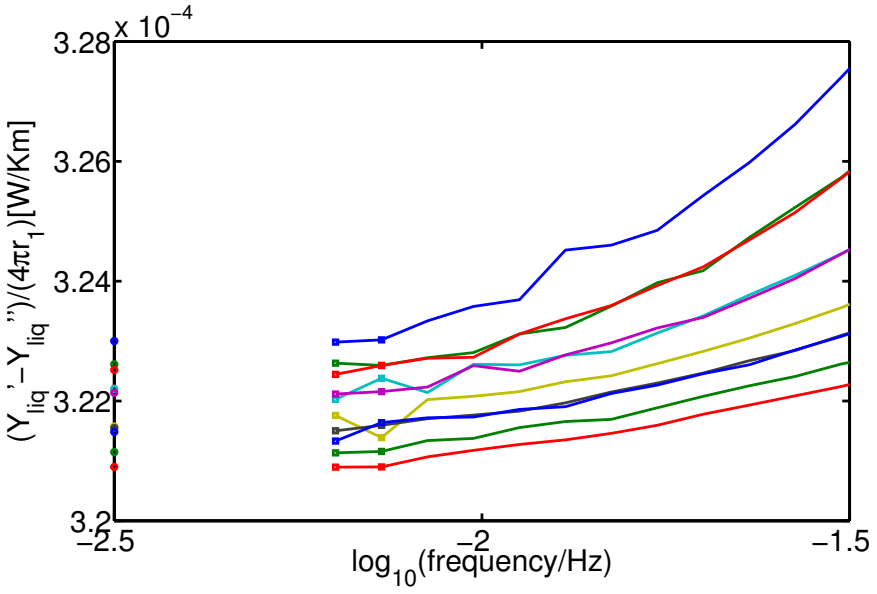

Figure 7.14 The thermal conductivity λ for the temperatures 235K, 236K, 237K, 238K, 239K, 240K and 241K. The value used to determine the specific heat using Eq. 7.15 is taken as the average of the two data points at lowest frequency.

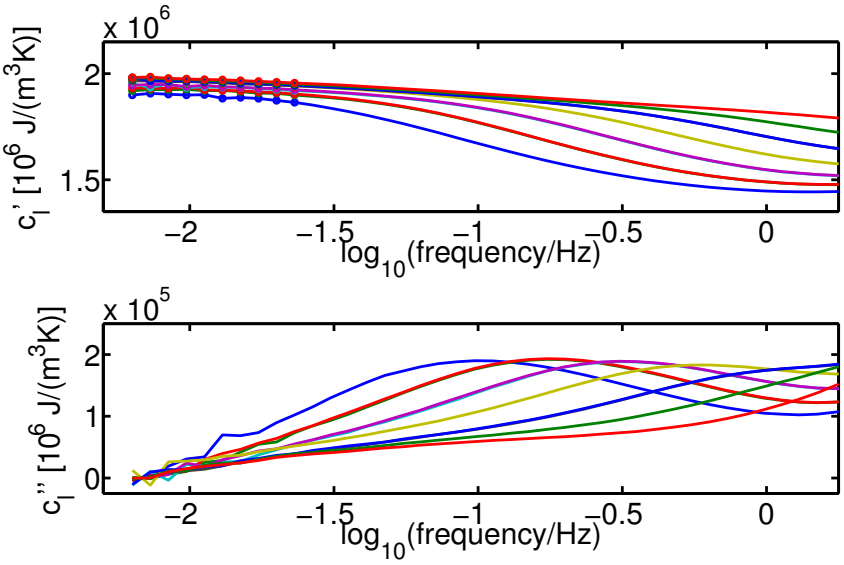

Figure 7.15 The longitudinal specific heat c_l found for the temperatures 235K, 236K, 237K, 238K, 239K, 240K and 241K

8 The cross response function β_S

The combined experiment can in principle be done in two ways. Either one applies an oscillating voltage to the PBG while measuring the change in temperature at the center with the thermistor, or one generates an oscillating heat current with amplitude P_{th} by Joule heating in the thermistor and measure the voltage generated in the PBG as the liquid attempts to expand. The equivalent diagram model of the whole system is shown in Figure 8.1. In this pilot test we have chosen to model the thermistor as an ideal heat generator in parallel with its heat capacity C_0. The value used for C_0 is the one found in the preceding chapter by fitting the full model of the thermal impedance to the measured impedance. To model the thermistor in this way is in some respect to simple; in the measurement of the specific heat one had to take the thermal structure of the thermistor into account [8]. In the equivalence diagram in Figure 8.1 we have stitched together the three models developed so far. These are, from the left, the heat capacity of the thermistor, in the middle, the equivalent diagram of the transfer matrix given by Eq. 6.5, and to the right, the model of the PBG used to measure the adiabatic bulk modulus. However, in this combined experiment we are working at frequencies far below the resonance frequency of the PBG. We therefor ignore the inertia of the shell and only include the stiffness of the PBG, C_m on the mechanical side of the model.

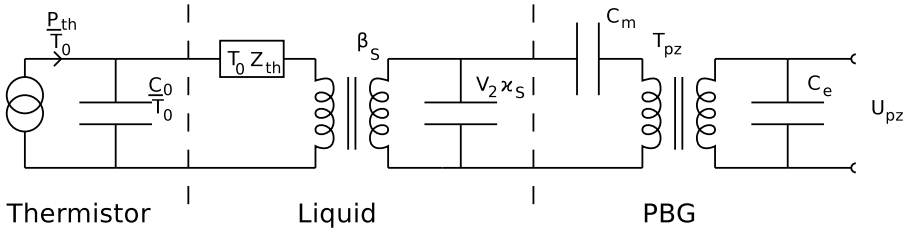

Figure 8.1 Equivalent diagram of the liquid in contact with the thermistor and the piezoelectric shell.

The voltage U_{pz} generated in the PBG carries information on the inverse of the pressure coefficient $1/\beta_S = \left(\frac{\partial V}{\partial S}\right)_p$. To relate the voltage amplitude measured by a voltmeter of high impedance ($I_{pz} = 0$) in response to a heat current P_{th} generated in the thermistor we multiply the transfer matrices of the three models that are combined in Figure 8.1:

$$\begin{pmatrix} \delta T \\ P_{th} \end{pmatrix} = \begin{pmatrix} 1 & 0 \\ \frac{i\omega C_0}{T_0} & 1 \end{pmatrix} \begin{pmatrix} i\omega T_0 Z_{th} V_2 \kappa_S \beta_S & T_0 Z_{th} \beta_S \\ i\omega V_2 \kappa_S \beta_S & \beta_S \end{pmatrix} \times \begin{pmatrix} \frac{1}{T_{pz}} + \frac{C_e}{C_m} T_{pz} & \frac{T_{pz}}{i\omega C_m} \\ i\omega C_e T_{pz} & T_{pz} \end{pmatrix} \cdot \begin{pmatrix} \delta U_{pz} \\ I_{pz} \end{pmatrix} \tag{8.1}$$

Multiplying these together gives a very large matrix which is omitted here, but in the case of $I_{pz} = 0$ the voltage to power response becomes

$$\left(\frac{U_{pz}}{P_{th}}\right)_{I_{pz}=0} = \frac{T_{pz}}{C_e i\omega} \frac{1}{(1 + C_0 i\omega Z_{th}(\omega)) \left(1 + \left(1 + T_{pz}^2 \frac{C_m}{C_e}\right) \frac{V_2 \kappa_S(\omega)}{C_m}\right)} \frac{1}{T_0 \beta_S(\omega)} \tag{8.2}$$

8.0.1 Estimating the measured piezoelectric voltage

In table 8.0.1 we list the parameters that is used to estimate measured piezoelectric voltage U_{pz}. From the measurement of the bulk modulus we have $T_{pz}/C_e = 10^{11} V\mathrm{m}^{-3}$. At 1Hz the factor $C_0 Z_{th} = 10^{-1}$ while $V_2 \kappa_S(1\mathrm{Hz})/C_m = 1$. From the values of the specific heat and the estimated expansion coefficient we get $\frac{1}{T_0 \beta_S} \approx \frac{\alpha_p}{c_l} = 3{\times}10^{-10}\mathrm{m}^3\mathrm{J}^{-1}$. From this we find that $\frac{T_{pz}}{C_e} \frac{1}{\beta_S} = 30 V/J$. Using a power amplitude of roughly $P_{th} = 0.3\mathrm{mW}$ in order to keep the temperature in the center below 1K, we estimate the measured voltage to $U_{pz} \approx 3\mathrm{mV}$. The absolute value of the measured voltage at 240K is shown in Figure 8.2 and it seems like our estimate is in the right range.

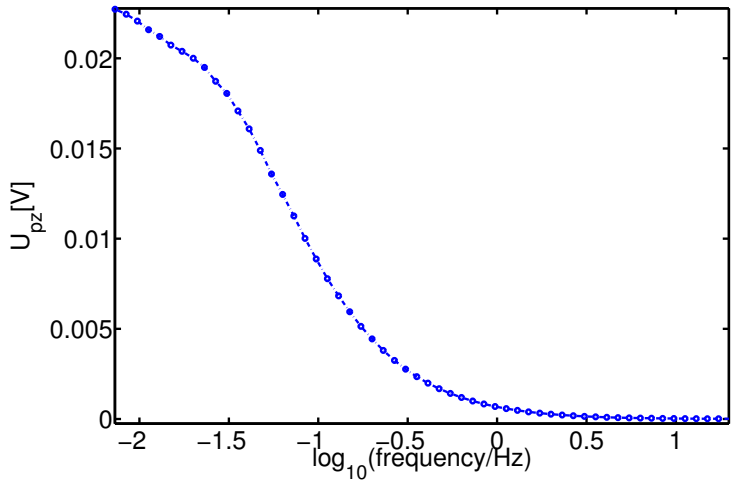

Figure 8.2 Absolute value of the measured piezoelectric voltage U_{pz} at 240K.

To get a feel for the system we consider Figure 8.3. It shows the measured ratio of the complex amplitudes of piezoelectric voltage and power $\frac{U_{pz}}{P_{th}}$ at three temperatures. One low temperature (blue curve), one intermediate (green) and a high temperature (red). At intermediate and high temperature one can see the hole resonance. Inspecting the figure closely one also see that there is a "bump" in the low-frequency end of the spectrum. It is seen both at low and high temperature, suggesting that it is a phenomenon that is not affected by the glass transition, and gives an additive contribution to the response. A first guess could be that we see the pyro-electric effect. This should be present at frequencies matching the characteristic time of heat diffusion in a sphere the

C_m	$7.5 \times 10^{-16} \frac{\mathrm{m}^3}{\mathrm{Pa}}$
T_{pz}	$2.4 \times 10^{3} \frac{\mathrm{C}}{\mathrm{m}^3}$
C_e	$15 \times 10^{-9} \mathrm{F}$
T_0	240K
$c_l(1\mathrm{Hz})$	$1.6 \times 10^{6} \frac{\mathrm{J}}{\mathrm{Km}^3}$
C_0	$1 \times 10^{-4} \frac{\mathrm{J}}{\mathrm{K}}$
$\alpha_p(1\mathrm{Hz})$	$5 \times 10^{-4} \mathrm{K}^{-1}$
$Z_{th}(1\mathrm{Hz})$	$10^{3} \frac{\mathrm{K}}{\mathrm{W}}$
$V_2\kappa_S(1\mathrm{Hz})/C_m$	~ 1

Table 8.1 Parameters used to estimate the signal in the cross response experiment at 240K. The parameters were found in Chapter 7.

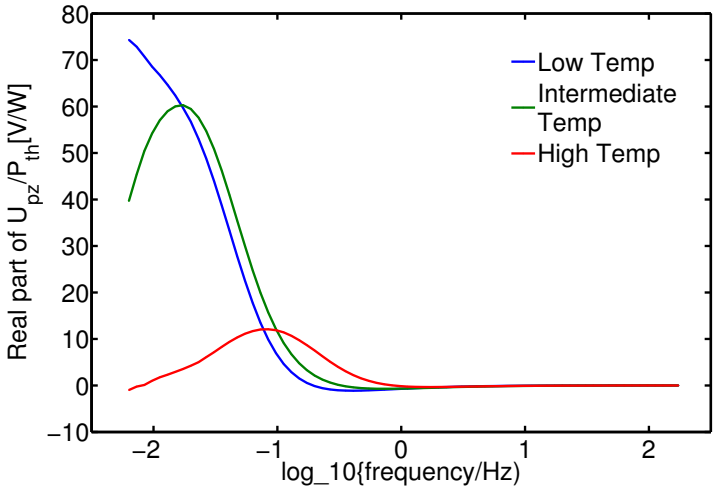

Figure 8.3 Measured ratio of the complex amplitudes of piezoelectric voltage and power $\frac{U_{pz}}{P_{th}}$ at three temperatures. At intermediate and high temperature we see the hole resonance.

size of our system. Using the values of thermal conductivity and specific heat found in the preceding chapter, one finds that for a sphere with radius $r = 9$mm (like our sphere) the characteristic frequency is around 1mHz. The process we see here is a little faster than that. In any case it is difficult to say what cases the shape of the curves unless you have a model to put into Eq. 8.2 in place of $1/\beta_S$. The model used in Chapter 3 in order to simulate the cooling by heating effect is one possibility.

Figure 8.4 is a zoom in on the real part of the measured response in the region where the thermal impedance is peaking (compare with Figure 7.13). There seems to be sign of relaxation.

8.0.2 The pressure coefficient

In order to find the pressure coefficient, or rather $\frac{1}{T_0\beta_S}$ we invert Eq. 8.2, but with a small adjustment: Three more components are added to the model. Two of them

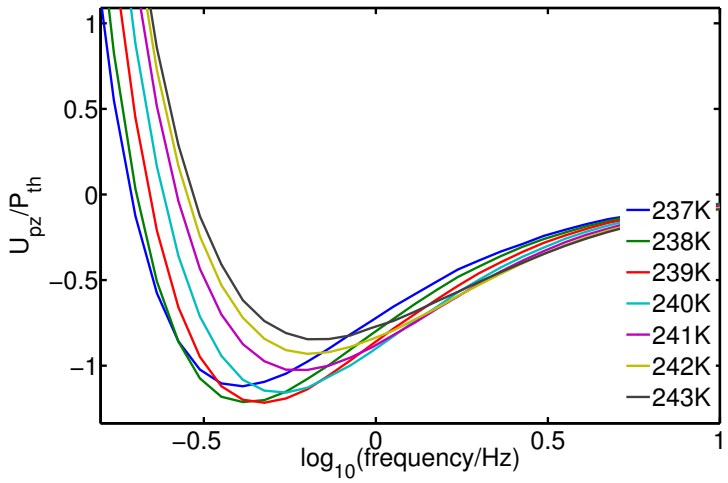

Figure 8.4 Zoom in on the real part of the ratio of piezoelectric voltage and power amplitude U_{pz}/P_{th} at the lowest temperatures.

are part of the electrical setup and is located outside the cryostat. The elements are a capacitance $C_p = 10\text{nF}$ and a resistance $R_p = 100\text{M}\Omega$ which is placed in parallel with the electrical capacitance of the PBG, C_e. The third element included is a resistance R_h in parallel with the normalized mechanical capacitance of the liquid $V_2\kappa_S/C_M$. This models the Poiseuille flow in the hole of the PBG, but the results turn out not to be very sensitive to the inclusion of that element. The result of the inversion is seen in Figure 8.5 and Figure 8.6. In the two figures the axes are not the same. This is done to make it easier to see what happens in the figures. In any case, it is clear that we have not gotten all information out of the measured response. It immediately strikes you that there is something fishy about the way the curves separate (or not) when temperature is changed. It is as if all the curves in the real part are forced to meet in a single point around $f = 10\text{Hz}$. It is not clear to me how to interpret these curves. There is one aspect of the result that seems promising though: The actual numerical value of the measured quantity fits with the estimated value based on the numbers in table 8.0.1. Also it is clear that there is a signal without to much noise, so it seems that one does not have to increase the power delivered at the center of the sphere in order to see a signal.

8.1 Possible developments of the measurement

There are three things that need to be done:

1. Make a simulation of the problem, using a model for the pressure coefficient to put into Eq. 8.2. This way one would get a better idea of what to expect from the measured response.
2. Try the opposite experiment, where one measures the temperature response in the center to an oscillating piezoelectric voltage over the PBG. Unpublished results produced by a group of students at Glass and Time have observed the same

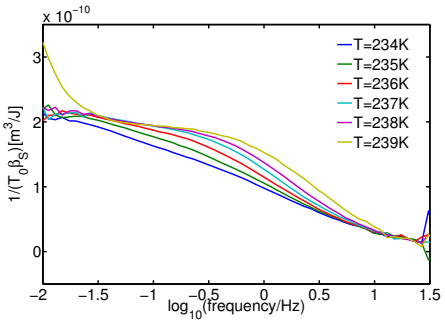

Figure 8.5 Real part of $\frac{1}{T_0\beta_S}$.

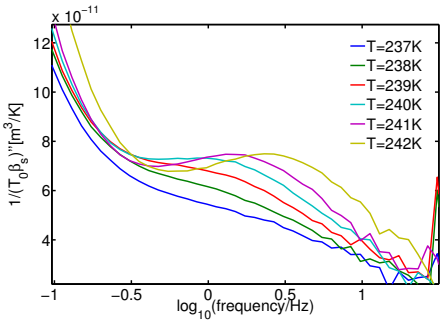

Figure 8.6 Imaginary part of $\frac{1}{T_0\beta_S}$.

spurious behavior as we do here in the opposite experiment. The students used the same model to invert the data as we do here. This leads to the following suggestion:

3. The model used to invert the data, is probably to simple, that is, the model of the thermistor. In the previous chapter, we saw that in order to get a good fit to the measured thermal impedance, one needed to include the thermal structure of the bead, as given by Eq. 7.18. It would just be a matter of inverting that matrix and then put it into the equivalent network model depicted in Figure 8.1. This is a plausible solution to the problem as the thermal structure becomes important exactly in the range of frequencies where we expect to see the structural relaxation in the response functions.

Bibliography

[1] T. E. Christensen. *En metode til bestemmelse af den frekvensafhaengige varmefylde af en underafkoelet vaeske ved glasovergangen.* IMFUFA, Roskilde University, TEXT 184, 1989.

[2] T. Christensen and N. B. Olsen. Determination of the frequency-dependent bulk modulus of glycerol using a piezoelectric spherical shell. *Physical Review B*, 49(21):15396–15399, 1994.

[3] T. Christensen and N. B. Olsen. Comparative measurements of the electrical and shear mechanical response in some supercooled liquids. *Journal of Non-Crystalline Solids*, 172-174:357–361, 1994.

[4] T. Christensen and N. B. Olsen. Quasistatic measurements of the frequency-dependent bulk and shear modulus of supercooled liquids. *Journal of Non-Crystalline Solids*, 172-174:362–364, 1994.

[5] T. Christensen and N. B. Olsen. A rheometer for the measurement of high shear modulus covering more than seven decades of frequency below 50 khz. *Review of Scientific Instruments*, 66(10):5019–5031, 1995.

[6] T. Christensen and N. B. Olsen. Thermoviscoelasticity of glass-forming liquids. *Journal of Non-Crystalline Solids*, 235-237:296–301, 1998.

[7] J. Papini and J. Heebøll-Christensen. Pyroelectricity-a new application for the piezoelectric bulk transducer. Master's thesis, Roskilde University, 2008.

[8] Bo Jakobsen, N. B. Olsen, and T. Christensen. Frequency-dependent specific heat from thermal effusion in sphercial geometry. *Physical Review E*, 81:061505, 2010.

[9] N. L. Ellegaard, T. Christensen, P. V. Christiansen, N. B. Olsen, U. R. Pedersen, T. B. Schröder, and J. C. Dyre. Single-order-parameter description of glass-forming liquids: A one-frequency test. *Journal of Chemical Physics*, 126:074502, 2007.

[10] T. Christensen and J. C. Dyre. Solution of the spherically symmetric linear thermoviscoelastic problem in the inertia-free limit. *Physical Review E*, 78:021501, 2008.

[11] T. Hecksher. *Relaxation in supercooled liquids.* PhD thesis, Roskilde University, 2011.

[12] N. O. Birge and S. R: Nagel. Specific-heat spectroscopy of the glass transition. *Physical Review Letters*, 54:2674–2677, 1985.

[13] T. Christensen. *J. Phys. (Paris) Colloq.*, C8:635, 1985.

[14] A. A. Minakov, S. A. Adamovsky, and C. Schick. *Thermochim. Acta*, 377:173, 2001.

[15] T. Christensen, N. B. Olsen, and J. C. Dyre. Conventional methods fail to measure $c_p(\omega)$ of glass-forming liquids. *Physical Review E*, 75:041502, 2007.

Part III

Appendices

A Balance equations of momentum and energy

A.1 Temperature of the liquid filled shell

I will model the temperature of the liquid as a continuous function of t and r. For this we need to look further into heat diffusion in spherical symmetry.

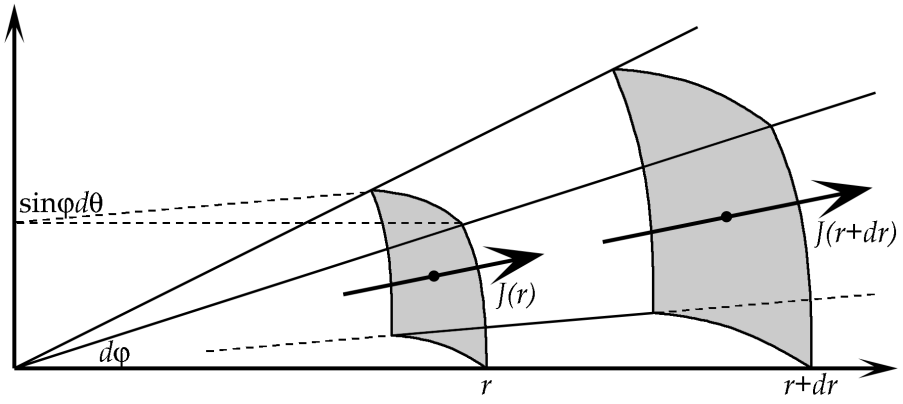

Figure A.1 The heat flow in a differential volume. The heat change in the volume over time must be the difference between the heat inflow and the heat outflow (if we assume no heat is produced in the volume).

We specify a differential volume element in spherical coordinates $r^2 \sin\phi \, dr d\phi d\theta$ in the distance r from the center and assume that heat only flows in the radial direction from the outside to the center. Notice that the heat flow by definition follows the positive r-direction, so in our case we let $-4\pi r^2 J(r)$ be the flow of heat inward through the surface of a sphere with radius r, see figure A.1. If we assume that no heat is produced inside the volume then the change in heat over time must be the difference between heat inflow and heat outflow,

$$\delta Q = -\left((r+dr)^2 J(r+dr) - r^2 J(r)\right) 4\pi \cdot \delta t, \tag{A.1}$$

extend the equation with the factor $r^2 dr$,

$$\begin{aligned}\delta Q &= -\frac{(r+dr)^2 J(r+dr) - r^2 J(r)}{r^2 dr} 4\pi r^2 dr \cdot \delta t \\ &= -\left(\frac{J(r+dr) - J(r)}{dr} + \left(\frac{2}{r} + \frac{dr}{r^2}\right) J(r+dr)\right) 4\pi r^2 dr \cdot \delta t, \end{aligned} \tag{A.2}$$

and let dr go to zero (notice that this will make $4\pi r^2 dr$ approach the volume of a spherical shell with infinitesimal thickness, we call this V_0),

$$\delta Q = -\left(\frac{dJ(r)}{dr} + \frac{2}{r} J(r)\right) V_0 \cdot \delta t. \tag{A.3}$$

When we consider small changes in heat in a differential volume element with no heat production it is fair to assume this as a thermodynamically reversible process, and so the heat δQ is described by $T_0 \delta S$, and furthermore we apply the thermodynamic expansion of δS:

$$T_0 \delta S = T_0 \left(\frac{\partial S}{\partial T}\right)_V \delta T + T_0 \left(\frac{\partial S}{\partial V}\right)_T \delta V = c_V \delta T + T_0 K_T \alpha_p \delta V, \tag{A.4}$$

with $c_V \equiv T_0 \left(\frac{\partial S}{\partial T}\right)_V$, $K_T \equiv V_0 \left(\frac{\partial p}{\partial V}\right)_T$, and $\alpha_p \equiv \frac{1}{V_0}\left(\frac{\partial V}{\partial T}\right)_p$, we get

$$c_V \delta T + T_0 K_T \alpha_p \delta V = -\left(\frac{dJ(r)}{dr} + \frac{2}{r} J(r)\right) V_0 \cdot \delta t. \tag{A.5}$$

T_0 should be interpreted as a constant, in our calculations we will assume it to be the starting temperature for our measurement, literally T_0.

Divide equation A.5 with V_0 and let C_V define the volume specific heat capacity, $C_V = \frac{T_0}{V_0}\left(\frac{\partial S}{\partial T}\right)_V$,

$$C_V \delta T + T_0 K_T \alpha_p \frac{\delta V}{V_0} = -\left(\frac{dJ(r)}{dr} + \frac{2}{r} J(r)\right) \delta t. \tag{A.6}$$

Now divide the equation with δt and let it go to zero to obtain the differential expression,

$$C_V \frac{\partial \delta T}{\partial t} + T_0 K_T \alpha_p \frac{\partial}{\partial t} \frac{\delta V}{V_0} = -\left(\frac{dJ(r)}{dr} + \frac{2}{r} J(r)\right). \tag{A.7}$$

Insert Fourier's Law of heat conduction, $J(r) = -\lambda \frac{\partial \delta T}{\partial r}$,

$$C_V \frac{\partial \delta T}{\partial t} + T_0 K_T \alpha_p \frac{\partial}{\partial t} \frac{\delta V}{V_0} = \lambda \left(\frac{\partial^2 \delta T}{\partial r^2} + \frac{2}{r} \frac{\partial \delta T}{\partial r}\right)$$

Recognize equation A.8 as a second order partial differential equation. We will be able to solve this if we can find expressions for the divergence of the displacement field $\nabla \bullet \bar{u} \equiv \frac{\delta V}{V_0}$

A.2 Mechanical displacement and stress field of the liquid

Specify a differential volume element in spherical coordinates $r^2 \sin\phi \, dr d\phi d\theta$ in the distance r from the center, see figure A.2. If $\bar{u}(r, \phi, \theta, t)$ is the displacement field of the liquid we write the force on the differential volume by Newton's second law,

$$d\bar{F} = dm \cdot \frac{\partial^2 \bar{u}}{\partial t^2} = \rho dV \cdot \frac{\partial^2 \bar{u}}{\partial t^2}, \tag{A.8}$$

with ρ of course being the density of the liquid.

Invoking the theory of stress and strain tensors we assume that all force on the differential volume is supplied by the stress tensor, $\bar{\sigma}(r, \phi, \theta, t)$, according to the definition that stress times the normal vector to an area of a surface constitutes a force on the area, $\bar{\sigma} \cdot \bar{n}_A A = \bar{F}_A$.

In this way we get forces acting on all six sides of the differential volume as shown i figure A.3, and assuming that the spherical coordinates diagonalize the stress tensor we have no skew forces on any surface.

Therefore we get a radial force balance on dV from the difference between stress on the inner and outer surface of the volume,

$$\begin{aligned} F_r &= dA(r+dr) \cdot \sigma_{rr}(r+dr) - dA(r) \cdot \sigma_{rr}(r) \\ &= \sin\phi \, d\phi d\theta \cdot \left((r+dr)^2 \sigma_{rr}(r+dr) - r^2 \sigma_{rr}(r) \right), \end{aligned} \tag{A.9}$$

but the forces in the tangential directions will also have small effect on this balance since they have a small component in the radial direction,

$$\begin{aligned} F_\phi &= 2 \cdot dA(\phi) \cdot \sigma_{\phi\phi}(r) \cdot \sin\left(\frac{1}{2} d\phi\right) \\ &= 2(r \sin\phi \, dr d\theta) \sigma_{\phi\phi}(r) \sin\left(\frac{1}{2} d\phi\right), \end{aligned} \tag{A.10}$$

$$\begin{aligned} F_\theta &= 2 \cdot dA(\theta) \cdot \sigma_{\theta\theta}(r) \cdot \sin\left(\frac{1}{2} \sin\phi \, d\theta\right) \\ &= 2(r \, dr d\phi) \sigma_{\theta\theta}(r) \sin\left(\frac{1}{2} \sin\phi \, d\theta\right). \end{aligned} \tag{A.11}$$

The resulting force balance will then be the difference between radial forces plus the radial component of the tangential forces

$$\begin{aligned} \rho r^2 dr \frac{\partial^2 \bar{u}}{\partial t^2} &= (r+dr)^2 \sigma_{rr}(r+dr) - r^2 \sigma_{rr}(r) \\ &- 2r \, dr \left(\sigma_{\phi\phi}(r) \frac{\sin(\frac{1}{2} d\phi)}{d\phi} + \sigma_{\theta\theta}(r) \frac{\sin(\frac{1}{2} \sin\phi \, d\theta)}{\sin\phi \, d\theta} \right), \end{aligned} \tag{A.12}$$

rearrange the equation and we have

$$\begin{aligned}\rho\frac{\partial^2\bar{u}}{\partial t^2} &= \frac{\sigma_{rr}(r+dr)-\sigma_{rr}(r)}{dr}+\left(\frac{2}{r}+\frac{dr}{r^2}\right)\sigma_{rr}(r+dr)\\ &- \frac{2}{r}\left(\sigma_{\phi\phi}(r)\frac{\sin(\frac{1}{2}d\phi)}{d\phi}+\sigma_{\theta\theta}(r)\frac{\sin(\frac{1}{2}\sin\phi\, d\theta)}{\sin\phi\, d\theta}\right).\end{aligned} \tag{A.13}$$

Now letting the infinitesimal quantities dr, $d\phi$, and $d\theta$ go to zero we get the result

$$\rho\frac{\partial^2\bar{u}}{\partial t^2}=\frac{\partial\sigma_{rr}}{\partial r}+\frac{2}{r}\sigma_{rr}-\frac{1}{r}\sigma_{\phi\phi}-\frac{1}{r}\sigma_{\theta\theta}. \tag{A.14}$$

Next step is to find expressions for the stress tensor, $\bar{\sigma}(r,\phi,\theta,t)$. We have already assumed that in the spherical symmetry the stress tensor is described only by the diagonal elements, σ_{rr}, $\sigma_{\phi\phi}$, and $\sigma_{\theta\theta}$, now we define pressure to be the average of these stresses

$$-p=\frac{1}{3}\left(\sigma_{rr}+\sigma_{\phi\phi}+\sigma_{\theta\theta}\right). \tag{A.15}$$

The pressure changes according to the thermodynamic derivatives

$$\delta p=\left(\frac{\partial p}{\partial V}\right)_T\delta V+\left(\frac{\partial p}{\partial T}\right)_V\delta T, \tag{A.16}$$

by the Maxwell relations

$$\delta p=\left(\frac{\partial p}{\partial V}\right)_T\delta V+\left(\frac{\partial V}{\partial T}\right)_p\left(\frac{\partial p}{\partial V}\right)_T\delta T. \tag{A.17}$$

Insert the definition of the isothermal bulk modulus, $K_T=-V_0\left(\frac{\partial p}{\partial V}\right)_T$, and the isobaric expansion coefficient, $\alpha_p=\frac{1}{V_0}\left(\frac{\partial V}{\partial T}\right)_p$, and write the pressure

$$\frac{1}{3}\left(\sigma_{rr}+\sigma_{\phi\phi}+\sigma_{\theta\theta}\right)=K_T\frac{\delta V}{V_0}+K_T\alpha_p\delta T. \tag{A.18}$$

The relative change in volume, $\delta V/V_0$, can be described in terms of the strain tensor, $\bar{\epsilon}(r,\phi,\theta,t)$. Assuming that the liquid in the cavity is an isotropic material, the strain tensor will be diagonalized in the same spherical coordinate system as the stress tensor, $\bar{\epsilon}$ is described with the diagonal elements, ϵ_{rr}, $\epsilon_{\phi\phi}$, and $\epsilon_{\theta\theta}$, so we get

$$\frac{\delta V}{V_0}=\frac{\delta V_r+\delta V_\phi+\delta V_\theta}{V_0}=\frac{\delta r}{r_0}+\frac{\delta\phi}{\phi_0}+\frac{\delta\theta}{\theta_0}=\epsilon_{rr}+\epsilon_{\phi\phi}+\epsilon_{\theta\theta}. \tag{A.19}$$

As seen from this equation the diagonal elements of $\bar{\epsilon}$ are expressed by the relative change in length in each coordinate direction as part of a relative volume change. In

figure A.4 the volume dV is displaced to dV' by $\bar{u}(r,\phi,\theta,t)$, from this figure we get the three expressions

$$\epsilon_{rr} = \frac{((r+dr+\bar{u}(r+dr))-(r+\bar{u}(r)))-(r+dr-r)}{(r+dr-r)} = \frac{\partial \bar{u}}{\partial r}, \tag{A.20}$$

$$\epsilon_{\phi\phi} = \frac{(r+\bar{u}(r))\,d\phi - r d\phi}{r d\phi} = \frac{\bar{u}(r)}{r}, \tag{A.21}$$

$$\epsilon_{\theta\theta} = \frac{(r+\bar{u}(r))\sin\phi\,d\theta - r\sin\phi\,d\theta}{r\sin\phi\,d\theta} = \frac{\bar{u}(r)}{r}. \tag{A.22}$$

Hooke's Law defines a linear relation between stress, $\bar{\sigma}$, and strain, $\bar{\epsilon}$, and since we assume that both tensors are diagonalized in the same coordinate system this becomes a set of relations between σ_{rr} - ϵ_{rr}, $\sigma_{\phi\phi}$ - $\epsilon_{\phi\phi}$, and $\sigma_{\theta\theta}$ - $\epsilon_{\theta\theta}$. In this relation we have both the bulk modulus, K_T, that describes a volume changing but shape maintaining deformation, and the shear modulus, G, that describes a shape changing but volume maintaining deformation.

The first relation we simply get from equation A.18,

$$\frac{1}{3}\left(\sigma_{rr}+\sigma_{\phi\phi}+\sigma_{\theta\theta}\right) = K_T\left(\epsilon_{rr}+\epsilon_{\phi\phi}+\epsilon_{\theta\theta}\right) + K_T\alpha_p\delta T. \tag{A.23}$$

The other three relations we get from the shear modulus and we are able to write one relation for each general direction [1, p.13]

$$\sigma_{rr} - \frac{1}{3}\left(\sigma_{rr}+\sigma_{\phi\phi}+\sigma_{\theta\theta}\right) = 2G\left(\epsilon_{rr} - \frac{1}{3}\left(\epsilon_{rr}+\epsilon_{\phi\phi}+\epsilon_{\theta\theta}\right)\right), \tag{A.24}$$

$$\sigma_{\phi\phi} - \frac{1}{3}\left(\sigma_{rr}+\sigma_{\phi\phi}+\sigma_{\theta\theta}\right) = 2G\left(\epsilon_{\phi\phi} - \frac{1}{3}\left(\epsilon_{rr}+\epsilon_{\phi\phi}+\epsilon_{\theta\theta}\right)\right), \tag{A.25}$$

$$\sigma_{\theta\theta} - \frac{1}{3}\left(\sigma_{rr}+\sigma_{\phi\phi}+\sigma_{\theta\theta}\right) = 2G\left(\epsilon_{\theta\theta} - \frac{1}{3}\left(\epsilon_{rr}+\epsilon_{\phi\phi}+\epsilon_{\theta\theta}\right)\right). \tag{A.26}$$

By combining these four relations we get

$$\sigma_{rr} = \left(K_T + \frac{4}{3}G\right)\epsilon_{rr} + \left(2K_T - \frac{4}{3}G\right)\epsilon_{\phi\phi} - K_T\alpha_p\delta T, \tag{A.27}$$

$$\sigma_{\phi\phi} = \sigma_{\theta\theta} = \left(K_T + \frac{2}{3}G\right)\epsilon_{rr} + \left(2K_T - \frac{2}{3}G\right)\epsilon_{\phi\phi} - K_T\alpha_p\delta T. \tag{A.28}$$

For further reference, by rearranging equation A.27 one has

$$\sigma_{rr} = \left(K_T + \frac{4}{3}G\right)\nabla \bullet u - 4G\epsilon_{\theta\theta} - \beta_V\delta T. \tag{A.29}$$

This is an instance of the Duhamel-Neumann constitutive relation [1] connecting mechanical and thermodynamic properties which reads

$$\sigma_{ij} = K_T \nabla \bullet u \delta_{ij} + 2G\left(\epsilon_{ij} - \frac{1}{3}\nabla \bullet u \delta_{ij}\right) - \beta_V \delta T \delta_{ij}. \tag{A.30}$$

By putting equations A.27 and A.28 into equation A.14 we get the following beautiful relation

$$\begin{aligned}
\rho\frac{\partial^2 \bar{u}}{\partial t^2} &= \left(K_T + \frac{4}{3}G\right)\frac{\partial^2 \bar{u}}{\partial r^2} + \left(2K_T - \frac{4}{3}G\right)\left(\frac{1}{r}\frac{\partial \bar{u}}{\partial r} - \frac{\bar{u}}{r^2}\right) - K_T\alpha_p\frac{\partial \delta T}{\partial r} \\
&+ \frac{2}{r}\left(\left(K_T + \frac{4}{3}G\right)\frac{\partial \bar{u}}{\partial r} + \left(2K_T - \frac{4}{3}G\right)\frac{\bar{u}}{r} - K_T\alpha_p\delta T\right) \\
&- \frac{2}{r}\left(\left(K_T + \frac{2}{3}G\right)\frac{\partial \bar{u}}{\partial r} + \left(2K_T - \frac{2}{3}G\right)\frac{\bar{u}}{r} - K_T\alpha_p\delta T\right) \\
\rho\frac{\partial^2 \bar{u}}{\partial t^2} &= \left(K_T + \frac{4}{3}G\right)\left(\frac{\partial^2 \bar{u}}{\partial r^2} + \frac{2}{r}\frac{\partial \bar{u}}{\partial r} - \frac{2\bar{u}}{r^2}\right) - K_T\alpha_p\frac{\partial \delta T}{\partial r},
\end{aligned} \tag{A.31}$$

knowing that $\bar{u}$ is displaced only in the radial direction we can write this equation as

$$\rho\frac{\partial^2 \bar{u}}{\partial t^2} = \left(K_T + \frac{4}{3}G\right)\nabla\left(\nabla \cdot \bar{u}\right) - K_T\alpha_p\nabla\delta T, \tag{A.32}$$

and thus we conclude this section having found the equation that governs the displacement field in the sphere.

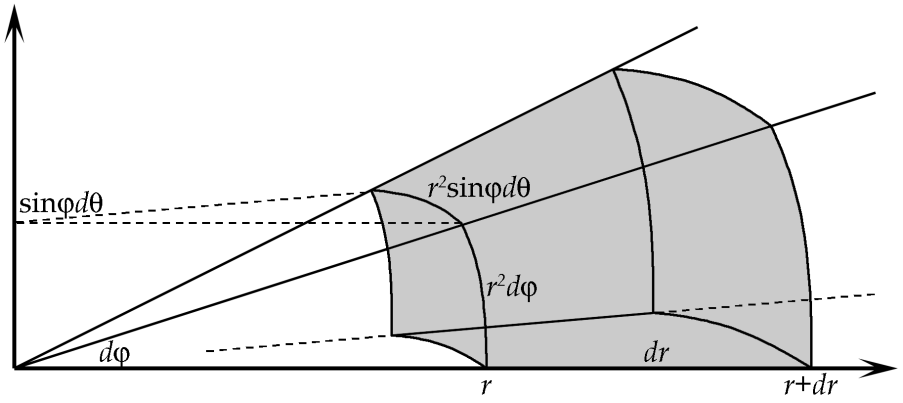

Figure A.2 The infinitesimal differential volume can be viewed as simple box and as such the volume can be calculated as the product of three sides, $dV = r^2 \sin\phi dr d\phi d\theta$.

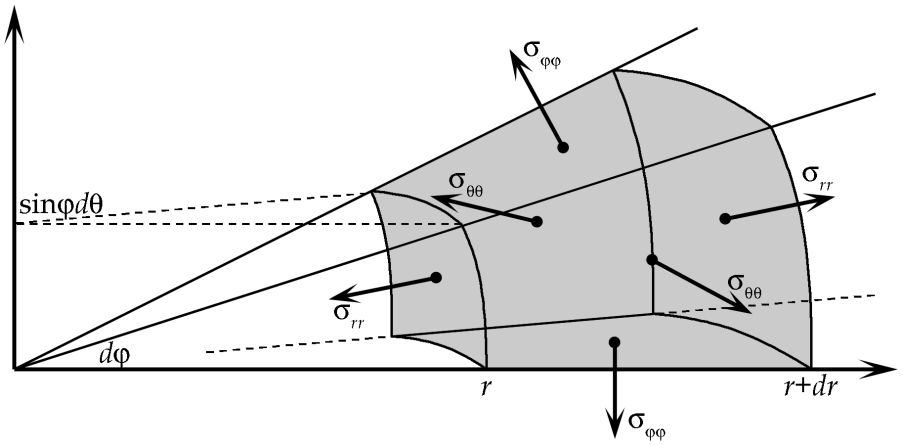

Figure A.3 The force on the differential volume is supplied from the stress tensor which specifies the drag in the volume surfaces in all possible directions.

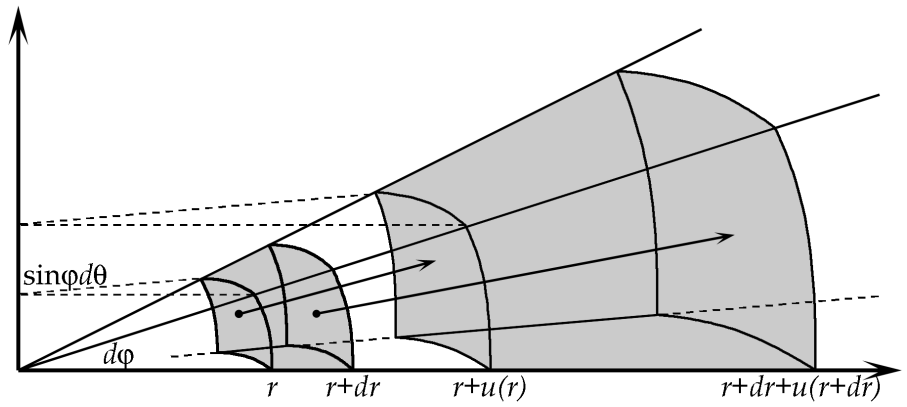

Figure A.4 The diagonal elements of the strain tensor are found by considering the displacement of the volume dV into dV' by the displacement field $\bar{u}(r, \phi, \theta, t)$.

B The moulding device and moulding scheme

The moulding device is shown in Figure B.1. It is made of teflon to make it easy to remove the sphere after moulding. There are two main parts of the moulding device. They consist of two cylindrical blocks, with half spheres cut out in each block having the same base radii, 9.55mm. These two parts are the two smallest pieces shown in Figure B.1; The one in front of the photo, and the one to the right. Lets call them piece A and B respectively.

In piece B there are two tracks where wires are embedded and on the face of the half-sphere in piece B you can see the small NTC-bead connected to the wires. In piece A, there is a hole in the bottom of the cavity. This is to allow liquid to flow in and out in the moulding proces. When filling piece A with the melt in step 3, there is a teflon-plug inserted into the hole. This is removed in step 4.

There is also a hollow cylinder, piece C, with a hight equal to the hight of the two moulding parts put on top of each other. Its inner radius fits with the outer radius of pieces A and B, and its purpose is to make sure that when piece A and B meet face to face, the two half-spheres meet in an exact sphere when put together.

step 1 in moulding proces

First glucose is grinded in a bowl of aluminum, and then put into a exicator which sucks water out of the sample for 24 hours.

step 2 in moulding proces

Then the bowl is put into an oven which melts the Glucose at 158℃(the melting temperature of Glucose). The melt is kept at this temperature for 5 minutes, short enough to avoid charamelization.

step 3 in moulding proces

The melt is quickly poured into piece A (with the plug put into the hole) and B. The two parts then cool in an oven preset to 60℃. Now the flow is slow, so that turned up-side down for a few seconds, the content does not lew the cavities of pieces A and B. The reason for this is that the next step in the moulding proces is to put piece

B inside piece C, and on top of that, turned up-side down, we put piece A, with its content facing downwards.

step 4 in moulding proces

The two halfspheres are joined by placin piece A and B inside piece C, the plug in piece A is removed. This way the NTC-bead is trapped in the center of the resulting sphere. Then the molding device is put in to an oven at temperature preset to 100℃. Here the sample sits for 1 hour so that the two half-spheres melt together forming one sphere.

step 5 in moulding proces

Now the temperature of the oven is slowly ramped down to 40℃(a bit above the caloroverimetric glass transition temperature). The final temperature is reached after 24 hours. This way the liquid have time to contract sucking in exceeding liquid from the hole in piece A, avoiding large tensions that risk cracking of the sphere.

step 6 in moulding proces

The temperature is lowered to 25℃, and waits there for 2 hours, the sample now being a solid glass. The sphere is then removed from the moulding device, in three steps. First the piece A and B is pushed out of piece C. Then by tightening the screew in piece A, shown in the photo in Figure B.1, piece A is pushed away from the sample. Finally the sample is loosened from piece B by pulling it out by the wires.

step 7 in moulding proces

Now the sphere is coated with a very thin layer of clear cellulose varnish in order to prevent the uptake of water from the atmosphere. The resulting sphere of glucose is seen sitting in piece B in Figure B.2. In this particular case you can see som bubbles of air trapped inside the sample. This constitutes the biggest problem in the proces, since a bubble of air on the NTC-bead destroys the thermal contact to the glucose.

Figure B.1 Photo of the three parts constituting the moulding device. See the text above for an explanation.

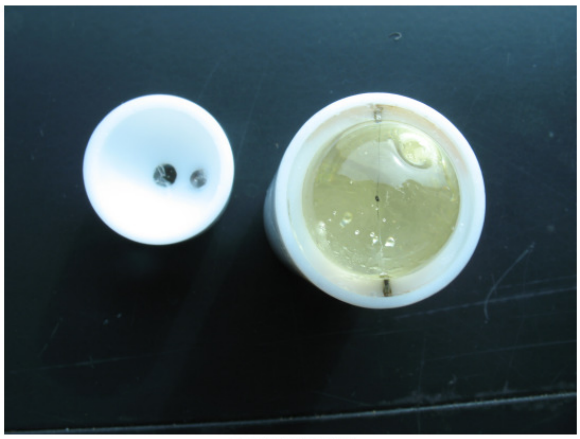

Figure B.2 The resulting sphere of glucose, with some bubbles of air trapped in it.

Bibliography

[1] L. D. Landau and E. M. Lifshitz. *Theory of Elasticity.* Elsevier, 1986.

C Reprint of publications

Journal of Non-Crystalline Solids 357 (2011) 346–350

Contents lists available at ScienceDirect

Journal of Non-Crystalline Solids

journal homepage: www.elsevier.com/ locate/ jnoncrysol

A combined measurement of thermal and mechanical relaxation

Tage Christensen *, Bo Jakobsen, Jon Papini, Tina Hecksher, Jeppe C. Dyre, Niels Boye Olsen

DNRF Centre "Glass and Time", IMFUFA, Department of Sciences, Roskilde University, Postbox 260, DK-4000 Roskilde, Denmark

ARTICLE INFO

Article history:
Received 18 April 2010
Received in revised form 29 June 2010

Keywords:
Glass transition;
Thermoviscoelasticity;
Prigogine–Defay ratio

ABSTRACT

In order to describe relaxation the thermodynamic coefficient $\frac{1}{\beta_S} = \left(\frac{\partial V}{\partial S}\right)_p$ can be generalized into a complex frequency-dependent cross response function. We explore theoretically the possibility of measuring $\frac{1}{\beta_S}(\omega)$ for a supercooled liquid near the glass transition. This is done by placing a thermistor in the middle of the liquid which itself is contained in a spherical piezoelectric shell. The piezoelectric voltage response to a thermal power generated in the thermistor is found to be proportional to $\frac{1}{\beta_S}(\omega)$ but factors pertaining to heat diffusion and adiabatic compressibility $\kappa_S(\omega)$ do also intervene. We estimate a measurable piezoelectric voltage of 1 mV to be generated at 1 Hz for a heating power of 0.3 mW. Together with $\kappa_S(\omega)$ and the longitudinal specific heat $c_l(\omega)$ which may also be found in the same setup a complete triple of thermoviscoelastic response functions may be determined when supplemented with shear modulus data.

1. Introduction

The recent finding [1] that a class of liquids — the strongly correlating liquids — may be described by a single "order" parameter makes it urgent to devise methods that measure thermal and mechanical relaxation and their interconnection. It would be an advantage if they can be measured in the same setup on the same sample. The classical Prigogine–Defay test of a one "order" parameter description has recently been rigorously reformulated for the equilibrium liquid in terms of (four) Dynamic Prigogine–Defay ratios [2]. One of these, $\Lambda_{Sp} = -(T_0/c_p)''(\kappa_S)''/((1/\beta_S)'')^2$ is from an experimental viewpoint the easiest to access. It contains the complex frequency-dependent specific heat $c_p(\omega)$, adiabatic compressibility $\kappa_S(\omega)$ and adiabatic pressure coefficient $\beta_S(\omega) \equiv (\delta p(\omega)/\delta T(\omega))_S$. We can measure $\kappa_S(\omega)$ by the so-called piezoelectric bulk modulus gauge (PBG) [3]. The PBG is a hollow sphere with a thin wall of a piezoelectric ceramic material. Pressure/volume changes of a contained liquid are detectable due to the piezoelectric effect. In the middle of the PBG we have now added a thermistor by which we can measure the longitudinal heat capacity $c_l(\omega)$ via the effusivity [4,5]. In this paper we study theoretically what can be deduced by combining the two sensors, i.e. how does the expansion of the liquid upon heating in the centre affect the piezoelectric shell.

2. Thermomechanical response of a differential volume element

The thermal interaction with matter is described in terms of the conjugated variables temperature, T and entropy, S. We name the interaction as an energy bond. It is a scalar bond since the variables are scalars. The mechanical interaction is described in terms of the strain and stress tensors but this interaction can be separated in a pure scalar part by the trace of these tensors and the deviatoric traceless part of these tensors. The conjugated variables of the scalar mechanical energy bond may then be taken as volume, V and minus pressure, $-p$. The deviatoric parts of the strain and stress tensors describe shear deformations and are not coupled to the scalar parts for symmetry reasons (The Curie–Prigogine principle [6–8]) but the scalar bonds however are coupled. The response δS and δV to perturbations δT and $-\delta p$ defines the constitutive properties of matter:

$$dV/V_0 = -\kappa_T dp + \alpha_p dT \tag{1}$$

$$dS/V_0 = -\alpha_p dp + \frac{1}{T_0} c_p dT \tag{2}$$

Since the perturbations excite thermal and acoustical waves the constitutive equations are defined for a differential volume element, V_0 of a linear dimension, R much smaller than the characteristic thermal diffusion length and acoustical wave length associated with the time scale of the perturbations (Figs. 1 and 2).

Eqs. (1) and (2) are valid in equilibrium thermodynamics. When it comes to describing the relaxation of supercooled liquids they are replaced with corresponding equations of linear irreversible thermodynamics

$$dV(t)/V_0 = -\int_{-\infty}^{t} \kappa_T(t-t')dp(t') + \int_{-\infty}^{t} \alpha_p(t-t')dT(t') \tag{3}$$

* Corresponding author.
E-mail address: tec@ruc.dk (T. Christensen).

0022-3093/$ – see front matter © 2010 Elsevier B.V. All rights reserved.
doi:10.1016/j.jnoncrysol.2010.07.051

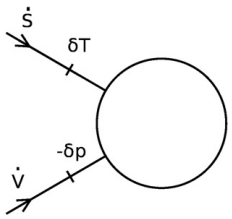

Fig. 1. The two scalar energetic interactions with a differential volume element. Differential means that the wavelengths of the thermal and mechanical perturbations are much longer than the dimensions of the volume element.

$$dS(t)/V_0 = -\int_{-\infty}^{t}\alpha_p(t-t')dp(t') + \int_{-\infty}^{t}\frac{1}{T_0}c_p(t-t')dT(t') \tag{4}$$

The thermodynamic coefficients are now replaced by response functions. These relaxing response functions may be consider in the frequency domain instead by defining e.g. the complex frequency-dependent compressibility as:

$$\kappa_T(\omega) = i\omega\int_0^{\infty}\kappa_T(t)e^{-i\omega t}dt. \tag{5}$$

Now dV, dS, dp and dT should be interpreted as the complex amplitudes of harmonically varying perturbations and the constitutive equations of linear irreversible thermodynamics (3) and (4) becomes

$$dV/V_0 = -\kappa_T(\omega)dp + \alpha_p(\omega)dT \tag{6}$$

$$dS/V_0 = -\alpha_p(\omega)dp + \frac{1}{T_0}c_p(\omega)dT \tag{7}$$

They can now be treated exactly like the equilibrium Eqs. (1) and (2). The response functions like $\kappa_T(\omega)$ and $c_p(\omega)/T_0$ pertaining to the conjugated variables of a single energy bond are auto response functions. $\alpha_p(\omega)$ on the other hand is a cross response function connecting a variable from the thermal bond to a variable from the mechanical bond. The three functions give a complete description of the thermomechanical response. For relaxing system they are not completely independent since the knowledge of the cross response function and one of the auto response functions for all frequencies makes it possible to calculate the other auto response function [9,10]. Moreover if the liquid relaxation is described by a single order parameter the relaxational part of the triple of relaxation functions are proportional and the dynamic Prigogine–Defay ratio [2]

$$\Lambda_{Tp} = \frac{c_p''\kappa_T''}{T_0\left(\alpha_p''\right)^2} \tag{8}$$

is equal to 1.

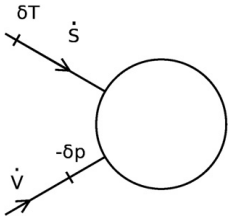

Fig. 2. Another response situation. Here entropy and pressure are the input variables and marked on the energy bond nearest to the system. In Fig. (1) temperature and pressure were the input variables.

There are three other different possibilities of pairs of independent controlling variables than $(dT,-dp)$, namely (dS,dV), $(dS,-dp)$, (dT,dV) leading to other triples of response functions and other variants of the dynamic Prigogine–Defay ratio. It is thus convenient to introduce the four auto response functions (connecting conjugated variables of the same bond),

$$c_V = \frac{T}{V}\left(\frac{\partial S}{\partial T}\right)_V \quad , \quad c_p = \frac{T}{V}\left(\frac{\partial S}{\partial T}\right)_p$$

$$\kappa_T = -\frac{1}{V}\left(\frac{\partial V}{\partial p}\right)_T \quad , \quad \kappa_S = -\frac{1}{V}\left(\frac{\partial V}{\partial p}\right)_S$$

and the four cross response functions (connecting variables of different bonds),

$$\alpha_p = \frac{1}{V}\left(\frac{\partial V}{\partial T}\right)_p = -\frac{1}{V}\left(\frac{\partial S}{\partial p}\right)_T,$$

$$\frac{1}{\alpha_S} = -V\left(\frac{\partial T}{\partial V}\right)_S = V\left(\frac{\partial p}{\partial S}\right)_V,$$

$$\beta_V = \left(\frac{\partial p}{\partial T}\right)_V = \left(\frac{\partial S}{\partial V}\right)_T,$$

$$\frac{1}{\beta_S} = \left(\frac{\partial T}{\partial p}\right)_S = \left(\frac{\partial V}{\partial S}\right)_p$$

Strictly speaking – defining these 8 functions as partial derivatives – they are at first just constant real thermodynamic coefficients but they may be generalized into complex functions just like $\kappa_T(\omega)$, $\alpha_p(\omega)$ and $c_p(\omega)$ and they are thought of in this sense in the following. An extensive table of relations between these functions is given in the appendix of reference [4]. Here we just notice that β_S is related to α_p and c_p by

$$\frac{1}{T_0\beta_S} = \frac{\alpha_p}{c_p}. \tag{9}$$

All of the response functions can be related to fluctuations of the thermodynamic variables [11]. For example $1/\beta_S$ is proportional to correlations between temperature and volume fluctuations. It was recently found [1] that a class of liquids — the strongly correlating liquids — may be described by a single "order" parameter and it was explicitly shown [12] by computer NVT simulations of the Kob–Andersen binary Lennard–Jones system that

$$\Lambda_{TV}(\omega) = -\frac{c_V''\left(\frac{1}{\kappa_T}\right)''}{T_0(\beta_V'')^2} \tag{10}$$

was 1 within 20%.

As we shall see it will probably be the triple $T_0/c_p(\omega), \kappa_S(\omega), 1/\beta_S$ that is experimentally easiest accessible and it will be the *Sp*-variant of the Prigogine–Defay ratio

$$\Lambda_{Sp} = -\frac{\left(\frac{T_0}{c_p}\right)''\kappa_S''}{\left(\left(\frac{1}{\beta_S}\right)''\right)^2} \tag{11}$$

that shall test the one-parameter'ness of real liquids.

3. Thermomechanical response of a finite spherical volume element

When considering a real experiment with perturbations varying at a frequency $f=\omega/(2\pi)$ it is not always possible to be in a situation of homogeneous fields. The wavelength of sound λ_{sound} and the heat diffusion length, $|l_D|$ may be comparable to or smaller than the sample size R. If we consider frequencies below 1 kHz then roughly $\lambda_{sound}>1$m

and for $R<1$cm we can neglect mechanical waves i.e. neglect inertia in the continuum description [4]. However the heat diffusion length, $|l_D| = |\sqrt{D/(i\omega)}|$ of a supercooled liquid with a typical heat diffusion constant of $D=0.1\text{mm}^2/\text{s}$ varies from $4\mu m$ to 4mm when frequency varies from 1 kHz to 1 mHz and thus heat diffusion cannot be neglected for a sample size of 1 cm. By the coupling between the temperature field and the strain field that α_p induces, the strain and stress fields also become inhomogeneous. This implies that even in spherical geometry the two pressures, the radial $\delta p_r = -\sigma_{rr}$ and the mean (hydrostatic) $\delta p = -1/3(\sigma_{rr}+\sigma_{\theta\theta}+\sigma_{\varphi\varphi})$ are not equal if shear modulus is comparable to bulk modulus. When interacting mechanically with a sphere through its surface we don't have access to δp but only to δp_r. For this reason shear modulus enters – via the boundary conditions – the description of the thermomechanical response of a finite sphere although it wasn't present in the thermomechanical response of a differential volume element, Eqs. (6) and (7). Consider generally a finite amount of liquid lying in between radii r_1 and r_2 depicted in Fig. 3. In the inertia-free limit the general problem of the relation between the variables, radial pressure, δp_r, temperature change, δT, volume displacement, δV and entropy displacement, δS at the two radii has been solved [4] in the frequency domain in terms of a transfer matrix:

$$\begin{pmatrix} \delta p_r \\ \delta T \\ \delta V \\ \delta S \end{pmatrix}_{r_2} = \mathbf{T}(r_2, r_1) \begin{pmatrix} \delta p_r \\ \delta T \\ \delta V \\ \delta S \end{pmatrix}_{r_1} \tag{12}$$

In general $\mathbf{T}$ is a complicated object. An interesting result was found when two conditions hold: 1) frequencies are high enough to be in the "thermally thick limit" with respect to r_2, i.e. $|l_D| \ll r_2$ and 2) $r_1 \ll r_2$: When studying in this case the combined response to thermal stimuli at radius r_1 and mechanical stimuli at radius r_2 one can neglect the mechanical boundary condition at r_1 and the thermal boundary condition at radius r_2 ending up with a reduced transfer matrix given as

$$\begin{pmatrix} \delta T \\ \delta S \end{pmatrix}_{r_1} = \begin{pmatrix} i\omega Z_{th} T_0 V_2 \kappa_S \beta_S & i\omega Z_{th} T_0 \beta_S \\ V_2 \kappa_S \beta_S & \beta_S \end{pmatrix} \begin{pmatrix} \delta p_r \\ \delta V \end{pmatrix}_{r_2}, \tag{13}$$

where $V_2 = \frac{4\pi}{3} r_2^3$ and Z_{th} is the thermal impedance,

$$Z_{\text{th}}(\omega) = \frac{1}{4\pi\lambda r_1 \left(1 + \sqrt{i\omega r_1^2 c_l(\omega)/\lambda}\right)}, \tag{14}$$

λ is the heat conductivity. The specific heat, c_l entering the thermal impedance is the so-called longitudinal specific heat. c_l is the amount of heat absorbed per Kelvin upon a temperature increment if the associated expansion is forced to be longitudinal. This is in contrast to the isobaric specific heat for which the expansion is isotropic. The longitudinal specific heat can be related to the isochoric specific heat, c_V by [4]

$$c_l = \frac{\frac{1}{\kappa_S} + \frac{4}{3}G}{\frac{1}{\kappa_T} + \frac{4}{3}G} c_V, \tag{15}$$

where G is shear modulus. Using the identities [4]

$$\frac{c_p}{c_V} = \frac{\kappa_T}{\kappa_S} \quad \text{and} \quad \kappa_T - \kappa_S = \frac{c_p}{T_0 \beta_S^2} \tag{16}$$

together with (15) the deviation between the longitudinal specific heat and isobaric specific heat may be expressed by

$$\frac{1}{c_p} = \frac{1}{c_l} - \frac{1}{T_0 \beta_S^2} \frac{\frac{4}{3}G}{1 + \frac{4}{3}G\kappa_S}. \tag{17}$$

This expression has the advantage of giving $c_p(\omega)$ in terms of the quantities $c_l(\omega), \kappa_S(\omega), \beta_S(\omega)$ and $G(\omega)$ that are possible to access experimentally by our new device supplemented with the Piezoelectric Shear modulus Gauge [13].

Eq. (13) is equivalent to equation (138) of reference [4]. The determinant of (13) is zero although a transfer matrix relating proper conjugated variables should have determinant 1. The reason is that we are studying a limiting case where $|i\omega Z_{\text{th}} T_0 V_2 \kappa_S \beta_S^2| \gg 1$. Thus the inverse relation is

$$\begin{pmatrix} \delta p_r \\ \delta V \end{pmatrix}_{r_2} = \begin{pmatrix} \beta_S & -i\omega Z_{th} T_0 \beta_S \\ -V_2 \kappa_S \beta_S & i\omega Z_{th} T_0 V_2 \kappa_S \beta_S \end{pmatrix} \begin{pmatrix} \delta T \\ \delta S \end{pmatrix}_{r_1}, \tag{18}$$

This is equivalent to equation (139) of reference [4], but there was a typo: the common T_0 factor in the matrix of that formula should be deleted. The simplified transfer matrix can be represented by the equivalent diagram of Fig. 4. The equivalent diagram is in a sense a more correct description since it leads to a transfer matrix deviating from Eq. (13) by a negligible term that however endows it with a determinant of 1.

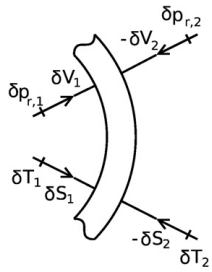

Fig. 3. Depiction of the four thermal and mechanical interactions at the boundaries at r_1 and r_2 in spherical geometry.

4. The combined experiment

The adiabatic compressibility $\kappa_S(\omega)$ can be measured using the piezoelectric bulk modulus gauge (PBG) [3]. The PBG is a hollow sphere of radius 1 cm with a thin wall of a piezoelectric ceramic material. The thickness t is 0.5 mm. The sphere may be filled by a liquid at elevated temperature, where it is fluent. The PBG transforms the mechanical compliance of the liquid into an electric compliance (the capacitance), that can be simply measured by an LCR-meter or by other means. In order to make combined thermomechanical experiments we have placed a thermistor in the middle of the PBG (see Fig. 5). By the thermistor itself we can measure the longitudinal heat capacity $c_l(\omega)$ via the effusivity [5]. Combining the two devices makes it, in principle, possible to get the cross response function $1/\beta_S$. That is, nearly all ingredients of Λ_{sp} can be found for the same sample in the same device. However if $c_l(\omega)$ differs significantly from $c_p(\omega)$ [4] as

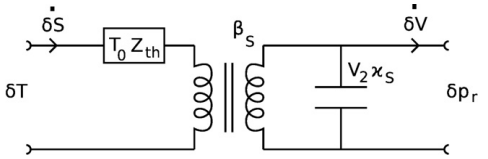

Fig. 4. Equivalent diagram of the liquid.

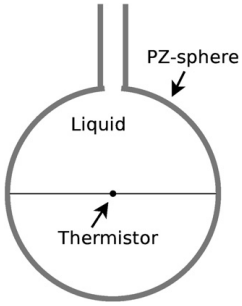

Fig. 5. The combined measurement of c_l, κ_S, β_S.

may be judged by Eq. (17) a supplementary measurement of the shear modulus is needed. We may produce an oscillating heat current with amplitude P_{th} by Joule heating in the thermistor and measure the piezoelectric voltage U_{pz} generated in the PBG as the liquid attempts to expand. This voltage contain information on $1/\beta_S = \left(\frac{\partial V}{\partial S}\right)_p$ but it is also dependent of the thermal interaction of the thermistor with the liquid and the mechanical interaction of the liquid with the PBG. In order to filter these factors out we may look at the equivalent diagram, Fig. 6 of the whole system. For simplicity we model the thermistor as an ideal heat generator in parallel with its heat capacitance C_0 of approximately 5.5×10^{-5} J/K. (For a more detailed model of the thermal structure of the thermistor, see reference [5]). In the equivalence diagram in Fig. 6 the PBG consist of a mechanical compliance, C_m, a transducer ratio, T_{pz} and an electric (clamped) capacitance C_e. They can be expressed [3] in terms of the dielectric constant, ϵ_{33}, the elastic compliance, $(s_{11}+s_{12})/2$ and the piezoelectric constant, d_{13} of the piezoelectric material pz29 together with the radius, r_2 and shell thickness, t (see Table 1).

By the equivalence diagram one finds that the generated piezoelectric voltage amplitude U_{pz} measured by a voltmeter of high impedance ($I_{pz}=0$) in response to a heat current amplitude P_{th} generated in the thermistor becomes

$$\left(\frac{U_{pz}}{P_{th}}\right)_{I_{pz}=0} = \frac{T_{pz}}{C_e i\omega} \frac{1}{(1+C_0 i\omega Z_{th}(\omega))\left(1+\left(1+T_{pz}^2\frac{C_m}{C_e}\right)\frac{V_2\kappa_S(\omega)}{C_m}\right)} \frac{1}{T_0\beta_S(\omega)} \quad (19)$$

We see that in principle β_S may be found by this third cross experiment with a thermistor in the PBG. However the signal is also influenced in its frequency dependence by the thermal impedance of the liquid and the adiabatic compressibility but both of these can be found by the experiments of the thermistor alone respectively the PBG alone. The frequency dependence in the thermal impedance has a characteristic diffusion time constant that is almost independent of the change of c_l at the glass transition whereas the factor containing the compressibility of course will change the position of its characteristic time scale as temperature is changed. It is interesting to estimate this signal. At 1 Hz $C_0 Z_{th}$ is of the order of 1 and so is the factor containing the compressibility. From the values in the Table 1 we find $\frac{T_{pz}}{C_e} = 10^{11}\mathrm{Vm}^{-3}$. Typical values of the expansion coefficient and the specific heat of a liquid are $\alpha_p = 5\times10^{-4}\mathrm{K}^{-1}$ and $c_p = 2\times10^6\mathrm{JK}^{-1}\mathrm{m}^{-3}$ and thus $\frac{1}{T_0\beta_S} = \frac{\alpha_p}{c_p} = 2.5\times10^{-10}\mathrm{m}^3\mathrm{J}^{-1}$. From this we find $\frac{T_{pz}}{C_e}\frac{1}{T_0\beta_S} = 25\,\mathrm{V/J}$. Using a power amplitude P_{th} of 0.3 mW in order to keep temperature change in the centre below 1 K we thus expect a signal of the order of 1 mV at 1 Hz which is readily detectable.

Table 1
Properties and lumped parameters of the piezoelectric bulk modulus gauge modeled in Fig. 6.

r_2		9.5×10^{-3} m
t		0.5×10^{-3} m
ϵ_{33}		26×10^{-9} F/m
$\frac{s_{11}+s_{12}}{2}$		6×10^{-12} m^2/N
d_{13}		26×10^{-9} C/N
k_p	$\frac{d_{13}}{\sqrt{\epsilon_{33}(s_{11}+s_{12})/2}}$	0.64
C_m	$\frac{s_{11}+s_{12}}{2}\frac{4\pi r_2^4}{t}$	1.5×10^{-15} m^3/Pa
T_{pz}	$\frac{2d_{13}}{(s_{11}+s_{12})}\frac{1}{r_2}$	4×10^3 C/m^3
C_e	$\epsilon_{33}\left(1-k_p^2\right)\frac{4\pi r_2^2}{t}$	40×10^{-9} F

5. Conclusion

Of the four dynamic Prigogine–Defay ratios one special namely, $\Lambda_{Sp} = -(T_0/c_p)''(\kappa_S)''/((1/\beta_S)'')^2$ seems from an experimental viewpoint to be the most directly accessible. By combining the devices of the two techniques 1) measurement of the adiabatic compressibility $\kappa_S(\omega)$ with the Piezoelectric Bulk modulus Gauge and 2) measurement of the longitudinal specific heat $c_l(\omega)$ by thermal effusion in spherical geometry a third cross response function, $1/\beta_S(\omega)$ may be measured. That is, nearly all ingredients of Λ_{Sp} could be found for the same sample in the same device. However $c_l(\omega)$ may differ from $c_p(\omega)$ [4], in which case a supplementary measurement of the shear modulus is needed.

References

[1] U.R. Pedersen, T. Christensen, T. Schrøder, J.C. Dyre, Feasibility of a single-parameter description of equilibrium viscous liquid dynamics, Phys. Rev. E 77 (2008) 011201.
[2] N.L. Ellegaard, T. Christensen, P.V. Christiansen, N.B. Olsen, U.R. Pedersen, T.B. Schrøder, J.C. Dyre, Single-order-parameter description of glass-forming liquids: a one-frequency test, J. Chem. Phys. 126 (2007) 074502.

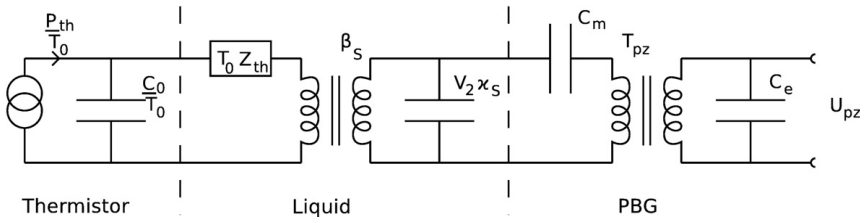

Fig. 6. Equivalent diagram of the liquid in contact with the thermistor and the piezoelectric shell (PBG).

[3] T. Christensen, N.B. Olsen, Determination of the frequency-dependent bulk modulus of glycerol using a piezoelectric spherical-shell, Phys. Rev. B 49 (1994) 15396.
[4] T. Christensen, J.C. Dyre, Solution of the spherically symmetric linear thermo-viscoelatic problem in the inertia-free limit, Phys. Rev. E 78 (2008) 021501.
[5] B. Jakobsen, N.B. Olsen, T. Christensen, Frequency dependent specific heat from thermal effusion in spherical geometry, Phys. Rev. E 81 (2010) 061505.
[6] P. Curie, Oeuvres, Societe Francaise de Physique, Paris, 1908.
[7] I. Prigogine, Etude Thermodynamique des Phenomenes Irreversibles, Desoer, Liege, 1947.
[8] S.R.D. Groot, P. Mazur, Non-equilibrium Thermodynamics, North-Holland Publishing Co., Amsterdam, 1962.
[9] N.P. Bailey, T. Christensen, B. Jakobsen, K. Niss, N.B. Olsen, U.R. Pedersen, T.B. Schrøder, J.C. Dyre, Glass-forming liquids: one or more "order" parameters? J. Phys. Condens. Matter 20 (2008) 244113.
[10] J. Meixner, H.G. Reik, in: S. Flügge (Ed.), Principen der Thermodynamik und Statistik, Handbuch der Physik, vol. 3, Springer, Berlin, 1959.
[11] T.B. Schrøder, N.P. Bailey, U.R. Pedersen, N. Gnan, J.C. Dyre, Pressure–energy correlations in liquids. III. Statistical mechanics and thermodynamics of liquids with hidden scale invariance. J. Chem. Phys. 131 (2009) 234503.
[12] N.P. Bailey, U.R. Pedersen, N. Gnan, T.B. Schrøder, J.C. Dyre, Pressure–energy correlations in liquids. II. Analysis and consequences. J. Chem. Phys. 129 (2008) 184508.
[13] T. Christensen, N.B. Olsen, A rheometer for the measurement of a high-shear modulus covering more than 7 decades of frequency below 50 kHz, Rev. Sci. Instrum. 66 (1995) 5019–5031.

Do all liquids become strongly correlating at high pressure?

Jon J. Papini* and Thomas B. Schrøder, and Jeppe C. Dyre†
DNRF Centre "Glass and Time", IMFUFA, Department of Sciences, Roskilde University, Postbox 260, DK-4000 Roskilde, Denmark
(Dated: March 25, 2011)

We present molecular dynamics simulations studying the influence of pressure on the correlation between the thermal equilibrium fluctuations of virial W and potential energy U, focusing on liquids that are not strongly correlating at low pressure (i.e., do not have a WU correlation coefficient above 0.9). The systems studied are the two hydrogen-bonded liquids GROMOS methanol and TIT5P water, the ionic liquid defined by a united-atom model of the 1-butyl-3-methyl-imidazolium nitrate, and for reference the standard single-component Lennard-Jones liquid. The simulations were performed for pressures varying from 0 GPa to 10 GPa. For all systems studied we find that the virial / potential energy correlation increases with increasing pressure. This suggests that if crystallization is avoided, all liquids become strongly correlating at sufficiently high pressure.

The properties of strongly correlating liquids were recently discussed in several papers [1]. These liquids by definition exhibit strong correlations between their constant-volume equilibrium fluctuations of the potential energy U and the virial [2, 3] $W \equiv -1/3 \sum_i \mathbf{r}_i \cdot \nabla_{\mathbf{r}_i} U(\mathbf{r}_1, ..., \mathbf{r}_N)$, where $\mathbf{r}_i$ is the position of particle i. Recall that, if p is the pressure, V the volume, N the number of particles, and T the temperature, the average virial $\langle W \rangle$ gives the configurational contribution to the pressure [2, 3]:

$$pV = Nk_BT + \langle W \rangle . \quad (1)$$

If Δ denotes the instantaneous deviations from equilibrium mean values, the WU correlation is quantified by the correlation coefficient R defined by

$$R = \frac{\langle \Delta W \Delta U \rangle}{\sqrt{\langle (\Delta W)^2 \rangle \langle (\Delta U)^2 \rangle}} . \quad (2)$$

Perfect correlation gives $R = 1$; strongly correlating liquids are defined [1] by $R \geq 0.9$ for fluctuations monitored in the NVT ensemble, i.e., at constant volume and temperature.

The computer simulations of Ref. 1 indicate that the correlation coefficient R tends to increase at increasing pressure, but no systematic studies have been carried out of the effect of pressure on the correlation. The simulations of Ref. 1 showed that van der Waals type liquids and metallic liquids are generally strongly correlating. In contrast, liquids composed of molecules whose interactions have competing or directional interactions are generally not strongly correlating. The latter classes of liquids include the hydrogen-bonded liquids, the covalently bonded liquids, and the (strongly) ionic liquids. Since previous works indicated that R increases at increasing pressure, the question arises whether all liquids become strongly correlating at sufficiently large pressure. This is the guiding question of the present brief report.

Simulations of four different model liquids were performed with NVT molecular dynamics using the Gromacs package [4]. For each model samples of different densities were created and mixed during 1 ps (argon units) at a high temperature, followed by a ramping down to the desired isotherm. Here the systems were equilibrated at constant temperature during 10 - 500 ns. The data for each state point shown below represent an average taken over five statistically independent samples, with a sampling frequency of 0.2 ps and production runs of length 10 ns. The following systems were studied: 1) *The single-component Lennard-Jones liquid* defined by the pair potential $v_{LJ}(r) = 4\epsilon \left[(\sigma/r)^{12} - (\sigma/r)^6\right]$. This system serves as a reference strongly correlating liquid. The results reported below refer to standard argon units ($\sigma = 0.34$ nm, $\epsilon = 0.997$ kJ/mol). Samples consisting of $N = 864$ particles were studied. 2) *Methanol*: The GROMOS force field was used [5, 6], which is composed of three sites representing respectively the methyl group, the oxygen atom, and the oxygen-bonded hydrogen atom (H). The masses are, respectively, 15.035 u, 15.999 u, 1.008 u; the Coulomb interactions are given by the following charges: 0.176 e, -0.574 e, and 0.398 e. The sites interact with sites on other methanol molecules by additional Lennard-Jones interactions with the constants $\epsilon_{MM} = 0.9444$ kJ/mol, $\epsilon_{OO} = 0.8496$ kJ/mol, $\epsilon_{MO} = 0.9770$ kJ/mol, $\sigma_{MM} = 0.3646$ nm, $\sigma_{OO} = 0.2955$ nm and $\sigma_{MO} = 0.3235$ nm. The van der Waals interactions are cut off smoothly between 0.9 nm and 1.1 nm. The M-O distance is fixed at 0.136 nm, the O-H distance at 0.1 nm, and the M-O-H bond angle at 108.53°. Samples consisting of $N = 1728$ molecules were studied. 3) *TIP5P*: In this water model [7] each water molecule is described by five sites: one site represents the oxygen atom (O), two sites represent the hydrogen atoms, and two sites locate the centers of negative charge that correspond to the oxygen lone-pair electrons. The potential parameters and charges used are the same as in Ref. 1. Sample consisting of $N = 512$ molecules were studied.

*Electronic address: papini@ruc.dk
†Electronic address: dyre@ruc.dk

4) *[BMIM]$^+$[NO$_3$]$^-$*: A united-atom model of the ionic liquid 1-butyl-3-methyl-imidazolium nitrate [8] based on the GROMOS [5] force field. The same parameters were used as in Ref. 8.

As an example of WU correlations Fig. 1 shows the equilibrium fluctuations as a function of time of the TIP5P water model's normalized virial and potential energy. Figure 1(a) gives data from a simulation at zero pressure at $T = 475$ K. The fluctuations of W and U are rather uncorrelated ($R = 0.18$). At lower temperatures the correlation is even lower; indeed near the density maximum the correlation is close to zero [1]. Figure 1(b) gives data from a simulation at $p = 8$ GPa at the same temperature. Here the correlation is much larger ($R = 0.64$).

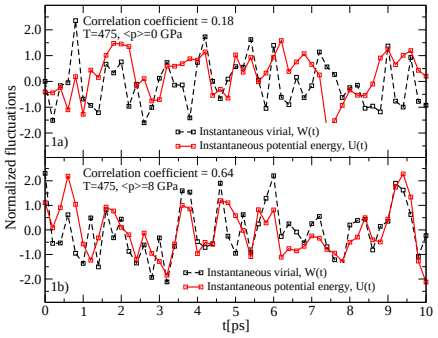

FIG. 1: Time series from simulation of 512 molecules of TIP5P water in the NVT ensemble at two different pressures. (a) At zero pressure the correlation between normalized fluctuations of the virial, $\triangle W(t)/\sqrt{\langle(\triangle W)^2\rangle}$ and that of the potential energy, $\triangle U(t)/\sqrt{\langle(\triangle U)^2\rangle}$, is weak, with a correlation coefficient of $R = 0.18$. As shown in Ref. 1 this low correlation is related to the existence of a density maximum at lower temperature where the WU correlation is almost zero. (b) At the pressure 8 GPa the WU correlation is considerably stronger ($R = 0.64$).

To systematically investigate the influence of pressure on the WU correlation we calculated the correlation coefficient as a function of pressure along isotherms for the four liquids. Figure 2 shows that the correlation increases with increasing pressure for all systems. The low correlation in the case of the single component Lennard-Jones (SCLJ) liquid at T=310 K reflects the fact that only the last three points stem from liquid-state simulations.

In Fig. 3 the correlation coefficient was plotted instead as a function of the relative volume change, $\triangle V = (V_0 - V)/V_0$, where V_0 is the highest volume at the given temperature corresponding to the lowest pressure of the simulation. In three cases the lowest pressure was around 1 bar, but for Methanol the lowest pressure was of order 0.1 GPa. Water crystallizes upon compression before it reaches the correlation coefficient $R > 0.9$ that defines a strongly correlating liquid.

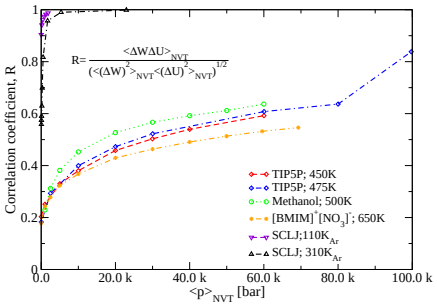

FIG. 2: The WU correlation coefficient R plotted as a function of pressure along isotherms for the following systems: 1) The standard, single-component Lennard-Jones liquid (two isotherms), 2) the ionic liquid [BMIM]$^+$[NO$_3$]$^-$, 3) methanol, and 4) the TIP5P water model (two isotherms; the last point represents a crystallized sample). In all cases the correlation increases with pressure.

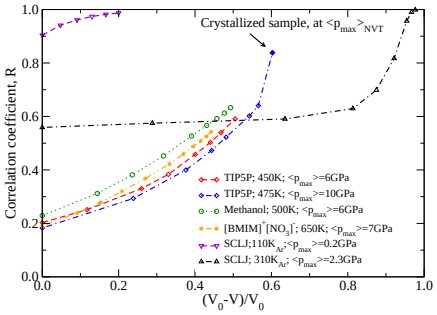

FIG. 3: The correlation coefficient R plotted against the volume decrease relative to the volume V_0 at the lowest pressure of the given isotherm. Data were taken from 10 ns of simulations of each liquid. The higher density isotherm (450 K) of TIP5P water shows stronger correlation than its less dense counterpart (475 K) at the same pressure.

In summary, all liquids studied show increasing virial / potential energy correlations as pressure increases. These simulations indicate that if crystallization is avoided, all liquids become strongly correlating at sufficiently high pressure. As a potentially important consequence of this, note that the major part of planet Earth is molten silica at extremely high pressure; our simulations suggest that this liquid is strongly correlating and thus simpler than it is at ambient pressure.

I. ACKNOWLEDGMENTS

Nuno Micaelo is gratefully acknowledged for providing the coordinates of an equilibrated sample of the united atom model of 1-butyl-3-methyl-imidazolium nitrate. The center for viscous liquid dynamics "Glass and Time" is sponsored by The Danish National Research Foundation.

[1] U. R. Pedersen, N. P. Bailey, T. B. Schrøder, and J. C. Dyre, Phys. Rev. Lett. **100**, 015701 (2008); U. R. Pedersen, T. Christensen, T. B. Schrøder, and J. C. Dyre, Phys. Rev. E **77**, 011201 (2008); T. B. Schrøder, U. R. Pedersen, N. P. Bailey, S. Toxvaerd, and J. C. Dyre, Phys. Rev. E **80**, 041502 (2009); N. P. Bailey, U. R. Pedersen, N. Gnan, T. B. Schrøder, and J. C. Dyre, J. Chem. Phys. **129**, 184507 (2008); N. P. Bailey, U. R. Pedersen, N. Gnan, T. B. Schrøder, and J. C. Dyre, J. Chem. Phys. **129**, 184508 (2008); T. B. Schrøder, N. P. Bailey, U. R. Pedersen, N. Gnan, and J. C. Dyre, J. Chem. Phys. **131**, 234503 (2009); N. Gnan, T . B. Schrøder, U. R. Pedersen, N. P. Bailey, and J. C. Dyre, J. Chem. Phys. **131**, 234504 (2009); N. Gnan, C. Maggi, T . B. Schrøder, and J. C. Dyre, Phys. Rev. Lett. **104**, 125902 (2010); U. R. Pedersen, T. B. Schrøder, and J. C. Dyre, Phys. Rev. Lett. **105**, 157801 (2010).

[2] M. P. Allen and D. J. Tildesley, *Computer Simulation of Liquids* (Oxford University Press, 1987).

[3] J. P. Hansen and J.R. McDonald, *Theory of Simple Liquids*, 3ed edition, (Academic, New York, 2005).

[4] H. J. C. Berendsen, D. van der Spoel, and R. van Drunen, Comput. Phys. Commun. **91**, 43 (1995); E. Lindahl, B. Hess, and D. van der Spoel, J. Mol. Model. **7**, 306 (2001).

[5] W. R. P. Scott, P. H. Hünenberger, I. G. Tironi, A. E. Mark, S. R. Billeter, J. Fennen, A. E. Torda, T. Huber, P. Krüger, and W. F. van Gunsteren, J. Phys. Chem. A **103**, 3596 (1999).

[6] W. F. Van Gunsteren, S. R. Billeter, A. A. Eising, P. H. Hünenberger, P. Krüger, A. E. Mark, W. R. P. Scott, and I. G. Tironi *Biomolecular Simulation: The GROMOS96 manual and user guide* (Zürich: Hochschulverlag AG an der ETH Zürich, Switzerland, 1996).

[7] M. W. Mahoney and W. L. Jorgensen, J. Chem. Phys. **112** 8910 (2000).

[8] N. M. Micaelo, A. M. Babtista, and C. M. Soares, J. Phys. Chem. B **110**, 14444 (2006).

[9] A. Carre, J. Horbach, S. Ispas, and W. Kob, EPL **82**, 17001 (2008).

[10] H. J. C. Berendsen, J. R. Grigera, and T. P. Straatsma, J. Phys. Chem. **91**, 6269 (1987).